1

The Fundamentals of Solar Energy Photocatalysis

Xin Li[1] *and Jiaguo Yu*[2]

[1] *Institute of Biomass Engineering, South China Agricultural University, 483 Wushan Road, Tianhe District, Guangzhou 510642, P. R. China*
[2] *China University of Geosciences, Laboratory of Solar Fuel, Faculty of Materials Science and Chemistry, 388 Lumo Road, Wuhan 430074, P. R. China*

1.1 Background

Solar energy semiconductor photocatalysis has long been considered to be the best solution to various kinds of energy and environmental problems. During the past decades, the solar energy semiconductor photocatalysis has attracted more and more attention. Based on Figure 1.1a, the total number of academic papers on the photocatalysis published since 1996 has reached 64 011, with increasing publication year by year. Especially, there are almost 8000 papers published in 2019 in the field of photocatalysis. Among all different research fields, the number of papers in photocatalytic pollutant degradation is the largest, which is much more than the total number of publications in both photocatalytic H_2 evolution and CO_2 reduction (Figure 1.1b).

So far, hundreds of solar energy semiconductor photocatalysts have been exploited and applied in the different photocatalytic fields, including the plasmonic metals, metal oxides/hydroxides, sulfides, nitrides, metal-free polymers, organic semiconductors, and their composites. Although some reviews covered the progresses of these kinds of semiconductors, there are few books systematically summarizing the advances in these semiconductors. Therefore, it is timely to provide a comprehensive book to thoroughly elaborate the exploitation and application of typical kinds of solar energy semiconductors in the different photocatalytic fields. We believe that this book can help the researchers easily grasp the recent achievements for various kinds of semiconductors and inspire their new ideas in developing new solar energy semiconductors for efficient photocatalysis.

1.2 History of Solar Energy Photocatalysis

Due to its green and renewable advantages, photocatalysis has been one of the most active directions in the field of chemistry in recent years.

Semiconductor Solar Photocatalysts: Fundamentals and Applications, First Edition.
Edited by Jiaguo Yu, Xin Li, and Jingxiang Low.

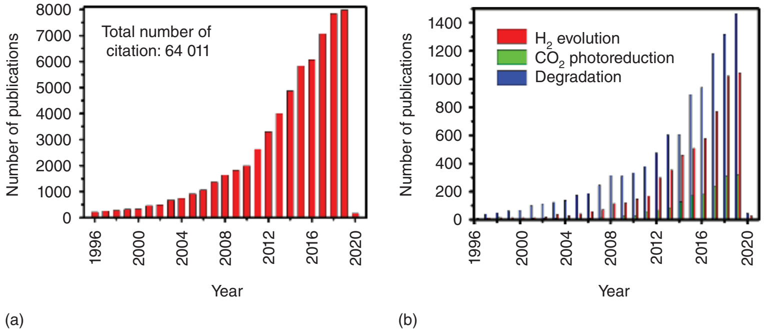

Figure 1.1 The number of publications on photocatalysis found by searching with the following keywords: (a) topic: (photoca*), (b) topic 1: (photoca*), and topic 2: (hydrogen or H-2 or H_2), (carbon dioxide or CO_2 or CO-2), or (degradat*). Source: Science Core Collection 26 November 2019.

Semiconductor photocatalysis can be traced back to 1839. Becquerel [1] first discovered the photoelectric phenomenon, although he did not explain it theoretically.

In 1955, Brattain and Garrett [2] gave a reasonable explanation for the photoelectric phenomena, marking the birth of photoelectrochemistry.

Especially in 1972, Fujishima and Honda first found that n-type semiconductor rutile TiO_2 single crystal electrode could achieve the photocatalytic decomposition of H_2O to O_2 under the ultraviolet (UV) light (with 380 nm wavelength), while on the counter electrode Pt simultaneously produces H_2 [3]. This great discovery has caused a sensation all over the world, which revealed the possibility of using solar energy to decompose water for hydrogen production – or to convert solar energy directly into chemical energy – thus opening up a new era of semiconductor photocatalysis research and attracting worldwide attention. Because of its far-reaching significance in the development of new energy and the protection of ecological environment, heterogeneous semiconductor photocatalysis has become a hot spot, attracting the extensive attention of researchers in many fields, such as chemistry, physics, and materials.

In the middle and late 1970s, Carey et al. [4] and Bard and coworker [5] utilized the TiO_2 suspension to degrade polychlorinated biphenyls and cyanides, respectively, under UV irradiation, which set off a research upsurge of environmental photocatalysis technology with the main purpose of decomposing environmental pollutants.

Schrauzer also confirmed that TiO_2 with rutile and anatase mixed crystal phases can realize the photocatalytic decomposition of chemisorbed water into H_2 and O_2 with a 2 : 1 stoichiometric ratio [6].

At the same time, Bard and his coworkers have guided and promoted the development of photoelectrochemistry. They first extended the theory of photoelectrochemistry (microelectrode model) to the photocatalysis of semiconductor particles, advancing the semiconductor photocatalysis technology greatly in theory. They not only used electron paramagnetic resonance (EPR) spectroscopy to characterize the free radicals such as hydroxyl ($^{\bullet}OH$) and hydroperoxyl ($^{\bullet}OOH$) radicals in the processes of photocatalytic oxidation and photocatalytic reduction of O_2 [7, 8], respectively, but also used Pt-decorated TiO_2 photocatalyst to decompose acetic acid for generating methane (CH_4), which proved that the heterogeneous photocatalysis process has similar principles to the photoelectrochemical (PEC) process [9, 10]. In terms of its charge transfer mechanism, the suspended semiconductor particle photocatalyst can be regarded as a short-circuited PEC cell [11, 12].

In 1978, Halmann found that CO_2 dissolved in the electrolyte could be reduced to formic acid (HCOOH), formaldehyde, and methanol (CH_3OH) by using p-GaP single crystal, carbon rod, and K_2HPO_4–KH_2PO_4 buffer solution as cathode, anode, and electrolyte, respectively, under the necessary applied bias voltage [13].

In the same year, Somorjai first used $SrTiO_3$ to achieve the photocatalytic conversion of CO_2 and water vapor to CH_4 [14].

In 1979, Inoue et al. [15] systematically reported that WO_3, TiO_2, ZnO, CdS, GaP, SiC, and other semiconductor catalysts suspend in the saturated aqueous solution of CO_2 could achieve the photoreduction of CO_2 to HCOOH, formaldehyde (HCHO), CH_3OH, and CH_4 under the illumination of xenon lamp and high-pressure mercury lamp. More importantly, the reaction mechanism of CO_2 photoreduction was proposed.

In 1980, Kawai and Sakata reported that H_2 was produced by photocatalytic reforming biomass and its derivatives (glycine, glutamic acid, proline, white gelatin protein) in water using $Pt/RuO_2/TiO_2$ photocatalyst. Only H_2 and CO_2 products were released from the photocatalytic processes [16].

Sequentially, Pt/TiO_2 [17] and (Pt) $SrTiO_3$ [18, 19] have also been proved to exhibit good photocatalytic activity for the decomposition of water into H_2. Therefore, since the early 1980s, heterogeneous photocatalysis technology has gradually formed two main research directions: environmental photocatalysis and energy photocatalysis.

Along with the two main research directions, researchers from the fields of physics, chemistry, materials science, and environmental science have made a series of remarkable achievements in developing new semiconductor materials, revealing the mechanism of photocatalysis process and improving the quantum efficiency of photocatalysis reaction. Table 1.1 systematically summarizes a series of notable advances in the development of efficient heterogeneous photocatalysts. As seen from Table 1.1, among various kinds of photocatalysts, TiO_2-based photocatalysts were undoubtedly the most studied, because TiO_2 has many advantages, such as low cost, nontoxicity, strong oxidation–reduction ability, light and chemical corrosion resistance, and excellent stability. However, it remains a great challenge to design and develop high-performance TiO_2-based photocatalytic materials. The key problems lie in how to enhance the quantum efficiency of TiO_2 photocatalysis, promote the separation of photogenerated charge carriers, and expand the visible light response range. So far, TiO_2 modification methods have been widely developed, such as dye and quantum dot (QD) sensitization [30]; cocatalyst loading [17, 21–23, 70, 73, 74]; metal and non-metal ion doping [31, 37, 39, 40]; reasonable control of defects and exposed crystal facets [57, 66, 67]; nanostructure modification (including the construction of colloidal nanocrystals, hierarchical structures, hollow microspheres, and nanosheet structures) [29, 44, 45, 52, 53, 77]; formation of

Table 1.1 Some crucial advances in the development of efficient heterogeneous photocatalysts.

No.	Photocatalysts	Highlights	Group	References (year)
1	TiO_2 photoelectrode	The discovery of Fujishima–Honda effect of TiO_2	Fujishima and Honda	[3] (1972)
2	TiO_2 powders	Photodechlorination of polychlorinated biphenyls	Carey	[4] (1976)
3	TiO_2 powders	Photocatalytic oxidation of CN^- in aqueous solutions	Bard	[5] (1977)
4	TiO_2 powders	Overall water splitting on TiO_2 consisting of mixtures of anatase and rutile	Schrauzer	[6] (1977)
5	Pt–TiO_2 particle systems	Bard's concept, "a short-circuited photoelectrochemical cell"	Bard	[9, 11, 12, 20] (1978)
6	P-type GaP photocathode	Photo-assisted electrolytic reduction of CO_2 in aqueous phase	Halmann	[13] (1978)
7	TiO_2, CdS, and SiC powders	Photocatalytic reduction of carbon dioxide in aqueous suspensions of semiconductor powders	Inoue	[15] (1979)
8	Pt/TiO_2 powders	Decompose H_2O into H_2 and O_2 under UV irradiation	Sato and White	[17, 21] (1980)
9	RuO_2/TiO_2/Pt powders	Photocatalytic reforming of carbohydrates into hydrogen	Kawai	[16] (1980)
10	Platinized or Pt-free $SrTiO_3$ single crystals	Production of H_2	Wagner	[18, 19] (1980)
11	Pt and RuO_2 co-loaded TiO_2 sol	First report on the photocatalytic water decomposition by loading dual cocatalysts (with a quantum yield of $30 \pm 10\%$)	Grätzel	[22, 23] (1981)
12	$SrTiO_3$–NiO	The utilization of NiO as H_2-evolution cocatalysts	Domen	[24] (1982)
13	CdS–TiO_2	Improved photocatalytic efficiency through inter-particle electron transfer	Grätzel	[25] (1984)
14	$Zn_xCd_{1-x}S$ solid solutions	The utilization of solid solutions for H_2 evolution	White	[26] (1985)
15	$SrTiO_3$–Ni@NiO	The utilization of Ni@NiO core/shell H_2-evolution cocatalysts	Domen	[27, 28] (1986)
16	TiO_2 particles	Size quantization effects of small-particle titania	Anpo	[29] (1987)
17	Colloidal TiO_2 films	TiO_2-based solar cells sensitized by Ru-based dyes	Grätzel	[30] (1991)
18	TiO_2 colloids	Metal ion-doped quantum-sized (2–4 nm) TiO_2 colloids	Hoffmann	[31] (1994)
19	TiO_2 polycrystalline film	Light-induced amphiphilic surface of TiO_2	Fujishima	[32] (1997)

Table 1.1 (Continued)

No.	Photocatalysts	Highlights	Group	References (year)
20	$BiVO_4$ particles	First report on the $BiVO_4$ photocatalyst	Kudo	[33, 34] (1998)
21	$In_{1-x}Ni_xTaO_4$ ($x = 0$–0.2) solid solutions	Ni-doped indium–tantalum oxide	Zou	[35] (2001)
22	(WO_3 or Fe_2O_3)/dye-sensitized TiO_2	First report on the concept of “direct Z-scheme”	Grätzel	[36] (2001)
23	TiO_2 films/powders	First report on N-doped TiO_2	Asahi	[37] (2001)
24	Pt-loaded anatase TiO_2 and rutile TiO_2	The Z-scheme water splitting using IO_3^-/I^- redox mediator	Arakawa	[38] (2001)
25	TiO_2 photoelectrodes	First report on C-doped TiO_2	Khan	[39] (2002)
26	TiO_2 powders	First report on F-doped TiO_2	Yu	[40] (2002)
27	Ta_3N_5	First report on the Ta_3N_5 photocatalyst	Domen	[41] (2002)
28	TaON	First report on the TaON photocatalyst	Domen	[42] (2002)
29	$AgInZn_7S_9$	$AgInZn_7S_9$ solid solution photocatalyst for H_2 evolution	Kudo	[43] (2002)
30	Hierarchical TiO_2	First application of hierarchical TiO_2 in photocatalysis	Yu	[44, 45] (2003)
31	$NiO/NaTaO_3$:La photocatalyst	An apparent quantum yield of 56% at 270 nm	Kudo	[46] (2003)
32	$(AgIn)_xZn_{2(1-x)}S_2$ solid solution (Pt-loaded)	An apparent quantum yield of 20% for H_2 evolution at 420 nm	Kudo	[47] (2004)
33	GaN:ZnO solid solutions	Overall water splitting on $(Ga_{1-x}Zn_x)(N_{1-x}O_x)$ solid solution photocatalyst	Domen	[48–50] (2005)
34	CdS–Au–TiO_2 nanojunctions	All-solid-state Z-scheme system	Tada	[51] (2006)
35	Mesoporous anatase hollow microspheres	Fabrication of hollow TiO_2 microspheres by chemically induced self-transformation	Yu	[52, 53] (2006)
36	BiOX powders	First report on the BiOX (X = Cl, Br, I) photocatalysts	Zhang	[54] (2008)
37	TiO_2–graphene composites	The photocatalytic reduction of graphene oxide using TiO_2	Kamat	[55] (2008)
38	Au–TiO_2	The concept of plasmonic photocatalysts	Tatsuma	[56] (2005)

(*continued*)

Table 1.1 (Continued)

No.	Photocatalysts	Highlights	Group	References (year)
39	TiO_2 nanosheets	The fabrication of anatase TiO_2 crystals predominantly exposed with (101) facets	Lu and Qiao	[57] (2008)
40	MoS_2/CdS	The utilization of MoS_2 as H_2-evolution cocatalysts	Li	[58] (2008)
41	g-C_3N_4	First report on the g-C_3N_4 photocatalyst	Wang	[59] (2009)
42	Pt–PdS/CdS	The highest quantum efficiency of H_2 generation (93%) by loading Pt and PdS as dual cocatalysts on CdS	Li	[60] (2009)
43	CdS–ZnO	Demonstrated ZnO/CdS heterostructures based on the Z-scheme mechanism	Lu and Cheng	[61] (2009)
44	$(Pt/ZrO_2/TaON)–(Pt/WO_3)$	The highest quantum yield of 6.3% for Z-scheme systems	Domen	[62] (2010)
45	CdS–NiS	The utilization of NiS as H_2-evolution cocatalysts	Xu	[63] (2010)
46	Cu and Pt co-loaded TiO_2 nanotube arrays	Photocatalytic conversion of CO_2 and water vapor into hydrocarbon fuels	Grimes	[64] (2009)
47	Ag_3PO_4	First report on the Ag_3PO_4 photocatalyst	Ye	[65] (2010)
48	Hollow TiO_2 microspheres and photocatalytic selectivity	Tunable photocatalytic selectivity by using exposed (001) facets and designed surface chemistry	Yu	[66] (2010)
49	TiO_2 nanocrystals	First report on black hydrogenated TiO_2	Chen	[67] (2011)
50	CdS cluster/graphene composite	Photocatalytic H_2 evolution over graphene-based composite semiconductor	Yu	[68] (2011)
51	$BiVO_4$–(Ru/ $SrTiO_3$:Rh)	Construction of all-solid-state Z-scheme systems by using rGO as a solid-state electron mediator	Amal	[69] (2011)
52	$Cu(OH)_2$ cluster modified TiO_2	Utilization of $Cu(OH)_2$ as H_2-evolution cocatalysts	Yu	[70] (2011)
53	$Ni(OH)_2$ cluster modified TiO_2	Enhanced photocatalytic H_2 production activity of TiO_2 by $Ni(OH)_2$ cluster modification	Yu	[71] (2011)
54	CuS/ZnS porous nanosheet photocatalysts	A visible light-induced interfacial charge transfer (IFCT) mechanism for enhanced photocatalysis	Yu	[72] (2011)
55	Ultrafine Pt-loaded TiO_2 single crystals	CO_2 photoreduction to CH_4 with a super high yield of 1361 $\mu mol\ g\text{-}cat^{-1}\ h^{-1}$	Biswas	[73] (2012)

Table 1.1 (Continued)

No.	Photocatalysts	Highlights	Group	References (year)
56	(MoS_2 + graphene)/TiO_2 composites	2D–2D hybrid of MoS_2 and graphene as dual-electron cocatalysts for H_2 evolution	Yu	[74] (2012)
57	rGO–$Zn_xCd_{1-x}S$ nanocomposites	Noble metal-free photocatalysts for enhanced solar photocatalytic H_2 Production	Yu	[75] (2012)
58	Direct Z-scheme g-C_3N_4/TiO_2	Enhanced photocatalytic performance of direct Z-scheme g-C_3N_4/TiO_2 photocatalyst for decomposition of formaldehyde in air	Yu	[76] (2013)
59	Surface heterojunction	Surface heterojunction within single TiO_2 particles	Yu	[77] (2014)
60	Ternary NiS/$Zn_xCd_{1-x}S$/rGO nanocomposites	Co-loading of noble metal-free reduced graphite oxide (rGO) and NiS (reduction and oxidation cocatalysts) on $Zn_xCd_{1-x}S$	Yu	[78] (2014)
61	Carbon nanodot–C_3N_4	Overall water splitting by the metal-free photocatalysts	Kang	[79] (2015)
62	Hierarchical CdS–WO_3 heterostructure	A direct hierarchical Z-scheme CdS–WO_3 heterostructure for photocatalytic CO_2 reduction to CH_4	Yu	[80] (2015)
63	MS_2–CdS (M = W or Mo) nanohybrids	Wurtzite CdS nanocrystals hybridized with single-layer MS_2 nanosheets for efficient photocatalytic H_2 evolution	Zhang	[81] (2015)
64	1D poly(diphenylbutadiyne) (PDPB) nanostructures	Metal-free PDPB nanofibers for photocatalytic degradation of methyl orange and phenol	Remita	[82] (2015)
65	Graphene-g-C_3N_4 nanocomposites	Sandwich-like graphene-g-C_3N_4 hybrid nanostructures for enhanced visible light photoreduction of CO_2 to CH_4	Chai	[83] (2015)
66	g-C_3N_4/ZnO binary nanocomposite	A direct Z-scheme g-C_3N_4/ZnO system for photocatalytic reduction of CO_2 to CH_3OH	Peng	[84] (2015)
67	Ultrathin g-C_3N_4 nanosheet assemblies	Hierarchical amine-functionalized ultrathin g-C_3N_4 nanosheet assemblies for photoreduction of CO_2 to CH_4 and CH_3OH	Yu	[85] (2016)
68	Hybrid film of g-C_3N_4 and Ti_3C_2 nanosheets	Ti_3C_2 (with MXene phase) nanosheets as cocatalyst for photocatalytic O_2 evolution	Qiao	[86] (2016)
69	$SrTiO_3$:La, Rh, and $BiVO_4$:Mo powders embedded into an Au layer	Z-scheme systems for pure water (pH 6.8) splitting with a solar-to-hydrogen energy conversion efficiency of 1.1% and an apparent quantum yield of over 30% at 419 nm	Domen	[87] (2016)

(*continued*)

Table 1.1 (Continued)

No.	Photocatalysts	Highlights	Group	References (year)
70	FeCoW oxyhydroxides	Report on the lowest overpotential (191 mV) for the oxygen evolution reaction	Sargent and Vojvodic	[88] (2016)
71	Hollow cobalt-based bimetallic sulfide	Hollow $Zn_{0.30}Co_{2.70}S_4$ with higher electrocatalytic HER activity than most noble metal-free electrocatalysts	Zou	[89] (2016)
72	GaAs/InGaP/TiO_2/Ni photoanode, Pd/C/Ti mesh cathode	Solar-driven reduction of 1 atm of CO_2 to formate at 10% energy conversion efficiency	Lewis	[90] (2016)
73	Hierarchical g-C_3N_4 nanostructures	Hierarchical porous O-doped g-C_3N_4 nanotubes for photocatalytic CO_2 reduction to CH_3OH	Yu	[91] (2017)
74	Au/$La_2Ti_2O_7$ sensitized with black phosphorus	An efficient broadband solar-responsive photocatalyst for H_2 production	Majima	[92] (2017)
75	Black phosphorus nanosheets	Visible light photocatalytic H_2 evolution of black phosphorus nanosheets	Yang and Du	[93] (2017)
76	Ti_3C_2/CdS nanocomposites	Ti_3C_2 MXene cocatalysts significantly boosting photocatalytic H_2 production activity over CdS	Qiao	[94] (2017)
77	Ni/CdS nanoparticles	Photocatalytic H_2 evolution by dehydrogenation of 2-propanol	Xiao	[95] (2016)
78	In-plane (Cring)–g-C_3N_4 heterostructure	2D g-C_3N_4-based in-plane heterostructures for efficient photocatalytic H_2 production	Liu and Wei	[96] (2017)
79	$W_{18}O_{49}$/g-C_3N_4 heterostructure	First report on the non-metal plasmonic $W_{18}O_{49}$	Dong	[97] (2017)
80	Defective TiO_2	Photocatalytic NH_3 production from water and N_2 at atmospheric pressure and room temperature over surface oxygen vacancies of TiO_2	Shiraishi	[98] (2017)
81	Defective one-unit-cell $ZnIn_2S_4$ atomic layers	Defect-mediated electron–hole separation in one-unit-cell $ZnIn_2S_4$ layers for boosted solar-driven CO_2 reduction	Xie	[99] (2017)
82	$CsPbBr_3$ QD/GO	A $CsPbBr_3$ perovskite quantum dot/graphene oxide composite for photocatalytic CO_2 reduction	Kuang	[100] (2017)
83	Methylammonium lead iodide ($MAPbI_3$)	Photocatalytic H_2 generation from hydriodic acid using methylammonium lead iodide	Nam	[101] (2017)

Table 1.1 (Continued)

No.	Photocatalysts	Highlights	Group	References (year)
84	Black phosphorus/ g-C_3N_4	Metal-free photocatalyst for H_2 evolution in visible to near-infrared region	Majima	[102] (2017)
85	NiS/Ni/g-C_3N_4	Constructing Ni interface layers in the g-C_3N_4 nanosheets/amorphous NiS heterojunctions for efficient photocatalytic H_2 generation	Li	[103] (2017)
86	(Au/CoO_x–$BiVO_4$)/(ZrO_2/TaON)	Photocatalytic Z-scheme overall water splitting system with an apparent quantum efficiency of 10.3% at 420 nm	Zhang and Li	[104] (2018)
87	β-ketoenamine COFs	Diacetylene-functionalized covalent organic framework (COF) for photocatalytic hydrogen generation	Thomas	[105] (2018)
88	High-symmetry Cu_2O photocatalyst particle	Demonstrating that the holes and electrons are transferred to the illuminated and shadow regions of a single Cu_2O particle, respectively	Li	[106] (2018)
89	Ni_3C/CdS	Ni_3C nanoparticles as a new cocatalyst for photocatalytic H_2 evolution	Li	[107] (2018)
90	P-doped CdS	P-doped CdS for photocatalytic water splitting without sacrificial agents	Chen	[108] (2018)
91	Graphdiyne/TiO_2 nanofibers	Graphdiyne as a new photocatalytic CO_2 reduction cocatalyst	Yu	[109] (2019)
92	WO_3/g-C_3N_4	Firstly proposing the concept of step-scheme (S-scheme) heterojunction	Yu	[110] (2019)
93	TiO_2/CdS	The direct Z-scheme charge carrier migration pathway firstly confirmed by *in situ* irradiated X-ray photoelectron spectroscopy	Yu	[111] (2019)
94	C_3N_5	First report of a C_3N_5 photocatalyst	Kumar, and Shankar	[112] (2019)
95	Atomically thin $CuIn_5S_8$ layers	Selective visible light-driven photocatalytic CO_2 reduction to CH_4 mediated by atomically thin $CuIn_5S_8$ layers	Xie	[113] (2019)
96	Single-atom Cu/TiO_2 photocatalysts	Reversible and cooperative photoactivation	Hyeon, Kim, and Nam	[114] (2019)
97	Resorcinol–formaldehyde resins	Metal-free semiconductor photocatalysts for solar-to-hydrogen peroxide energy conversion	Shiraishi	[115] (2019)
98	$Y_2Ti_2O_5S_2$	Oxysulfide photocatalyst for visible light-driven overall water splitting	Domen	[116] (2019)
99	Al-doped $SrTiO_3$	Achieving the upper limit of quantum efficiency for overall water splitting	Domen	[117] (2020)

heterojunctions (by coupling with other semiconductors and nanocarbon materials) [55, 74]; etc. The following are some examples.

In 2001, the doping of N into TiO_2 (by replacing O in the lattice) [37] was first reported in the journal *Science*. The resulting $TiO_{2-x}N_x$ material showed high photocatalytic activity under the visible light ($\lambda < 500$ nm). The publication of this work started the research of the second-generation TiO_2 photocatalysts. Subsequently, the visible photocatalytic properties of S-, F-, and C-doped TiO_2 have been reported successively [39, 40]. Although these studies have greatly improved the light absorption of photocatalytic materials in the visible light region, the introduced modifiers, N or C atoms, are easy to disintegrate from the crystal lattice under the light irradiation. Therefore, the stability of these modified visible light photocatalytic materials is poor, and the reusability in practical application is limited to a certain extent [118].

In 2008, Yang and Qiao successfully synthesized TiO_2 nanoflakes with high exposure ratio of (001) crystal facets by using hydrogen fluride (HF) as crystal surface control agent [57]. Further studies showed that TiO_2 hollow nanospheres with high exposure ratio of the (001) crystal facets and surface fluorination had better photocatalytic degradation activity and good selectivity for methyl orange [66]. More interestingly, Yu et al. proposed the concept of surface (crystal surface) heterojunction [77]. By optimizing the ratio of different exposed crystal facets of TiO_2, the best photocatalytic activity for CO_2 reduction to CH_4 was achieved [77].

In 2003, Zhang and Yu constructed the hierarchical porous TiO_2 microspheres and confirmed that the hierarchical mesoporous and macroporous structures can effectively increase the photocatalytic degradation activity of *n*-pentane in the gas phase [44, 45]. Meanwhile, Yu et al. synthesized the mesoporous hollow TiO_2 microspheres by using a chemical-induced self-transformation strategy, whose photocatalytic activity was double that of P25 [53].

In 2011, Chen et al. first developed black TiO_2 with disordered surface structure and confirmed its high hydrogen production activity [67]. This study further stimulated the researchers to control the defects and surface structure of the photocatalysts, so as to improve the photocatalytic activity. In addition, various noble metal and non-noble metal cocatalysts (such as Pt, $Cu(OH)_2$, NiO, MoS_2, and graphene) have been widely developed and applied to greatly enhance the H_2 production and CO_2 reduction activities of TiO_2-based photocatalysts [22, 23, 27, 28, 64, 73, 74]. All in all, as the core photocatalyst, TiO_2 modification research and diversified applications will continue in full swing.

In addition to TiO_2-based photocatalysts, the development of non-TiO_2-based photocatalysts and the exploration of new mechanisms have been the recent focus of photocatalytic research. Since the 1980s, a variety of new non-TiO_2-based photocatalysts have been found, such as $SrTiO_3$ [18, 19], $Zn_xCd_{1-x}S$ [26], $BiVO_4$ [33, 34], $In_{1-x}Ni_xTaO_4$ [35], Ta_3N_5 [41], TaON [42], $AgInZn_7S_9$ [43], $(AgIn)_xZn_{2(1-x)}S_2$ [47], $(Ga_{1-x}Zn_x)(N_{1-x}O_x)$ [48–50], BiOX (X = Cl, Br, I) [54], Ag@AgCl [119], g-C_3N_4 [59, 120], C_3N_5 [112], resorcinol–formaldehyde resins [115], β-ketoenamine covalent organic frameworks (COFs) [105], $Y_2Ti_2O_5S_2$ [116], Ag_3PO_4 [65], etc. There is no doubt that g-C_3N_4 has become a dazzling new star in the field of photocatalysis in recent years [120–123]. Importantly, the appearance of graphene, a new type of two-dimensional (2D) ultrathin and highly conductive material, has injected infinite power into the design and development of new efficient photocatalysts. Various kinds of graphene-based composite photocatalyst materials are springing up [68, 74, 75, 124–127]. On the other hand, new photocatalytic mechanisms have been studied constantly. Bard first proposed the Z-scheme photocatalytic mechanism of biomimetic photosynthesis in 1979 [20]. In 2001, Arakawa and coworkers successfully constructed the first Z-scheme photocatalytic overall water splitting system with I^-/IO_3^- redox pairs, Pt-loaded rutile TiO_2 (H_2 production catalyst), and anatase TiO_2 (O_2 production catalyst) [38]. Domen achieved a quantum efficiency of 6.3% for photocatalytic overall water splitting under monochromatic light irradiation ($\lambda = 420.5$ nm), by using $Pt/ZrO_2/TaON$, Pt/WO_3, and I^-/IO_3^- as the H_2 production photocatalyst, O_2 production photocatalyst, and the electron mediator, respectively [62]. More recently, Zhang and Li reported a photocatalytic Z-scheme overall water splitting system with an apparent quantum efficiency (AQE) of 10.3% at 420 nm using $[Fe(CN)_6]^{3-}/[Fe(CN)_6]^{4-}$, $Au/CoO_x–BiVO_4$, and $ZrO_2/TaON$ as redox mediator, H_2-evolving, and O_2-evolving photocatalysts, respectively, which is so far the Z-scheme reaction system with the highest quantum efficiency for photocatalytic overall water splitting [104]. At the same time, all-solid-state and direct Z-scheme systems have been successfully developed and applied to photocatalytic decomposition of water and reduction of CO_2 [51, 69, 80, 84, 111, 128–130]. Moreover, a photoinduced interfacial charge transfer (IFCT) mechanism has been proved to be useful in the design and construction of novel visible light photocatalysts [72]. In particular, recently reported black phosphorus [92, 93], MXene cocatalyst [86, 94], graphdiyne [109], defective one-unit-cell $ZnIn_2S_4$ atomic layers [99], atomically thin $CuIn_5S_8$ layers [113], planar heterojunction [96], and van der Waals heterojunction [131, 132] provide a broader space for the design of 2D semiconductor photocatalysts. In addition, some other efficient hydrogen production systems such as Pt–PdS/CdS [60], non-noble metal (MoS_2/CdS [58], graphene/$Zn_xCd_{1-x}S$ [75], NiS/$Zn_xCd_{1-x}S$/graphene [78], Ni_3C/CdS [107], CdS–NiS [63], NiS/Ni/g-C_3N_4 [103], and C_3N_4–CdS–NiS [133]) as well as metal-free carbon dots/g-C_3N_4 [79] have been successfully constructed successively. All in all, the development of a series of non-TiO_2-based heterojunction photocatalytic materials, new mechanisms, and efficient systems will continue to advance the research in the field of photocatalysis.

1.3 Fundamental Principles of Solar Energy Photocatalysis

1.3.1 Basic Mechanisms for Solar Energy Photocatalysis

So far, four basic mechanisms have been extensively employed to describe the charge carrier generation and migration processes in heterogeneous photocatalysis, namely, inorganic semiconductor photocatalysis (Figure 1.2a), organic semiconductor photocatalysis (Figure 1.2b), surface plasmon resonance (SPR, Figure 1.2c), and

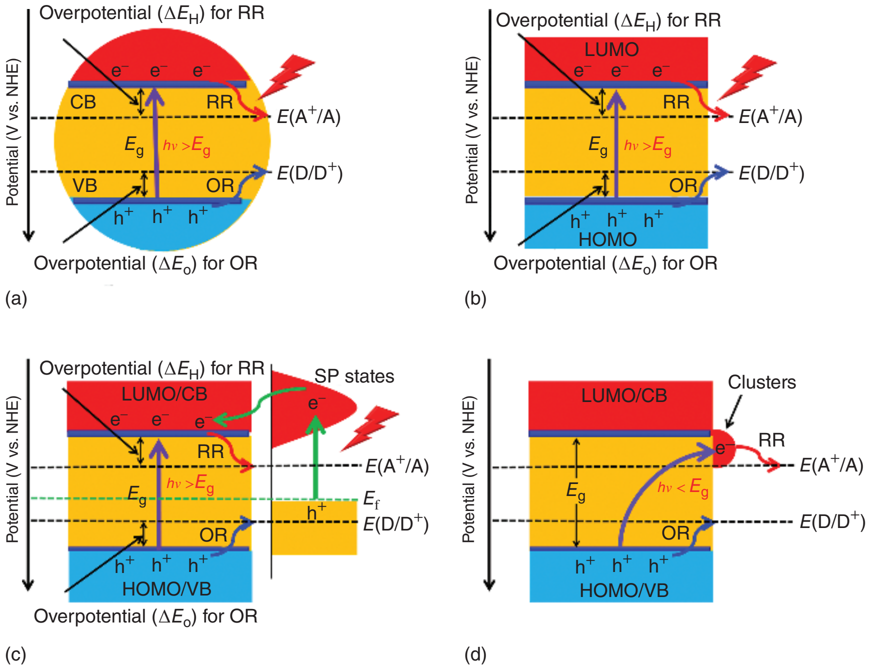

Figure 1.2 Photocatalytic mechanisms for (a) inorganic (TiO_2, CdS, WO_3, ZnO, $BiVO_4$, Si, etc.) and (b) organic (dyes, complexes, polymers, g-C_3N_4, etc.) semiconductors, (c) surface plasmon resonance (SPR) (Au, Ag, Cu, Bi, etc.), and (d) interfacial charge transfer (IFCT) (Cu(II), Fe(III), clusters, etc.). Source: Li et al. [134].

IFCT (Figure 1.2d). Among these four basic photocatalytic mechanisms, inorganic semiconductor photocatalysis and organic semiconductor photocatalysis are the most commonly used mechanisms for heterogeneous photocatalysis, and they share the similar principles. Typically, the electrons in the ground-state valence band (VB) or highest occupied molecular orbital (HOMO) could be photoexcited into the vacant conduction band (CB) or lowest unoccupied molecular orbital (LUMO) by absorption of the suitable incident photons. As a result, the separated photoinduced electrons and holes in CB/LUMO and VB/HOMO can rapidly migrate to the surface of the semiconductors and initiate the reduction and oxidation reactions, respectively. Clearly, the heterogeneous photocatalysis over the traditional inorganic semiconductors (i.e. TiO_2 [135], ZnO, WO_3 [136], CdS [107, 126, 137], and $BiVO_4$ [138]) and organic semiconductors (i.e. dyes [139], complexes [140–143], polymers [82, 144–147], graphene oxide [148], and g-C_3N_4 [120–123]) could be well explained by these two mechanisms, respectively. Notably, the photocatalytic activity for these two kinds of semiconductors could be further enhanced by different modification strategies, such as heteroatom doping, molecular doping and their co-doping, and vacancy creation [120, 149–152]. The third photocatalytic mechanism is the SPR, as shown in Figure 1.2c, which widely exists in the nanostructured noble metals (mainly Au and Ag), non-noble metal plasmonic metals (i.e. Bi and Cu) [153–161], and non-metal plasmonic materials. The plasmonic photocatalysis observed in the systems with contacted and separated semiconductors could be explained by SPR-mediated charge injection [162–173] and the near-field electromagnetic and scattering mechanisms [163, 174], respectively. On one hand, it is expected that regulation of composition, morphology, and structure of the metals can be used to further enhance the plasmonic photocatalysis. On the other hand, more and more novel plasmonic materials are expected to be exploited in the near future. Additionally, in some cases, it was found that some semiconductors can be excited by the incident photons with energy smaller than their corresponding bandgap energies, which could be well explained by the IFCT mechanism (Figure 1.2d). Creutz et al. first theoretically proposed the IFCT initiated by visible light in 2006 [175]. So far, the IFCT mechanism has been successfully used to explain the photocatalytic O_2 reduction or H_2 evolution over several clusters or chemical bonds (i.e. CuS, Cr_xO_y, Ag, Cu(II), and Fe(III)) that are modified wide band semiconductors. Clearly, these previously mentioned four mechanisms could be responsible for various kinds of heterogeneous photocatalysis reactions.

1.3.2 Thermodynamic Requirements for Solar Energy Photocatalysis

The energy band structure of a given semiconductor essentially determines the thermodynamic characteristics and largely affects the photocatalytic performance of the material. According to the theory of solid energy band, the electronic energy levels near the Fermi level of a semiconductor are separated, while they are continuous in bulk metal conductors. The band structure is generally composed of a low-energy VB (composed of electron filled orbits) and a high-energy CB (composed of an empty orbits). The energy gap between the VB and CB is the bandgap, expressed as E_g. The bandgap width of a given semiconductor determines its optical absorption performance. The relationship between the absorption wavelength threshold λ_g and the E_g of a semiconductor can be described by Eq. (1.1). It can be seen from the equation that the bandgap width of a semiconductor directly affects the light utilization for photocatalytic reactions. The wider the bandgap of a semiconductor is, the higher the energy of the photons it can absorb. These photons with higher energy correspond to shorter wavelength, and thus a semiconductor with a wider bandgap typically exhibits narrower absorption range, which is mainly concentrated in the UV region of the solar spectrum. In contrast, the narrower the bandgap is, the lower the energy of the photons a semiconductor can absorb, which corresponds to longer wavelength, indicating that the semiconductor can use more visible light in the solar spectrum. Because the visible light accounts for about 43% of the solar light, the development of narrow bandgap semiconductors and the broadening of the light response range of photocatalysts have become the focus of research.

$$\lambda_g = 1240/E_g(\text{eV}) \tag{1.1}$$

When the energy of the incident light equals or exceeds the bandgap energy of a semiconductor, the semiconductor can absorb the incident photons and excite electrons from the VB to the CB. The photogenerated electrons and holes could drive the reduction and oxidation reactions, respectively, which can lead to the redox reactions similar to those in the electrolysis process. In thermodynamics, the width of bandgap determines the absorption ability of a given semiconductor photocatalyst to photons, while the CB and VB positions of a semiconductor determine the possibility of photocatalysis. Therefore, the band structure (mainly the width of bandgap, the positions of CB and VB) and the redox potential of the adsorbed species essentially determine the light absorption capacity, the possibility of photocatalytic reaction, and the strength of the thermodynamic driving force.

From the thermodynamic viewpoint, to accomplish the photocatalytic reactions, the redox potentials for the surface reduction and oxidation half reactions should match well with the semiconductors' CB and VB levels, respectively. The standard redox potentials of several half reactions have been summarized in Table 1.2 [121, 127, 176]. Notably, the redox potential of almost all these reactions exhibit the same linear pH dependence ($V_{\mathrm{pH}} = V_{\mathrm{pH(0)}} - 0.059$ pH), except for that of pH-independent single-electron O_2 reduction ($E^0(O_2/O_2^-)$) [176, 177]. The reduction and oxidation half reactions in different photocatalytic systems are highlighted in Figure 1.3. Clearly, hydrogen evolution reaction (HER), CO_2 reduction reaction (CRR), and oxygen reduction reaction (ORR) are the three basic reduction half reactions for the different photocatalytic systems. The four-electron oxygen evolution reaction (OER), which is crucial for achieving solar fuel production (via overall water splitting and CO_2 reduction), is more challenging, due to its large overpotential and sluggish kinetics. Therefore, any factor that boosts the efficiency of these half reactions is beneficial for the enhancement of photocatalytic activity. The relative positions between band levels (at pH = 7 in aqueous solution) for some commonly used semiconductor photocatalysts relative to the redox potentials of typical half reactions and their potential applications are listed in Figure 1.4. Clearly, on one hand, the sufficiently positive VB potentials for some oxidative semiconductors (e.g. WO_3, ZnO, SnO_2, $SrTiO_3$, $BiVO_4$, Bi_2WO_6, BiOCl, and BiOBr) could drive the production of the $^{\bullet}OH$ radicals (on the left side of Figure 1.4), thus leading to their promising applications in the photodegradation of organic pollutants. On the other hand, more negative CB positions in some reductive photocatalysts (e.g. Ta_3N_5, TaON, CdS, g-C_3N_4, SiC, ZnS, BiOCl, Si, Bi_2S_3, and Cu_2O) could efficiently achieve the photocatalytic H_2 evolution and CO_2 reduction. It is noted that several semiconductors (e.g. Ta_3N_5, TaON, CdS, g-C_3N_4, SiC, ZnS, BiOCl, $SrTiO_3$, ZnO, and TiO_2) with suitable CB and VB positions for both H_2 and O_2 evolution are promising candidates for photocatalytic overall water splitting.

1.3.3 Dynamics Requirements for Solar Energy Photocatalysis

Thermodynamically speaking, the suitable band structure is necessary for semiconductor materials to drive the photocatalytic redox reactions, but it is not a sufficient condition for achieving the photocatalytic redox activity. This is because, in the process of photocatalysis, there are many dynamic factors that will affect the observed activity of a given photocatalyst. Generally, the overall photocatalytic quantum efficiency was significantly related to the kinetics of four successive kinetic processes: light harvesting, charge separation, charge carrier migration/transport, and surface

Table 1.2 Standard redox potentials for selected species.

Reaction	$E°'$ **(V) vs. NHE at pH 0**
H_2	
$2H^+ + 2e^- \rightarrow H_2(g)$	0
O_2 and N_2	
$O_2(g) + e^- \rightarrow O_2^{-\bullet}(aq)$	−0.33
$O_2(g) + H_2O + 2e^- \rightarrow HO_2^-(aq) + OH^-$	$-0.0649^{a)}$
$O_2(g) + H^+ + e^- \rightarrow HO_2^{\bullet}(aq)$	−0.046
$HO_2^-(aq) + H_2O + e^- \rightarrow {}^{\bullet}OH + 2OH^-$	$0.184^{a)}$
$O_2^{-\bullet}(aq) + H_2O + e^- \rightarrow HO_2^-(aq) + OH^-$	$0.2^{a)}$
$O_2(g) + 2H^+ + 2e^- \rightarrow H_2O_2(aq)$	0.695
$2H_2O(aq) + 4h^+ \rightarrow O_2(g) + 4H^+$	1.229
$OH^- + h^+ \rightarrow {}^{\bullet}OH$	2.69
$4OH^-(aq) + 4h^+ \rightarrow O_2(g) + 2H_2O$	0.401
$N_2(g) + 2H_2O + 6H^+ + 6e^- \rightarrow 2NH_4OH(aq)$	0.092
$O_3(g) + 2H^+ + 2e^- \rightarrow O_2(g) + H_2O$	2.075
Metal ion	
$MoO_4^{2-} + 4H_2O + 6e^- \rightarrow Mo(s) + 8OH^-$	$-0.913^{a)}$
$Co(OH)_2 + 2e^- \rightarrow Co(s) + 2OH^-$	$-0.733^{a)}$
$Ni(OH)_2 + 2e^- \rightarrow Ni(s) + 2OH^-$	$-0.72^{a)}$
$Cu_2O(s) + H_2O + 2e^- \rightarrow 2Cu(s) + 2OH^-$	$-0.365^{a)}$
$Co^{2+} + 2e^- \rightarrow Co(s)$	−0.277
$Ni^{2+} + 2e^- \rightarrow Ni(s)$	−0.257
$Mo^{3+} + 3e^- \rightarrow Mo(s)$	−0.2
$AgI + e^- \rightarrow Ag(s) + I^-$	−0.1522
$AgBr + e^- \rightarrow Ag(s) + Br^-$	0.0711
$AgCl + e^- \rightarrow Ag(s) + Cl^-$	0.2223
$Sn^{4+} + 2e^- \rightarrow Sn^{2+}$	0.15
$Cu^{2+} + e^- \rightarrow Cu^+$	0.159
$BiOCl + 2H^+ + 3e^- \rightarrow Bi(s) + H_2O + Cl^-$	0.1697
$Bi^{3+} + 3e^- \rightarrow Bi(s)$	0.308
$Cu^{2+} + 2e^- \rightarrow Cu(s)$	0.340
$Cu^+ + e^- \rightarrow Cu(s)$	0.520
$PdCl_4^{2-} + 2e^- \rightarrow Pd(s) + 4Cl^-$	0.64
$PtCl_4^{2-} + 2e^- \rightarrow Pt(s) + 4Cl^-$	0.758
$Rh^{3+} + 3e^- \rightarrow Rh(s)$	0.76
$Fe^{3+} + e^- \rightarrow Fe^{2+}$	0.771

(*continued*)

Table 1.2 (Continued)

Reaction	**$E^{\circ\prime}$ (V) vs. NHE at pH 0**
$Ag^+ + e^- \rightarrow Ag(s)$	0.7991
$IrCl_6{}^{3-} + 3e^- \rightarrow Ir(s) + 6Cl^-$	0.86
$Pd^{2+} + 2e^- \rightarrow Pd(s)$	0.915
$[AuCl_4]^- + 3e^- \rightarrow Au(s) + 4Cl^-$	0.93
$NiO_2 + 4H^+ + 2e^- \rightarrow Ni^{2+} + 2H_2O$	1.593
CO_2	
$CO_2 + e^- \rightarrow CO_2{}^-$	−1.9
$2CO_2(g) + 2H^+ + 2e^- \rightarrow HOOCCOOH(aq)$	−0.481
$CO_2(g) + 2H^+ + 2e^- \rightarrow HCOOH(aq)$	−0.199
$CO_2(g) + 2H^+ + 2e^- \rightarrow CO(g) + H_2O$	−0.11
$CO_2 + 4H^+ + 4e^- \rightarrow C + 2H_2O$	0.206
$CO_2 + 4H^+ + 4e^- \rightarrow HCHO + H_2O$	−0.07
$CO_2 + 6H^+ + 6e^- \rightarrow CH_3OH + H_2O$	0.03
$CO_2 + 8H^+ + 8e^- \rightarrow CH_4 + 2H_2O$	0.169
$2CO_2 + 8H_2O + 12e^- \rightarrow C_2H_4 + 12OH^-$	0.07
$2CO_2 + 9H_2O + 12e^- \rightarrow C_2H_5OH + 12OH^-$	0.08
$3CO_2 + 13H_2O + 18e^- \rightarrow C_3H_7OH + 18OH^-$	0.09
Other	
$N_2H_4(aq) + 4H_2O + 2e^- \rightarrow 2NH_4{}^+ + 4OH^-$	0.1
$H_2S(g) + 2h^+ \rightarrow S(s) + 2H^+$	0.144
$SO_2(aq) + 4H^+ + 4e^- \rightarrow S(s) + 2H_2O$	0.50
$H_3AsO_3(aq) + H_2O + 2h^+ \rightarrow H_3AsO_4(aq) + 2H^+$	0.56
$NO_2(g) + H_2O + h^+ \rightarrow NO_3{}^-(aq) + 2H^+$	0.80
$NO(g) + 2H_2O(l) + 3h^+ \rightarrow NO_3{}^-(aq) + 4H^+$	0.957
$H_2O_2(aq) + H^+ + e^- \rightarrow H_2O + OH^-$	1.14
$Cr_2O_7{}^{2-} + 14H^+ + 6e^- \rightarrow 2Cr^{3+} + 7H_2O$	1.36
$HO_2{}^{\bullet} + H^+ + e^- \rightarrow H_2O_2(aq)$	1.44
$H_2O_2(aq) + 2H^+ + 2e^- \rightarrow 2H_2O$	1.763

a) Superscripts denote standard redox potentials in basic solutions (pH = 14).
Source: Li et al. [176].

reaction (charge utilization) (Figure 1.5). In particular, it is well recognized that the overall photocatalytic quantum efficiency (η_c) is fundamentally determined by the product of efficiencies of the four tandem steps, including light harvesting efficiency (η_{abs}), charge separation efficiency (η_{cs}), charge migration and transport efficiency (η_{cmt}), and charge utilization efficiency (η_{cu}) for H_2 generation. The relationship between them could be calculated according to Eq. (1.2) [127, 151]:

$$\eta_c = \eta_{abs} \times \eta_{cs} \times \eta_{cmt} \times \eta_{cu} \tag{1.2}$$

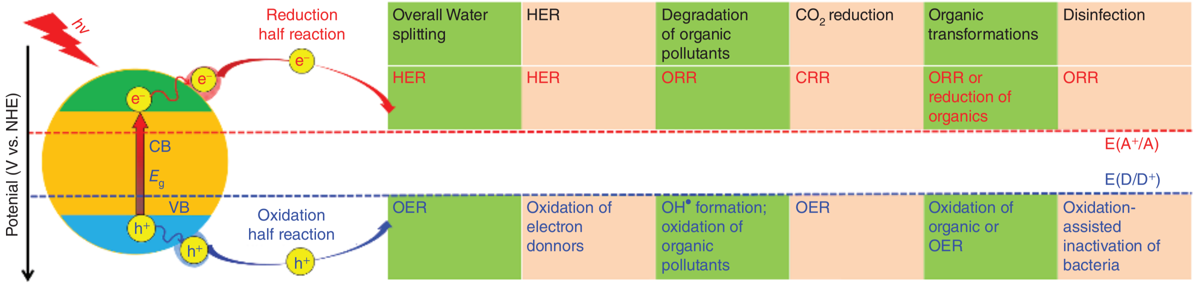

Overall Water splitting	HER	Degradation of organic pollutants	CO_2 reduction	Organic transformations	Disinfection
HER	HER	ORR	CRR	ORR or reduction of organics	ORR
OER	Oxidation of electron donnors	OH• formation; oxidation of organic pollutants	OER	Oxidation of organic or OER	Oxidation-assisted inactivation of bacteria

Figure 1.3 The reduction and oxidation half reactions in different photocatalytic reactions. OER, oxygen evolution reaction; HER, hydrogen evolution reaction; ORR, oxygen reduction reaction; and CRR, CO_2 reduction reaction. Source: Li et al. [134].

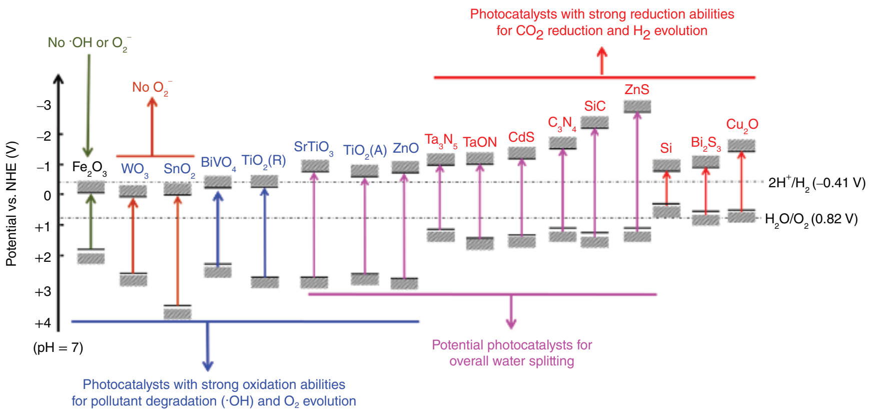

Figure 1.4 Band positions and potential applications of some typical photocatalysts (at pH 7 in aqueous solution). Source: Li et al. [176].

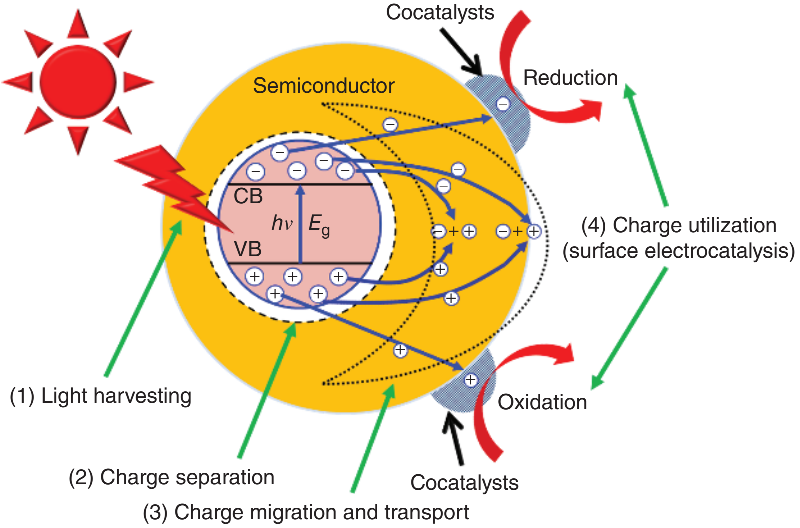

Figure 1.5 Kinetic processes of photocatalysis: (1) light harvesting, (2) the separation of photogenerated electron–hole pairs, (3) the migration and transport of photogenerated electrons and holes, and (4) the surface charge utilization for the reduction and oxidation of adsorbed reactants initiated by highly reactive electrons and holes, respectively. Source: Li et al. [176].

Therefore, to develop highly effective photocatalysts, all kinetic processes in the previously mentioned four steps must be comprehensively considered.

Among these kinetic processes, charge carrier dynamics, including trapping, recombination, and transfer, fundamentally determines their overall photocatalytic efficiency, which is significantly impacted by various factors such as the surface and interface properties, particle size, and shape of semiconductor materials [178]. Accordingly, understanding the charge carrier dynamics in semiconductors plays

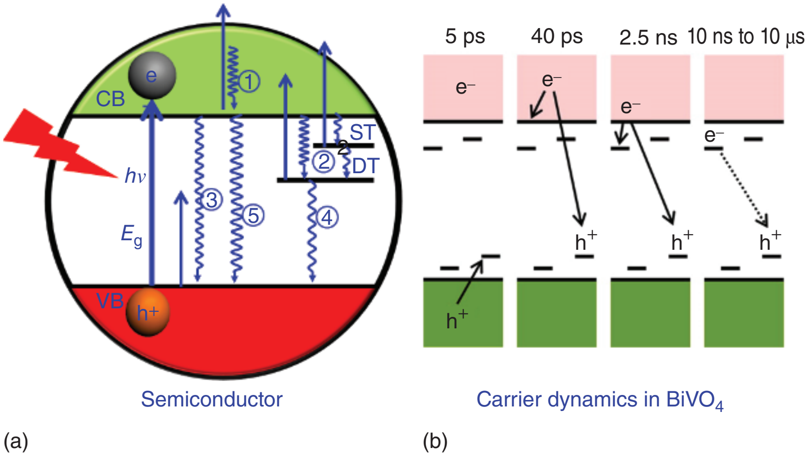

Figure 1.6 (a) Schematic illustration of charge carrier relaxation following above bandgap photoexcitation in semiconductors. The vertical straight lines with upward arrow indicate excitation processes, and the horizontal lines represent the bottom of the conduction band (CB), the shallow trap (ST) and deep trap (DT) states, and the top of the valence band (VB), respectively. The wavy lines with downward arrows indicate different relaxation processes: ① electronic relaxation within CB, ② trapping into ST and DT states and further trapping from ST to DT, ④ band edge electron–hole recombination, ⑤ trapped electron–hole recombination, and ⑥ exciton–exciton annihilation. Source: Zhang [179]. (b) Model of carrier dynamics in $BiVO_4$. Source: Ravensbergen et al. [180].

an essential role in exploring highly efficient photocatalysts for emerging photocatalytic applications. Interestingly, various time-resolved spectroscopic techniques including transient absorption and time-resolved fluorescence could be applied in investigating the surface and interfacial charge carrier trapping and recombination dynamics [179]. Figure 1.6a displays schematically the main pathways for charge carrier relaxation and the pump–probe scheme for monitoring the carrier dynamics [179]. The CB electronic and VB hole relaxation in band edge states (the excitonic state) on the time scale of 100 fs or less could result in their fast recombination on the order of nanoseconds or longer, with the strong band edge luminescence. However, the surface or internal defect states in the semiconductors could trap the charge carriers on a time scale of a few picoseconds to tens of picoseconds, thus resulting in the red-shifted trap state emission, owing to the nonradiative or radiative recombination. Generally, the nature, energy levels, or trap depth of the trap states could significantly affect the lifetimes of trap states, ranging from tens of picoseconds to nanoseconds or microsecond or even longer. For instance, the carrier dynamics in $BiVO_4$ thin films for PEC water splitting were carefully investigated by broadband transient absorption spectroscopy (TAS), as shown in Figure 1.6b [180]. The results indicated that the time scales for the hole trapping, the electron relaxation, and trapping process were approximately 5 ps, 40 ps, and 2.5 ns, respectively. Particularly, the trap-limited recombination was estimated to be on time scales longer than 10 ns. To guide the rational design of photocatalysts, the typical charge dynamics parameters of widely used semiconductors are summarized in Table 1.3.

Table 1.3 Comparison of the bandgap structures and charge carrier dynamics for typical semiconductors [134].

Catalyst (type)	**Bandgap structure (pH = 7, vs. NHE)**			**Charge carrier dynamics**		
	CB	**VB**	**E_g (eV)**	**Carrier lifetime**	**Minority carrier diffusion length**	**Charge mobility ($cm^2\ V^{-1}\ s^{-1}$ at 300 K)**
Si	−0.81	0.29	1.1	15 ns	~2–4 μm	1350
TiO_2 (anatase)	−0.52	2.7	3.20	>1 μs/80 μs/500 ps	10^4 nm	4/20
TiO_2 (rutile)			3.02	1 ms	10 nm	0.1/1
$SrTiO_3$	−0.75	2.75	3.5	50 ns	—	6–8
ZnO	−0.61	2.58	3.2	400 ps	250 nm	120–440 [181]/ 100–200/205
Cu_2O	−1.16	0.85	2.0	>117 ps	20–100 nm	—
SnO_2	0.04	3.54	3.5	~500–2000 ps	—	260
CdS	−0.9	1.5	2.4	50 ns	~1 μm	3–35/100–300
CdSe	−0.71	0.99	1.7	>500 ps/10–100 ns		600–700/~100
g-C_3N_4	−1.3	1.4	2.7	1 ns–100 ms/100–200 μs	—	—
Ta_3N_5	−0.75	1.35	2.1	<10 ps/2–12 ps	—	1.3–4.4
TaON	−0.75	1.75	2.5	10–140 ps	—	~17
GaN:ZnO				>500 ps	—	—
WO_3	−0.1	2.7	2.8	500 ns/10 μs	150 nm	1
α-Fe_2O_3	−0.03	2.17	2.2	8 ps	2–4 nm	0.2
$BiVO_4$	−0.3	2.1	2.4	40 ps–10 μs/40 ns	100 nm/70 nm	4×10^{-2} [182]
$CH_3NH_3PbI_3$				100 μs	>175 μm	$164 \pm 25(h^+)$/ $24.8 \pm 4.1(e^-)$
Graphene				0.4–1.7 ps		200 000

Source: Li et al. [134].

Obviously, all these semiconductors exhibit relatively short carrier lifetimes ranging from picoseconds to nanoseconds or microseconds, suggesting that the superfast charge recombination dynamics in semiconductors should be the main bottleneck in limiting photocatalytic efficiency. Notably, several semiconductors, such as TiO_2, CdS, WO_3, $BiVO_4$, and g-C_3N_4 with longer carrier lifetimes generally exhibit much better photoactivity than other semiconductors with shorter carrier lifetimes. In addition, it is well known that the longer minority carrier diffusion length and charge mobility ($cm^2\ V^{-1}\ s^{-1}$ at 300 K) are crucial for better photocatalysis, which could be employed as important design parameters for developing highly efficient photocatalysts. In a word, any modification strategy that could effectively prolong the charge carrier lifetimes of a given semiconductor could be used to boost its photocatalytic activity.

Notably, more attention should be paid on the effective mass of photogenerated charge carriers, which aids to understand the underlying physicochemical reasons responsible for the different photocatalytic activity of various semiconductor materials and phases. More recently, Yu's group performed the first-principles theoretical calculations to investigate the band structures, density of states, bond populations, optical properties, and charge carrier effective mass of wurtzite and zinc blende CdS and anatase, rutile, and brookite TiO_2 [183, 184]. Compared with other corresponding phases, wurtzite CdS and anatase TiO_2 exhibit the smaller effective masses of photogenerated charge carriers, thus leading to faster migration and lower recombination rates of photogenerated charge carriers from the interior to surface and much higher photocatalytic activity [183, 184]. Additionally, it should be noted that both indirect band structure and distortion-induced internal electric field could also promote the charge separation and diffusion of photogenerated charge carriers, thus beneficial for the enhanced photocatalysis. Accordingly, in future studies, more fundamental dynamics and band factors should be revealed to better understand the underlying reasons and to design better photocatalysts for practical applications.

1.4 Design, Development, and Modification of Semiconductor Photocatalysts

1.4.1 Design Principles of Semiconductor Photocatalysts

Clearly, to design better practical photocatalysts, five important features should be comprehensively considered, namely, low cost, nontoxicity, stability, visible light and near infrared (NIR) absorption, and efficiency (high activity and selectivity) (Figure 1.7). Based on these features, the well-known photocatalysts, such as TiO_2,

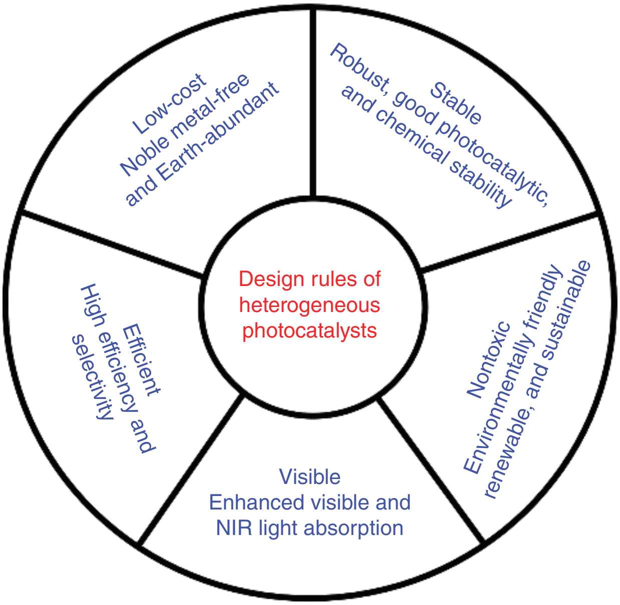

Figure 1.7 Design rules for heterogeneous photocatalysts. Source: Li et al. [185].

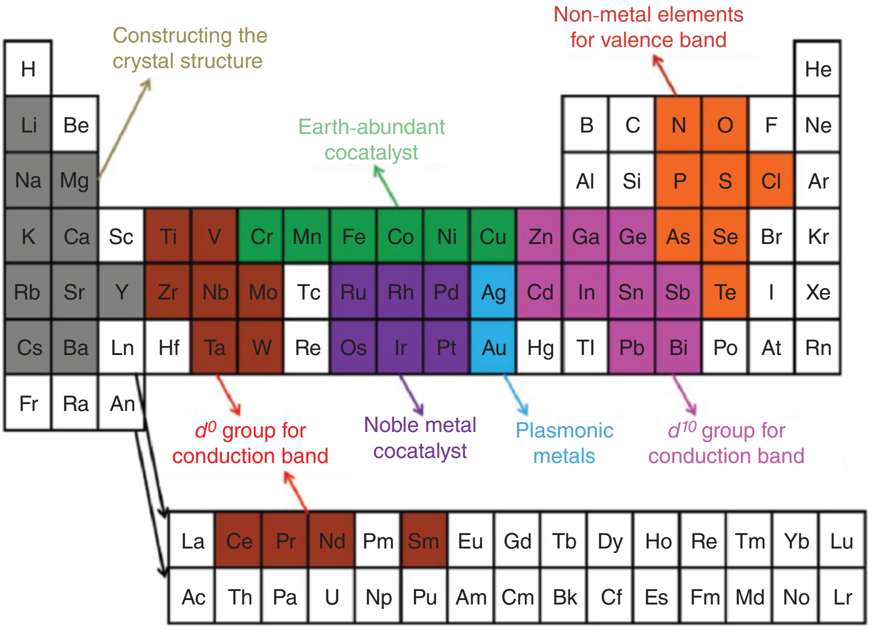

Figure 1.8 The roles of various kinds of elements in designing and developing the semiconductor-based photocatalysts for solar fuel production. Source: Li et al. [151].

g-C_3N_4, graphene, tungsten oxide (WO_3), and Bi-based semiconductors [186] should be very promising for a variety of applications.

According to these basic design principles, the basic roles of the different elements in exploring semiconductor photocatalysts are shown in Figure 1.8. As seen from Figure 1.8, the d^0 and d^{10} group elements are generally used to construct the CB of semiconductors, whereas the non-metal elements are suitable for fabricating the VB. Moreover, to greatly reduce the research and development cost, the use of Pt group cocatalysts (including Ru, Rh, Pd, Os, Ir, Pt, and plasmonic Ag and Au) should be minimized in the practical development process, despite their good electrocatalytic activity. Alternatively, the utilization of cocatalysts based on the first-row cheap transition metals (i.e. Fe, Co, Cu, and Ni) should be greatly increased. Additionally, alkaline Earth metals are usually employed to design the crystal structure of semiconductor photocatalysts due to their low toxicity, abundant reserves, and low price, which deserve more attention. In a word, cheap and nontoxic metal elements (such as W, Bi, Zn, Ta, Sn, Fe, Cu, and Mo) and non-metal elements should be given more attention in exploring semiconductor photocatalytic materials.

Among the five important features, the stability of photocatalysts is crucial for the long-term practical applications. Generally, on the basis of the relative positions of thermodynamic potentials and the band levels of semiconductors, there are three typical kinds of photocorrosion processes, namely, the reductive photocorrosion (as shown in Figure 1.9a), the oxidative photocorrosion (Figure 1.9b), and dual photocorrosion (Figure 1.9c) [187]. Some semiconductors with the proper CB and VB potentials are indeed stable without any photocorrosion (Figure 1.9d).

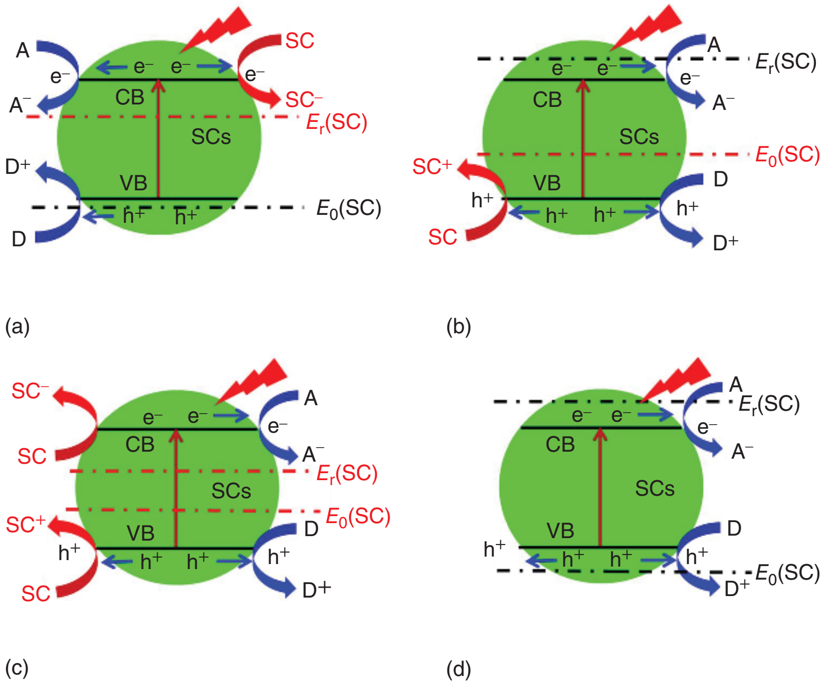

Figure 1.9 Schematic illustration of four kinds of photocorrosion: (a) reductive photocorrosion, (b) oxidative photocorrosion, (c) dual photocorrosion, and (d) stable. E_r(SC) and E_o(SC) are the thermodynamic reduction/oxidation potentials of semiconductors, respectively. Source: Li et al. [134].

The photocorrosion types for some commonly used semiconductors are shown in Figure 1.10. Various Ag-based semiconductors (e.g. Ag_3PO_4 [188], AgBr [189], Ag_2CO_3 [190], and AgI [191]) and typical non-oxide semiconductors (e.g. CdS [126, 192], GaAs, GaP, Ta_3N_5, and CdSe) easily suffer from the reductive and oxidative photocorrosion, respectively. Additionally, several semiconductors (i.e. Cu_2O [193] and SiC) exhibit extremely poor photostability due to the occurrence of dual photocorrosion.

Thus, apart from developing novel stable semiconductors, such as p-$CuRhO_2$ [194] and p-$AgRhO_2$ [195], five typical modification strategies (Figure 1.11) have been developed for effectively suppressing the unexpected photocorrosion of unstable semiconductors, namely, adding the suitable sacrificial electron donors (e.g. $S^{2-}/SO_3{}^{2-}$, lactic acid, triethanolamine, and CH_3OH) and electron acceptors (e.g. Ag^+) into solution; decorating with cocatalysts (e.g. cobalt phosphate (Co-Pi) or CoO_x [196, 197], noble metal, and Earth-abundant metal nanoparticles/clusters [198–200]); coupling with nanocarbon materials (such as graphene, carbon nanotubes, and ultrathin amorphous carbon layers [201–206]); creating heterojunctions; and constructing protective overlayers. Notably, creating heterojunctions and constructing protective overlayers have been proven to be the most promising two strategies to reduce the photocorrosion. In particular, the overall photocatalytic

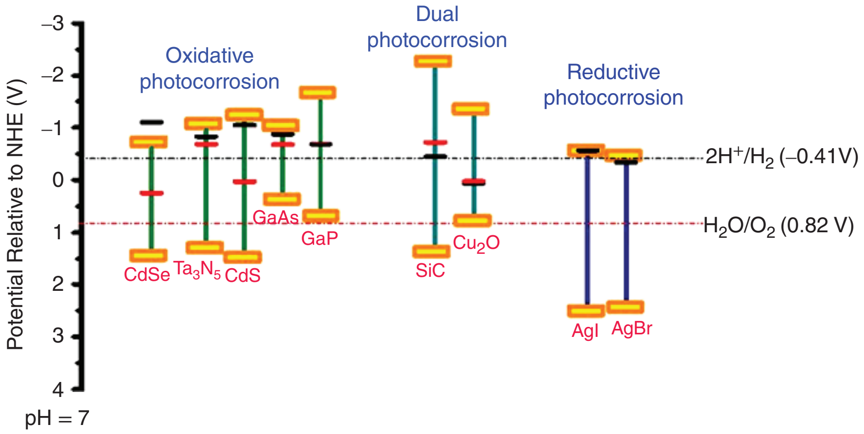

Figure 1.10 Band structures, thermodynamic reduction (black bar), and oxidation (red bar) potentials of typical semiconductors with oxidative, reductive, and dual photocorrosion. Source: Li et al. [134].

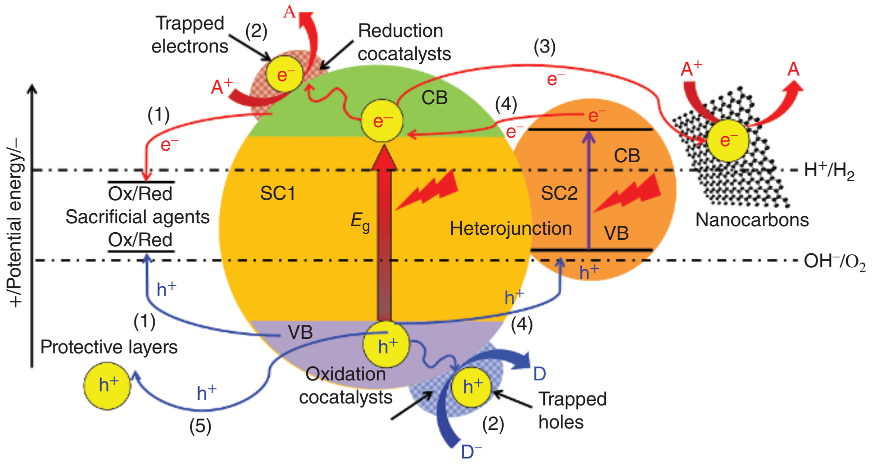

Figure 1.11 Strategies for inhibiting photocorrosion of unstable semiconductors: (1) adding sacrificial agents into solution, (2) depositing cocatalysts, (3) coupling with nanocarbon materials, (4) fabricating heterojunctions, and (5) constructing protective overlayers. Source: Li et al. [134].

activity of unstable Cu_2O and CdS semiconductors could be fundamentally boosted through constructing type-II heterojunctions (i.e. Cu_2O/TiO_2 [207–211] and CdS/TiO_2 [212–217]) and all-solid-state Z-scheme systems [218–220] due to the improved photostability. Additionally, various protective overlayers (i.e. TiO_2 [221–225], $SrTiO_3$ [226], g-C_3N_4 [227–229], Al_2O_3 [230], Ga_2O_3 [231], and SiO_2 [232–237]) have been constructed on the surface of semiconductors to effectively enhance the overall photocatalytic efficiency, through the favorable "passivation" and/or "catalysis" effects [238]. In future, it is anticipated that fabricating multiple heterojunctions can be used to rationally improve the photostability through making full use of possible synergism between them [239–245].

1.4.2 Classifications of Semiconductor Photocatalysts

So far, hundreds of semiconductors have been exploited and applied in different fields of photocatalysis [246]. According to their compositions, these photocatalysts could be classified into five types: metal oxide/hydroxide, non-oxide, novel, organic, and metal-free photocatalysts, which are summarized in Figure 1.12. Multicomponent metal oxide and sulfide solid solution photocatalysts are two kinds of most promising candidates for different photocatalysts. Unfortunately, no one photocatalyst could satisfy all requirements for practical photocatalytic applications [192]. Thus, heterojunction photocatalysts and various kinds of modification strategies have been developed to boost their photocatalytic efficiency. Herein, all these different potential photocatalysts will be thoroughly discussed in this book.

1.4.3 Modification Strategies of Semiconductor Photocatalysts

The main thermodynamic and dynamics processes in unit cells, bulk, and surface phases can be classified into three steps as shown in Figure 1.13, including (i) photoexcitation of electron–hole pairs in the unit cells of semiconductors, (ii) the charge separation/migration in bulk and the bulk (iii) and surface (iv) charge recombination, and surface charge-induced reduction (v) and oxidation (vi) reactions. Clearly, the overall photocatalytic performance is closely dependent on the thermodynamic and kinetic balance of all involved processes in the three steps, which is strongly determined by the surface/bulk properties and the electronic structures of a given photocatalyst.

Relatively speaking, the processes in the bulk and surface phases are more crucial for improving the overall photocatalytic efficiency than photoexcitation in the

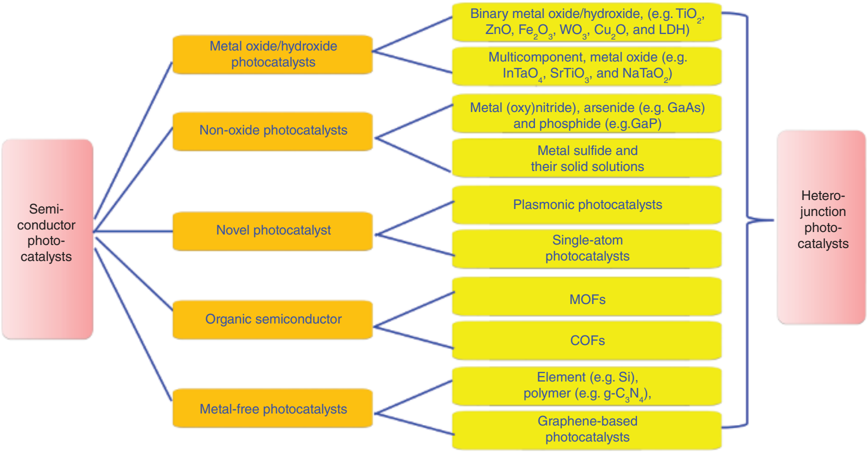

Figure 1.12 Classification of semiconductor photocatalysts.

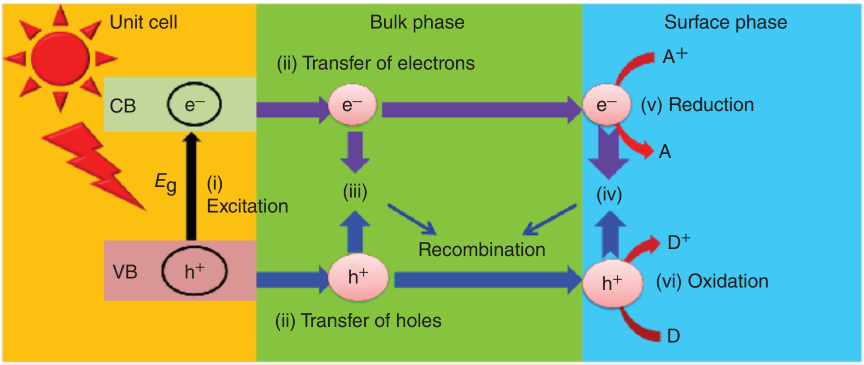

Different stages and corresponding enhancement stageies:		
(i) Excitation	(ii) Charge transfer and (iii) bulk recombination	(iv) Surface recombination, (v) reduction reaction, and (vi) oxidation reaction
Reduction of the band gap (energy band engineering), surface sensitization (plasmonic metals or (in)organic semiconductors), enlargement of the CB levels, and fabrication of the hierarchical or defect structures	Reduction of the diffusion distance (design of 0D nanocrystals, 1D nanorods/tubes, 2D nanosheets, 3D porous /hollow/hierarchical structures), enhancement of the electrical conductivity (doping or solid solution), enhancement of the crystallization degree, and construction of built-in or dipole-polarizability electrical fields	Load of the cocatalysts, exposition of the high-energy facets, enhancement of the surface area and reactive sites, construction of the direct z-scheme and type-II heterojunctions, use of the sacrificial agents, fabrication of the surface defects or coordinated unsaturated sites, and enhancement of the adsorption of reactants

Figure 1.13 Different photocatalytic processes and the corresponding enhancement strategies. Source: Li et al. [134].

unit cell, due to the occurrence of more and more visible light semiconductors. So far, various kinds of surface and interface modification strategies have been available for improving both charge carrier dynamics and sluggish surface reaction kinetics, thus achieving the highly active, selective, and stable solar-to-chemical energy conversion [247–250]. Particularly, the possible synergistic effects in the multifunctional integration and optimization of different modification strategies have been demonstrated to be of great significance for boosting the photocatalysis. For example, loading suitable amounts of plasmonic metals on semiconductors as cocatalysts can significantly boost the overall efficiency for different photocatalysts, owing to the simultaneous enhancement of all processes in the three stages through the plasmonic Schottky junction, including visible light harvesting, charge separation, and accelerated surface reaction kinetics [251], thus leading to the wide photocatalytic applications of the plasmonic metals cocatalysts [252–258]. Moreover, fabricating various kinds of hierarchical semiconductor structures at the micro/nanometer scale could simultaneously feature the light harvesting, charge separation, and adsorption of reactants, consequently resulting in boosted overall photocatalytic efficiency [85, 176, 259–265]. Additionally, loading suitable electrocatalysts as cocatalysts can significantly improve the surface electrocatalytic reduction and oxidation reactions (surface charge utilization), owing to the decreased onset overpotential, improved surface reaction kinetics, enhanced charge separation and photostability of semiconductors [196, 266, 267]. Of note, from the viewpoint of sustainable development, the stable and nontoxic Earth-abundant noble metal-free cocatalysts could greatly reduce the costs of practical photocatalytic applications, which are essentially important and promising for large-scale and long-time photocatalysis [70–72, 267–284]. Finally, constructing various semiconductor-based heterojunctions have been proven to be one of the most promising strategies to boost light absorption, charge separation, photostability, adsorption, and reaction kinetics [85, 124, 126, 127, 285, 286], for developing robust and efficient photocatalysts. In this section, we will thoroughly discuss the two most important strategies, constructing semiconductor-based heterojunctions and loading cocatalysts, which have been extensively applied in the different photocatalytic systems.

The formation of semiconductor-based heterojunctions has been proven to be an appealing strategy to improve the solar energy photocatalysis. So far, fabricating various kinds of heterojunctions [287–292], such as type-II/p–n heterojunctions [293–303], surface heterojunction (facet junctions) [77, 304–308], Schottky junctions (with metal and nanocarbons), direct Z-scheme systems [128, 130, 309–329], and S-scheme (or step-scheme) heterojunction [110, 330], have been successfully explored in the different heterogeneous photocatalysis systems. The charge separation mechanisms of these six types of heterojunctions are displayed in Figure 1.14.

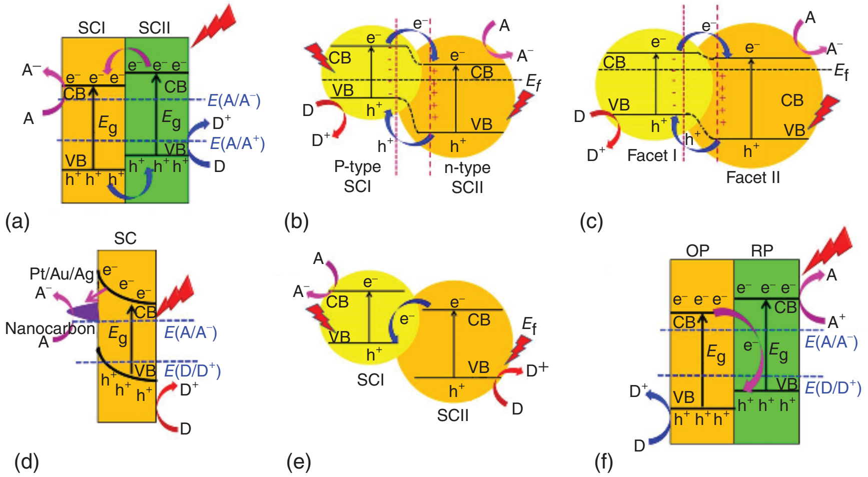

Figure 1.14 Typical photocatalytic heterojunction systems: (a) type-II heterojunctions, (b) p–n heterojunctions, (c) surface heterojunction, (d) Schottky junctions, (e) direct Z-scheme systems, and (f) step-scheme heterojunction. Symbols in the figure: A, acceptor; D, donor; SCI, semiconductor I; SCII, semiconductor II; OP, oxidation photocatalyst; RP, reduction photocatalyst; E_f, Fermi level; E_g, bandgap; CB, conduction band; and VB, valance band.

Among them, the type-II heterojunction has been dominantly studied during the past decades since Serpone et al. firstly fabricated interfaces between CdS and TiO_2 to improve the charge separation and transfer in 1984 [25]. Clearly, in type-II heterojunction, electrons and holes accumulate on SCI and SCII for reduction and oxidation reactions, respectively [287–289]. Thus, the photogenerated electrons and holes are spatially separated. However, the claimed charge transfer mode in type-II heterojunction is disputable, due to the huge electrostatic repulsive forces [128, 129, 331, 332]. Moreover, from a thermodynamic perspective, the weakened overall redox ability of the heterojunction is not beneficial for improving the photocatalytic reaction. Thus, the grievous fundamental problems greatly prevent the development of type-II heterojunction in the recent years. Similarly, although the p–n heterojunctions could achieve the favorable charge separation, they suffer from weakened redox ability during the photocatalysis.

More interestingly, surface heterojunction as an important kind of heterojunction has been recently developed and applied in photocatalysis. For instance, the co-exposed (001) and (101) facets in anatase TiO_2 formed in the presence of different amounts of HF have recently been reported. The results showed that when the ratio of (001) to (101) facets is 6 : 4, the maximum activity of photocatalytic CO_2 reduction to CH_4 can be achieved. The first-principles calculation further confirmed that the density states of anatase TiO_2 (001) and (101) crystal faces were significantly different, which resulted in the formation of typical surface heterojunction between TiO_2 (001) and (101) crystal faces [77]. Therefore, the formation of surface heterojunction can effectively promote the separation of charge carriers, so that the photocatalytic activity of CO_2 reduction can be significantly improved. Additionally, among these six types of heterojunctions, constructing the nanocarbon-based Schottky heterojunctions seems to be particularly attractive. So far, various kinds of nanocarbon materials, including carbon spheres, graphene, carbon nanotubes, carbon QDs, have been frequently exploited and applied in the field of photocatalysis. More importantly, nanocarbon materials could exhibit better adsorption activity toward reactive substances and promote the visible light absorption of semiconductors. For example, Yu and coworkers have successfully constructed CdS nanoclusters/graphene/Pt [68] and TiO_2 nanocrystals/graphene/MoS_2 [74] heterojunction composite photocatalysts, whose optimized photocatalytic activities were 4.87 and 39 times higher than the corresponding single semiconductor materials, respectively. The formation of Schottky heterojunction between nanocarbon materials and semiconductors could significantly promote the separation of photogenerated electron–hole pairs in the semiconductors, thus boosting the photocatalytic hydrogen production activity.

Furthermore, to remove the unfavorable influence of the undesirable conductors in all-solid-state Z-scheme photocatalysts [128, 331], Wang et al. developed ZnO/CdS Z-scheme heterojunction for improved H_2 evolution performance in 2009 [61]. Then, Yu et al. fabricated a direct Z-scheme g-C_3N_4/TiO_2 photocatalyst for improving photocatalytic formaldehyde decomposition in 2013 [76]. However, there is a lot of confusion over “direct Z-scheme”; not only it exhibits a lot of confusion with traditional Z-scheme and all-solid-state Z-scheme but also it suffers the consequences of the failure of traditional Z-scheme and all-solid-state

Z-scheme [128, 129, 331, 332]. Thus, S-scheme (or step-scheme) heterojunction, as a brand new concept describing the photocatalytic mechanism clearly and vividly, has been firstly proposed by Yu's group in 2019 [110]. An S-scheme heterojunction exhibits a completely different charge transfer route from type-II heterojunction. Distinctly, in S-scheme heterojunction, the powerful photogenerated electrons and holes accumulated in the CB of reduction photocatalyst (RP) and VB of oxidation photocatalyst (OP), respectively, could achieve the strong redox ability. Notably, the charge transfer route in S-scheme mode resembles "step" in macroscopic (from low CB to high CB) and letter of N in microscopic. In future, to develop better S-scheme photocatalysts, both thermodynamics and dynamics should be considered. Various kinds of design strategies, such as suitable cocatalyst loading, morphology control, and interface optimization, can be employed to lower photocatalytic reaction activation barrier and improve charge carrier separation and transfer.

In the future, some basic problems of heterojunction interface in photocatalysis are worthy of further deep study, such as the atomic structure and properties of solid–solid interface, the transport of photogenerated charge carriers across the interface, the formation and effect of interface defects, the decomposition mechanisms of organic molecules on the interface, and the formation process of solid–liquid interface. In this sense, the construction of heterojunction composite materials and the study of carrier separation mechanism with complex interface are still very important research topics in the field of photocatalysis, which could guide the design and development of novel composite semiconductors.

Since the pioneering works by Bard and his group reporting the concept of Pt islands (cocatalysts) on TiO_2 powder for photocatalytic applications [9, 11, 20], various effective electrocatalysts as active cocatalysts have been obtained to boost the surface electrocatalytic reactions of excited semiconductors. Interestingly, six basic configurations of the semiconductor/cocatalyst composite photocatalysts have been designed and developed over the past decades (Figure 1.15); namely, (a) semiconductor-supported single reduction or oxidation cocatalyst systems, (b) semiconductor–dual (reduction and oxidation) cocatalyst systems, (c) plasmonic metal–semiconductor–cocatalyst systems, (d) dye/QDs–semiconductor (irradiated or unirradiated)–cocatalyst systems, (e) dye/QDs–cocatalyst systems, and (f) semiconductor–carbon/metallic bridge-cocatalysts or semiconductor–cocatalysts with coated layers. Notably, the semiconductors in these six configurations could be replaced by the p–n and Z-scheme heterojunctions or homojunctions.

1.4.4 Development Approaches of Novel Semiconductor Photocatalysts

Because the electronic structure of a given semiconductor strongly determines the redox capacity during the photocatalysis, many researchers focus on studying the electronic structure of semiconductor photocatalytic materials. Generally, the element doping, defect engineering, and nanostructure design can effectively optimize the electronic structure of various kinds of semiconductor materials, so as to increase their visible or near-infrared photocatalytic activity. In addition to these traditional

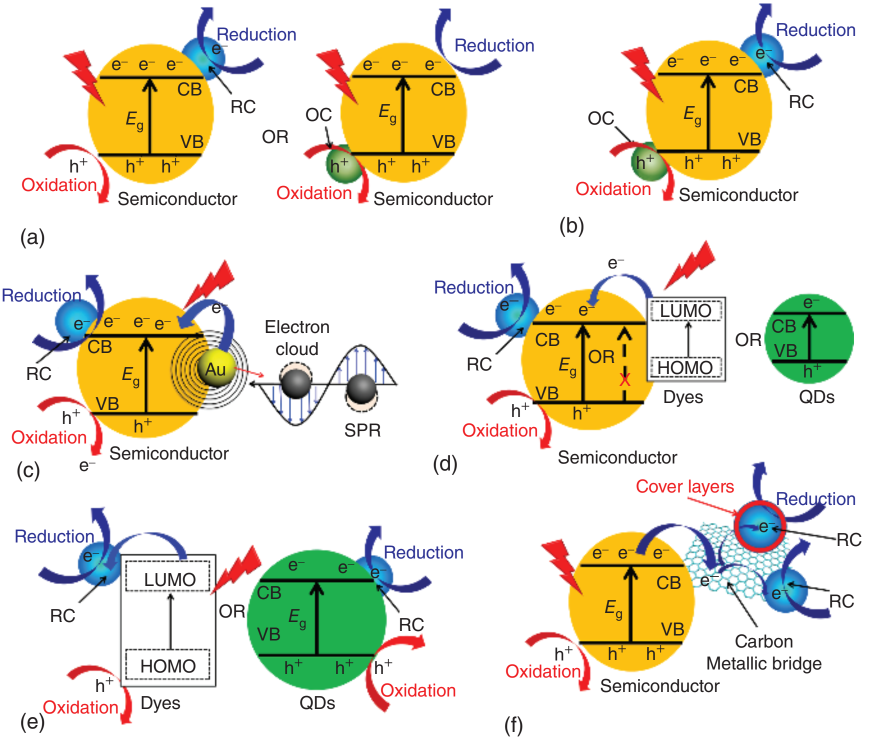

Figure 1.15 Schematic illustration for six configurations of the semiconductor/cocatalyst composites: (a) semiconductor-supported single reduction or oxidation cocatalyst systems, (b) semiconductor–dual (reduction and oxidation) cocatalyst systems, (c) plasmonic metal–semiconductor–cocatalyst systems, (d) dye/quantum dots–semiconductor (irradiated or unirradiated)–cocatalyst systems, (e) dye/quantum dots–cocatalyst systems, and (f) semiconductor–carbon/metallic bridge-cocatalysts or semiconductor–cocatalysts with coated layers. The abbreviations CB, VB, RC, OC, E_g, and QDs represent the conduction band, valance band, reduction cocatalyst, oxidation cocatalyst, bandgap, and quantum dots, respectively. Source: Li et al. [134].

modification strategies, the development strategies of new photocatalytic materials are as follows: solid solution engineering and first-principles calculation. This section will focus on the specific applications of these two strategies in the development of solar fuel photocatalytic materials.

The simplest and direct way to develop new photocatalytic materials is solid solution engineering, which has been successfully applied in photocatalytic H_2 production, degradation of pollutants, and CO_2 reduction. In order to reduce the workload of seeking new solid solutions, the high-throughput screening method provides a rapid experimental method for the development of semiconductor photocatalytic materials. The commonly used high-throughput screening approaches mainly include scanning electrochemical microscopy (SECM) [333, 334] and scanning printer [335]. For example, Bard's group confirmed that 5 mol% W-doped [334] or 2% W/6% Mo co-doped [336] $BiVO_4$, respectively, exhibited 3 and 10 times higher activity in PEC water oxidation by using SECM. The main reason for the improvement of photocatalytic activity is that W/Mo doping results in the distortion of $BiVO_4$ lattice structure, which promotes the separation of photogenerated electrons and holes. Additionally, they also found that the photocurrent of 12 mol% Zn-doped Bi_2WO_6 was the highest, which was 1.8 times as high as that of the pure Bi_2WO_6 sample. More importantly, these high-throughput screening methods can also be directly used to find efficient photocatalytic water splitting electrocatalysts [337–340].

Furthermore, the first-principles simulation method is also widely used in the design and development of new semiconductor and cocatalyst materials. The first-principles calculation is a quantum mechanical method based on density functional theory (DFT) and local density approximation. It can simulate the electronic structure, bonding properties, charge distribution, and optical properties of materials without experimental data. Many researchers use the first-principles method to simulate and calculate the electronic structure, band information, and the influencing factors of photocatalytic reaction. This method has been successfully applied to study the physical mechanism underlying the influence of element doping and substitution on the performance of photocatalytic materials and to design a batch of new photocatalytic materials. However, in most cases, the first-principles calculation mainly serves as supplementary theoretical analysis to the experiments, so as to better understand the structure–activity relationship of a given photocatalyst. For example, the first-principles calculation confirms that the energy band structure of TiO_2 (001) and (101) faces is significantly different [77]. In another work, the first-principles calculation predicted that N- and C-doped ZnO had better photocatalytic activity than S-doped ZnO, mainly because N- and C-doping can introduce vacancy state above the Fermi level of ZnO and lower its CB, resulting in an obvious reduction of its bandgap width and the increase of carrier concentration [341]. Recently, DFT calculations have shown that halogen atom doping can reduce the bandgap of single-layer g-C_3N_4, increase the visible light absorption, and reduce the work function, resulting in high photocatalytic activity [342]. More importantly, the high electronegativity of F atom makes it tend to occupy the VB and the HOMO of g-C_3N_4. In contrast, Cl, Br, and I atoms tend to occupy the CB and the LUMO of g-C_3N_4. Additionally, the first-principles calculation shows that layered MPS_3 (M = Fe, Mn, Ni, Cd, Zn) and $MPSe_3$ (M = Fe, Mn) are also potential 2D photocatalytic materials [343]. The energy gap of these single-layer structures is between 1.90 and 3.44 eV, and they have good absorption properties over a wide spectrum (including visible light and near-infrared range). The results show that the single-layer $MnPSe_3$ is a direct bandgap semiconductor with strong visible light absorption activity. It can completely decompose water in acidic or neutral environment and produce H_2 and O_2 at the same time. It can be predicted that charge carriers in $MnPSe_3$ has a high mobility, and the mobility of electrons and holes is very different. This indicates that the recombination of photogenerated electrons and holes of this new $MnPSe_3$ monolayer material can be effectively suppressed, and its photocatalytic quantum efficiency can be greatly improved, which is expected to become a new generation of photocatalyst that can efficiently utilize solar energy to catalyze the total decomposition of water.

At present, $MnPSe_3$ nanosheet can be prepared. It is hoped that in the near future, the single-layer structure can be successfully prepared, and further verify the theoretical prediction results. Similarly, based on the high-throughput calculation of DFT, $FeVO_4$ (2.51 eV), β-$Cu_2V_2O_7$ (2.42 eV), and β-Ag_3VO_4 (2.51 eV), and other new visible light water oxidation solid solution catalysts have been successively found [344, 345]. In contrast, there are few reports on the application of first-principles calculation in the screening of photocatalytic materials or the analysis of carrier dynamics before experiments. Therefore, in the future, more research should use the first-principles calculation to design the visible light-responsive photocatalyst with better photocatalytic activity.

In addition, it is worth noting that the first-principles calculation is also widely used in the development of electrocatalysts for photocatalytic H_2 evolution. In general, DFT calculation can be used to analyze and compare the geometry and electronic configuration of different electrocatalysts for H_2 evolution, the adsorption of H_2O, H and OH, and the free energy of H adsorption ($\Delta G(H^*)$), to explore the underlying mechanisms for the improvement of catalytic activity. Generally speaking, the strong adsorption of H_2O and the weak adsorption of H and OH are more favorable for the dissociation of H_2O and the desorption of H_2. In particular, $\Delta G(H^*)$ is an important index to measure the hydrogen evolution activity of a catalyst. The closer its value is to 0, the higher its catalytic activity is.

1.5 Processes and Evaluation of Solar Energy Photocatalysis

1.5.1 Processes of Solar Energy Photocatalysis

1.5.1.1 Photocatalytic Water Splitting

Hydrogen is a green energy with high heat of combustion, high efficiency, and zero discharge of pollution. At present, the production of H_2 is mainly from non-renewable primary energy, which will aggravate the shortage of the non-renewable energy sources and bring new environmental pollution problems. Although it is a very challenging work to efficiently convert solar energy into hydrogen energy by photocatalysis, it is one of the ideal ways to solve the problem of energy source shortage and environmental pollution fundamentally. Therefore, it has attracted increasing attention in the different communities. From the viewpoint of thermodynamics, producing H_2 and O_2 from water decomposition is an uphill reaction with large free energy change [151], that is to say, water decomposition is a chemical reaction that cannot occur spontaneously in thermodynamics. In the standard state, to decompose 1 mol of water into H_2 and O_2, at least 237 kJ of energy is required in theory (for example, see Eq. (1.3)). From the electrochemical point of view, the theoretical decomposition voltage of water is 1.23 eV. That is to say, when the voltage increases up to more than 1.23 eV, the electron has the ability to reduce H^+ to H_2, while the hole could oxidize the water and emit O_2. Therefore, in order to promote the decomposition of water, we must input enough energy to overcome the necessary change of Gibbs free energy. Compared with the downhill photocatalytic degradation of organic pollutants, the photocatalytic decomposition of water is usually very difficult. In general, visible light photocatalytic overall water splitting for H_2 production is even considered as the "Holy Grail" of chemistry [346]. However, photocatalytic water decomposition technology can use solar energy to drive water decomposition reaction to produce H_2. Water and sunlight are inexhaustible, and H_2 obtained from water can be transformed back to the form of water ($H_2 + 1/2O_2 \rightarrow H_2O$) after being used as energy. It is a completely sustainable development and utilization. Therefore, with the development of a series of new electrocatalysts for hydrogen release (used in electrolytic or PEC decomposition of water), and the discovery of many new visible light photocatalysts besides TiO_2, the technology of hydrogen production from water decomposition by solar photocatalysis has received more and more attention.

$$H_2O(l) \rightarrow H_2(g) + \frac{1}{2}O_2(g) \quad \Delta G^0 = 237.2\ \text{kJ/mol}, \Delta H^0 = 237\ \text{kJ/mol}, \quad \Delta E^0 = 1.23\ \text{V} \tag{1.3}$$

$$2H^+ + 2e^- \rightarrow H_2(g) \qquad \Delta E^0 = -0.41\ \text{V},\ \ \text{pH} = 7 \tag{1.4}$$

$$2H_2O(l) \rightarrow O_2(g) + 4H^+ + 4e^- \quad \Delta E^0 = +0.82\ \text{V}, \text{pH} = 7 \tag{1.5}$$

According to the types of photocatalyst and reactions, the photocatalytic hydrogen production systems can be divided into two categories: half-reaction hydrogen production systems and overall water splitting systems (Figure 1.16). Notably, the overall water splitting systems can be further divided into three sub-types: single photocatalyst, Z-scheme (liquid and all-solid-state), and heterojunction. Figure 1.17 shows the specific principles of photocatalytic H_2 production in these two kinds

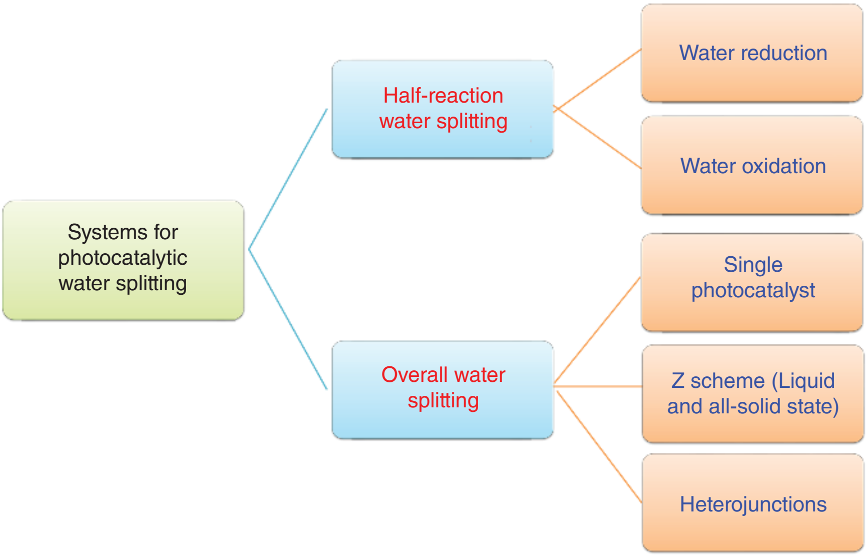

Figure 1.16 Systems for photocatalytic water splitting.

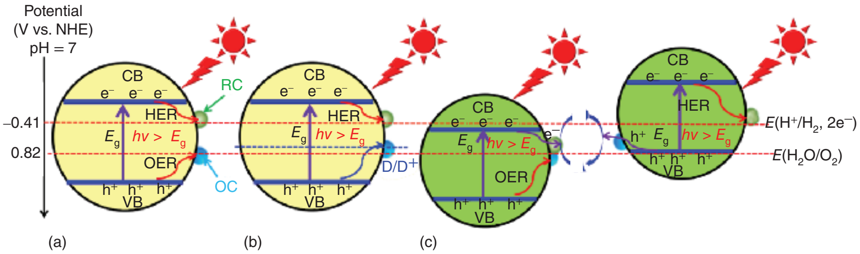

Figure 1.17 Three kinds of typical photocatalytic systems for water splitting: (a) overall water splitting by a single photocatalyst, (b) hydrogen generation from a half reaction of water splitting, and (c) Z-scheme overall water splitting by two different photocatalysts. HER: hydrogen evolution reaction; OER, oxygen evolution reaction; D, electron donors; A, electron acceptor; RC, reduction cocatalyst; and OC, oxidation cocatalyst. Source: Li et al. [127].

of reactions. Among them, the single catalyst system of overall splitting of water under visible light is the most difficult (as shown in Figure 1.17a). Most of the metal oxide photocatalysts and almost all of the metal sulfide photocatalysts can only complete the H_2 or O_2 production half reactions in the presence of sacrificial agents (Figure 1.17b). Although a large number of UV-responsive photocatalysts have been developed for water splitting, few progresses have been made in theoretical research [46]. In fact, using a single photocatalyst to achieve overall water splitting under visible light has strict requirements on the CB, VB, and bandgap width of a given semiconductor photocatalyst. Theoretically, such photocatalysts must meet the following thermodynamic requirements: the energy of photons must be greater than or equal to the theoretical minimum energy required for water splitting, i.e. 1.23 eV, which is approximately equal to the energy of photons of 1100 nm wavelength; the CB and VB positions must match the reduction and oxidation potentials of water, that is, the position of the CB bottom (E_{CB}) must be more negative than the redox potential of H^+/H_2 (−0.41 V vs. normal hydrogen electrode [NHE] at pH = 7), and the position of the VB top (E_{VB}) must be more positive than the redox potential of O_2/H_2O (0.82 V vs. NHE at pH = 7). Therefore, considering the existence of overpotential, the bandgap width of semiconductor should be at least greater than 1.8 eV [130]. The band structure of most metal oxide semiconductors does not meet the conditions of H_2 and O_2 production at the same time; on the other hand, the few photocatalysts that meet the preceding conditions are not responsive to the visible light due to their wide bandgap (for example, the E_g of TiO_2 and ZnO are 3.2 and 3.3 eV, respectively). Some non-oxide semiconductor photocatalysts (such as CdS and g-C_3N_4, with E_g values 2.4 and 2.7 eV, respectively) have visible light response, and their band positions can meet the requirements of the total splitting of water. However, their lower water oxidation overpotential or their own strong anodizing corrosion limits their application in the single-component visible light-driven overall water splitting system. On the contrary, the photocatalysts in the hydrogen evolution half reaction or comprising the Z-scheme systems do not need all the requirements simultaneously. For the photocatalytic H_2 production half reaction (as shown in Figure 1.17a), the semiconductor photocatalyst just needs to have a CB potential that is more negative than the redox potential of water reduction half reaction (that is, more negative than −0.41 V, at pH = 7, vs. NHE). The key point of optimizing this kind of reaction is to select the appropriate hydrogen evolution cocatalysts and electron donors with the appropriate redox potential to consume the photogenerated holes accumulating on the surface of the semiconductor. For the liquid-state Z-scheme system for simultaneous H_2 and O_2 production (Figure 1.17c), it is obvious that two types of photocatalysts are needed. But for either of the photocatalysts, it only needs to meet the potential requirements of photocatalytic H_2 production or O_2 production. For this kind of two-photon liquid-state Z-scheme system, the biggest advantage is that the active sites of H_2 production and O_2 production are effectively separated, so the undesired reverse reaction can be avoided. The electron transfer between the two photocatalysts in a Z-scheme system is a rate control step [347]. So far, various ionic redox pairs (such as IO_3^-/I^- and Fe^{3+}/Fe^{2+}), metal nanoparticles (such as Pt, Au, and Ag), and conductive carbon nanomaterials (such as graphene and carbon nanotubes) have been widely used in the construction of liquid and all-solid-state Z-scheme systems. However, there are some negative effects brought by the experience of electron mediator [348]: (i) under certain conditions, the redox intermediate will react with H_2 or O_2, and the photogenerated electrons and holes will selectively redox the electron mediator instead of H_2O; and (ii) if the electron mediator has a color, it will absorb part of the incident light. Therefore, the removal of the electron mediator can make the electrons and holes directly transfer between two kinds of semiconductor materials at high speed, which can improve the photocatalytic efficiency. Recently, direct Z-scheme photocatalytic systems (such as TiO_2/g-C_3N_4 [76], Ru/$SrTiO_3$: Rh–$BiVO_4$ [348], CdS–ZnO [61], and CdS–WO_3 [80, 349]) with no electron transporters have also been successfully constructed and applied in photocatalytic pollutant degradation, CO_2 reduction, and H_2 production [128]. In addition, it should also be noted that the Z-scheme reaction system itself is more complex than the traditional photolytic water splitting systems, increasing the possibility of side reactions and making it difficult to regenerate the deactivated catalyst. All in all, in addition to H_2 production half-reaction semiconductors, it is very important to select proper cocatalysts, as well as electron acceptors and electron donors with appropriate redox potentials for designing and constructing these two kinds of photocatalytic H_2 production systems.

Photocatalytic water splitting is usually very difficult to occur in systems without sacrificial agents. The sacrificial agents used in photocatalytic water decomposition systems can be divided into two categories (Figure 1.18): (i) electron donors, or hole trapping agents, for photocatalytic hydrogen production and (ii) electron acceptors, or electron trapping agents, for oxygen production. Commonly used electron donors mainly include biomass (e.g. sugar, cellulose, lactic acid) and other organic matter (e.g. triethanolamine, methane, CH_3OH, ethanol, ethylene diamine tetraacetic acid [EDTA]), as well as inorganic reductants (e.g. H_2S, Na_2S, K_2S, Na_2SO_3, $Na_2S_2O_4$, NaI, potassium thiocyanate [KSCN]). When biomass is used as the reducing agents, a fraction of the produced H_2 is released from the photocatalytic reforming biomass or biomass derivatives. However, this process couples solar energy and

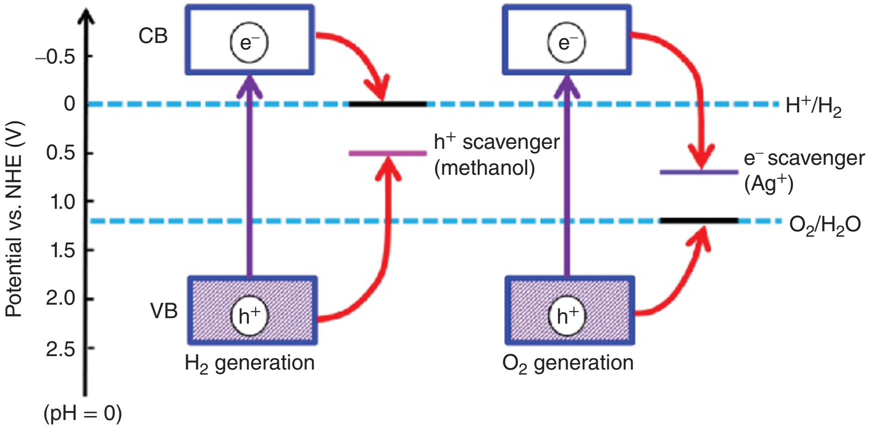

Figure 1.18 Photocatalytic H_2-generation and O_2-generation reactions in the presence of hole and electron sacrificial agents, respectively.

biomass energy, and its application value is obvious. In contrast, when Na_2S, K_2S, Na_2SO_3, $Na_2S_2O_4$, NaI, and KSCN are used as electron donors, even without any photocatalyst, HER will occur under UV irradiation [350]. Therefore, when we use these reductants as sacrificial agents for photocatalytic H_2 evolution, we should consider the photo-induced H_2 evolution behavior of these electron donors without photocatalyst. On the other hand, commonly used sacrificial agents for photocatalytic oxygen production reactions include Ag^+, Fe^{3+}, Ce^{4+}/Ce^{3+}, Fe^{3+}, $PtCl_2^-$, $AuCl_4^-$, $Na_2S_2O_8$, and $K_2S_2O_8$. Photogenerated electrons in the CB of semiconductor photocatalysts can be consumed by these oxidants in time, and the oxygen production reaction can be enhanced. However, it should be noted that although some oxidants (such as Ag^+) have a suitable oxidation potential, the reduced products (e.g. elemental Ag) may not be water soluble, which is deposited on the surface of the photocatalyst particles, hindering the light absorption, thus reducing the rate of OER and finally terminating the reaction. Therefore, it is generally observed that in the half-reaction system containing Ag^+, the oxygen production activity will gradually decrease over reaction time [34]. These reactions using sacrificial agents can be performed to evaluate whether a particular photocatalyst meets the thermodynamic and kinetic requirements for photocatalytic H_2 or O_2 production. However, even though a photocatalyst shows an activity of producing H_2 and O_2 in these reactions, the result does not guarantee that the photocatalyst has the activity for overall water splitting without a sacrificing agent. From this point of view, the term "water decomposition" should be treated differently from the hydrogen and oxygen production reactions in the presence of sacrificial agents. Water decomposition means that water can be completely decomposed to produce H_2 and O_2 at the stoichiometric ratio when there is no sacrificial agent. Additionally, for the specific half-reaction photocatalytic hydrogen production system, different sacrificial agents often have different H_2 production effects. For example, the photocatalytic H_2 production activity of g-C_3N_4 in the presence of triethanolamine as sacrificial agent is significantly higher than that observed using CH_3OH, ethanol, or EDTA as sacrificial agent [59]. Therefore, for a specific system, we should pay attention to optimize the type and concentration of sacrificial agents.

1.5.1.2 Photocatalytic CO_2 Reduction

The rapid consumption of fossil energy has led to the increase of CO_2 concentration in the atmosphere year by year, which has caused global warming and energy shortage problems. Therefore, reducing CO_2 emissions and sustainably transforming CO_2 have become hot spots for both alleviating environmental pressure and realizing the recycling of carbon resources. From the chemical point of view, the stable CO_2 molecules with standard formation heat of $-394.38\,\text{kJ mol}^{-1}$ are inert, thus making its chemical fixation and transformation very difficult. In the process of CO_2 reduction, H_2O is generally selected as the best hydrogen source and electron donor species.

Thermodynamically speaking, HCHO, HCOOH, CH_3OH, and CH_4 are the simplest products of CO_2 reduction by H_2O through the uphill reactions (see Table 1.4), due to the positive Gibbs free energy ΔG^0 of these reactions. These uphill reactions are obviously different from several spontaneous downhill CO_2 hydrogenation reactions (to CH_3OH, CH_4, and low carbon olefins; see Table 1.5) with negative ΔG^0 values. Therefore, a large amount of energy must be input to convert CO_2 and H_2O into different organic molecules. Among various facile technologies, photocatalytic CO_2 reduction has been considered as the most promising CO_2 conversion technology, which could convert abundant and renewable solar energy, water, and CO_2 into useful organic fuels without consuming auxiliary energy in the reaction process, thus effectively reducing the CO_2 emission into the atmosphere. Therefore, through artificial photosynthesis, solar fuels, such as alkanes, alkenes, and alcohols, and other organic substances could be obtained by abiotic reduction under the sunlight, thus truly realizing the recycling of the carbon element.

At present, due to the difficulty in achieving the half reaction of O_2 evolution, current studies mainly focus on the half reaction of CO_2 reduction through introducing the proper sacrificial agents to consume photogenerated holes. More importantly, these reduction half reactions are mainly dependent on the thermodynamic reduction potentials required, instead of the number of electrons involved in the reactions. The reaction difficulty is decreased in the following order:

Table 1.4 The standard molar enthalpy ΔH^0_{298} and the Gibbs free energy ΔG^0_{298} for the reduction reactions of CO_2 with H_2O.

Reaction	**ΔH^0_{298} (kJ mol^{-1})**	**ΔG^0_{298} (kJ mol^{-1})**
$CO_2(g) + H_2O(l) \rightarrow HCOOH(l) + 1/2O_2(g)$	541	275
$CO_2(g) + H_2O(l) \rightarrow HCHO(l) + O_2(g)$	795.8	520
$CO_2(g) + H_2O(l) \rightarrow CH_3OH(l) + 3/2O_2(g)$	727.1	703
$CO_2(g) + H_2O(l) \rightarrow CH_4(g) + 2O_2(g)$	890.9	818

Table 1.5 The standard molar enthalpy ΔH_{298}^0 and the Gibbs free energy ΔG_{298}^0 of CO_2 hydrogenation reactions [351].

Reaction	ΔH_{298}^0 (kJ mol^{-1})	ΔG_{298}^0 (kJ mol^{-1})
$CO_2 + H_2 \rightarrow CO + H_2O(g)$	41.2	28.6
$CO_2 + H_2 \rightarrow HCOOH(l)$	−31.2	33.0
$CO_2 + 3H_2 \rightarrow CH_3OH + H_2O(l)$	−131.0	−9.0
$CO_2 + 4H_2 \rightarrow CH_4 + 2H_2O(g)$	−164.9	−113.5
$2CO_2 + 6H_2 \rightarrow C_2H_4 + 4H_2O(g)$	−127.91	−57.52
$3CO_2 + 9H_2 \rightarrow C_3H_6 + 6H_2O(g)$	−249.84	−125.69
$4CO_2 + 12H_2 \rightarrow C_4H_8 + 8H_2O(g)$	−360.44	−179.95

Source: Data from Chen et al. [351].

HCOOH (−0.61 eV), CO (−0.53 eV), HCHO (−0.48 eV), CH_3OH (−0.38 eV), and CH_4 (−0.24 eV). The Latimer–Frost diagram of CO_2 reduction by multiple electrons and protons in pH = 7 ionic solution (Figure 1.19) further confirms that the increase of the number of electrons could greatly decrease the reduction potential, making the CO_2 reduction much easier. On the other hand, a more negative CB bottom potential could achieve much stronger reduction ability for selective reduction of CO_2 into different products. At this point, semiconductors with selectivity for HCOOH formation must be used to achieve the reduction of CO_2 into other energy products with more positive reduction potentials such as CO, CH_4, CH_3OH, and HCHO. Therefore, g-C_3N_4, SiC, CdS, and ZnS with relatively negative CB bottom potentials can selectively reduce CO_2 to different products such as HCOOH, HCHO,

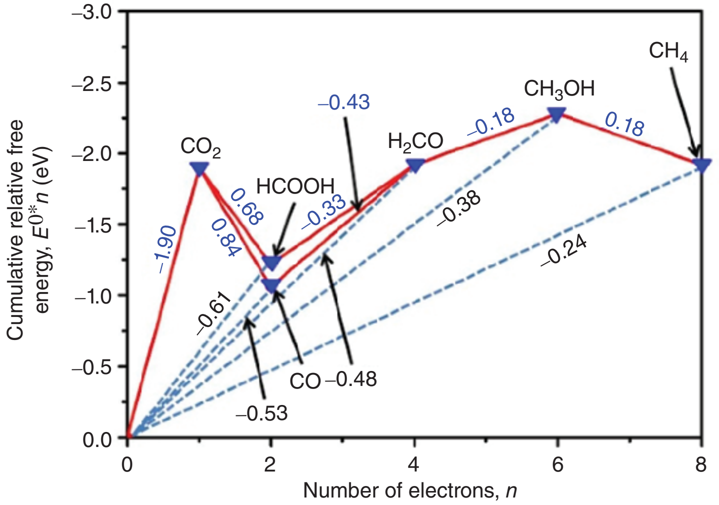

Figure 1.19 Latimer–Frost diagram for the multi-electron, multi-proton reduction of CO_2 in aqueous solution at pH 7. Source: Li et al. [352].

CH_3OH, or CH_4 [353–356]; whereas, rutile TiO_2 and $BiVO_4$ with relatively positive CB bottom potentials can reduce CO_2 and selectively produce CH_4, CH_3OH, or ethanol [357, 358]. Therefore, it is crucial to choose a semiconductor with suitable CB position in the selective reduction of CO_2 into different products.

Moreover, the dynamic factors, such as reaction conditions, the separation, and migration of photogenerated charge carriers, as well as the lifetime of electrons and holes, play key roles in highly efficient photoreduction of CO_2. Typically, the semiconductor photoreduction of CO_2 systems can be divided into two main categories: the aqueous suspension system (with dissolved CO_2 and carbonate) and the gas-phase reaction system (with water vapor and CO_2). The amount of H_2O in the aqueous suspension system is excessive, so it is impossible to adjust the ratio of H_2O/CO_2 by effective means for research. Therefore, more researchers choose the gas-phase system. Therefore, the gas–solid reaction model is used to analyze the influence of various factors on this kinetics of photocatalytic CO_2 reduction, as illustrated in Figure 1.20. It can be seen from the Figure 1.20 that in the process of photocatalytic reduction of CO_2, in addition to the excitation (process 1), charge transfer and separation (process 2), bulk recombination (process 3), and surface recombination (process 6) of photogenerated charge carriers, other important surface processes should also be considered, such as photocatalytic reduction of CO_2 (process 4) and water oxidation (process 5). In addition, we should pay attention to the undesired processes such as H_2 production on the surface of the photocatalyst (process 7) and

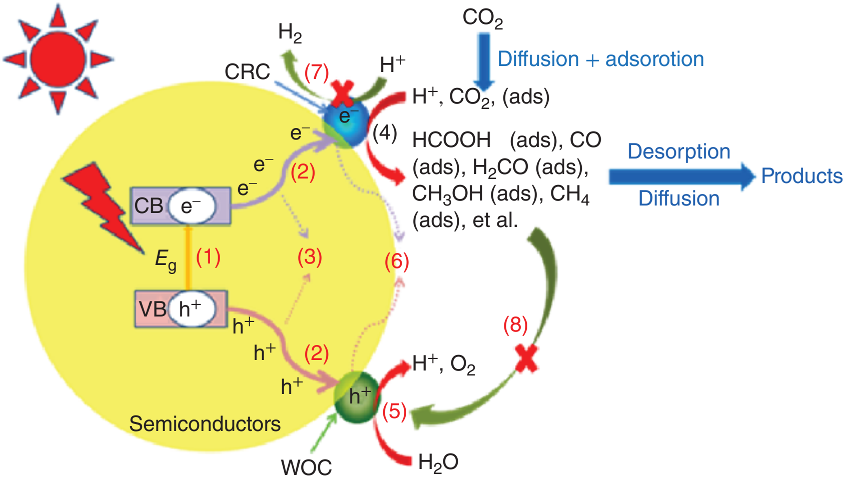

Figure 1.20 Processes involved in photocatalytic CO_2 reduction over a heterogeneous photocatalyst. CRC, CO_2 reduction cocatalysts; WOC, water oxidation cocatalysts. Step (1) the excitation of photogenerated electron–hole pairs; step (2) the separation of excited electrons and holes and their migration to the surface; step (3) the bulk charge recombination; step (4) the electrocatalytic reduction of CO_2 by photogenerated electrons trapped in the CRC or the surface active sites; step (5) the electrocatalytic oxidation of water by the photogenerated holes trapped in the WOC or the surface active sites; step (6) the surface charge recombination; step (7) the electrocatalytic H_2 evolution by trapped photogenerated electrons in the CRC or the surface active sites; and step (8) the electrocatalytic oxidation of reduction products over the WOC. Source: Li et al. [352].

re-oxidation of CO_2 reduction products (process 8). Therefore, from the viewpoint of system engineering, in order to build an efficient solar energy CO_2 conversion system, various possible factors, including the adsorption and activation of CO_2 by the photocatalytic materials, the efficiency of photogenerated electron–hole separation, the selection of cocatalysts, the promotion of target reactions (CO_2 reduction and water oxidation), and the inhibition of unexpected reactions (water reduction and re-oxidation of CO_2 reduction products), should be considered and optimized comprehensively.

In view of these key thermodynamic and kinetic factors affecting the efficiency of photocatalytic CO_2 reduction, Figure 1.21 systematically summarizes the corresponding design strategies of various high-efficiency photocatalytic CO_2 reduction photocatalysts [352]. These design strategies can be summarized into five aspects: (i) increasing the visible light absorption and excitation of photogenerated charge carriers, by means of elemental doping, introducing defects [359], building solid solutions, using the SPR effect [360], introducing photosensitizers, etc.; (ii) promoting carrier transfer and separation (mainly by building appropriate heterojunctions, such as Schott junction [355], type-II heterojunction [353, 354], direct Z-scheme system [80, 84], surface heterojunction [77, 361], and semiconductor/nanocarbon heterojunction [124, 125, 285, 362]); (iii) enhancing CO_2 adsorption and activation, such as increasing the surface area of the photocatalyst, introducing basic amino groups

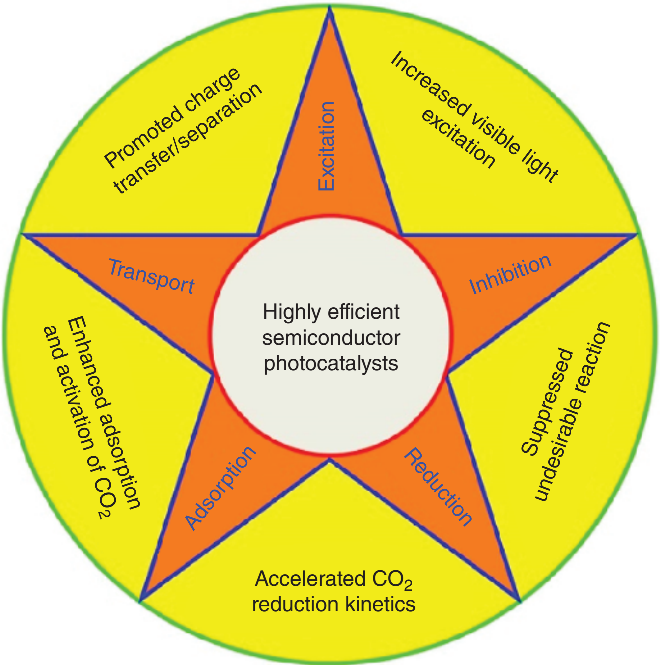

Figure 1.21 Factors influencing photocatalytic efficiency and corresponding design strategies for highly efficient photocatalysts used in the photocatalytic reduction of CO_2. Source: Li et al. [352].

[363, 364] or defect sites on the semiconductor surface; (iv) accelerating the reduction kinetics of CO_2 by loading various cocatalysts (such as Pt, AuCu alloy [365], RuO_x [366], and Ni@NiO [367]); and (v) inhibiting unexpected surface reactions, such as effectively inhibiting the H_2 generation reaction competing with carbon species for photogenerated electrons [368] and the re-oxidation reaction of the original product [369]. In the actual design of efficient CO_2 reduction photocatalysts, these modification strategies should be considered at the same time, so as to design the photocatalyst system with the best comprehensive performance.

In addition, the low selectivity and complex mechanism of photocatalytic reduction of CO_2 are also worthy of attention. So far, the use of photocatalytic reduction technology to synthesize organic compounds with CO_2 as raw material is still in the preliminary stage of research [134]. The key reason is that the conversion of CO_2 is not high and the selectivity of products is poor, due to the complex reaction mechanism. Considering the practical application of these compounds, it is highly desirable to control the selectivity of photocatalysts for a specific product and produce it with a purity as high as possible. However, the key factors affecting the selectivity of photocatalytic CO_2 reduction are still not well understood. So far, six typical strategies, including modulating surface morphological structures, tailoring surface chemical compositions, tuning the acidity–basicity of the supports, using the solvent effects, improving the interfacial properties, and loading suitable cocatalysts, have been explored to improve the product selectivity of the CO_2 photoreduction (as shown in Figure 1.22), which have been thoroughly discussed in a previous review [134].

1.5.1.3 Photocatalytic Degradation

In the past few decades, environmental pollution from discharge of toxic wastewater, solid waste, or flue gas has been regarded as a serious problem threating the sustainable development of human society. Semiconductor-based heterogeneous photocatalysis as an advanced oxidation process (AOP) has been extensively investigated for the pollution control and environmental remediation [370–375], due to its relatively easy operation and low costs. The photocatalytic degradation reactions could be generally classified into two types (Figure 1.23) [185]: (i) degradation of various organic pollutants (e.g. organic dyes, pharmaceuticals, antibiotics, pesticides, organic acids and aromatics, and recalcitrant polyfluorinated compounds [376, 377]) and toxic ions in aqueous solution and (ii) removal of gaseous pollutants (e.g. volatile organic compounds (VOCs), NO_x, ammonia, acetaldehyde, trichloroethylene, formaldehyde, and so on). Both types of photocatalytic reactions could be easily achieved in the laboratory by utilizing either photocatalyst powders or films immobilized on a support or substrate. However, industrial or pilot-scale applications of photocatalysis for environmental decontamination are still rare, due to unsatisfactory photocatalytic efficiency, selectivity, and stability of the currently developed photocatalysts.

According to the five design principles of semiconductor photocatalysts as shown in Figure 1.7, the potential practical photocatalysts for the degradation of pollutants could be evaluated. The stable, nontoxic, and inexpensive TiO_2 is the

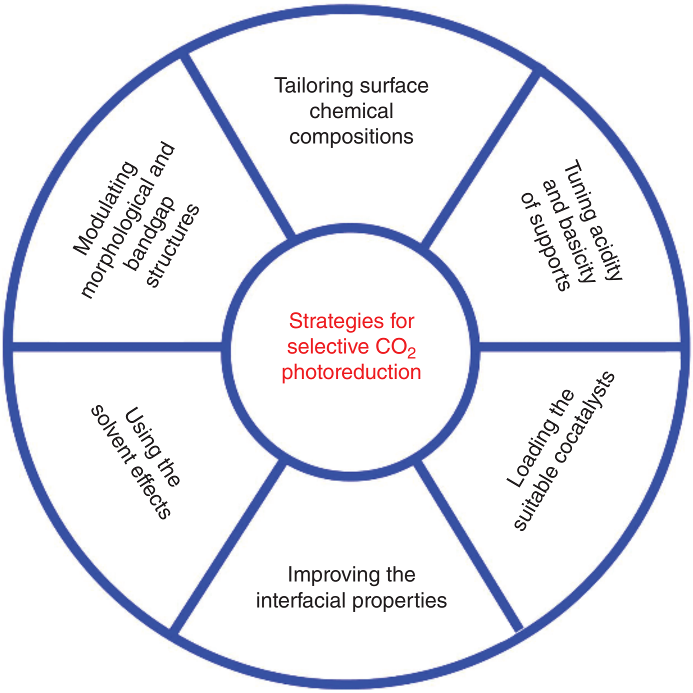

Figure 1.22 Typical strategies for selective CO_2 photoreduction. Source: Li et al. [134].

most frequently and thoroughly investigated semiconductor in environmental applications, because it has the excellent photoactivity for both reduction of O_2 and oxidation of surface H_2O/hydroxyl group to generate reactive oxygen species (ROS) such as the superoxide radical anion ($^\bullet O_2^-$) and $^\bullet OH$ radicals, owing to its suitable energy band structure. Notably, ZnO exhibits similar activity for the formation of $^\bullet O_2^-$ and $^\bullet OH$ radicals. However, its low photostability induced by Zn^{2+} release significantly restricts its extensive applications; actually, ZnO nanoparticles can undergo substantial dissolution even in the absence of light. In the last decade, the environmentally benign g-C_3N_4 materials have been widely recognized as a promising family of next-generation semiconductors for visible light-driven photocatalysis, owing to the unique 2D structure, tunable electronic properties, and excellent chemical stability. However, it should be noted that the photogenerated holes in g-C_3N_4 cannot drive the oxidation of surface H_2O/OH groups to $^\bullet OH$ radicals, and any $^\bullet OH$ radicals generated by g-C_3N_4 are the result of further transformation of the $^\bullet O_2^-$ radicals. In addition, it should be pointed out that some visible light-driven semiconductors with more positive VB potentials, such as WO_3, $BiVO_4$, and Bi_2WO_6, have excellent abilities for the oxidation of surface H_2O/OH groups to $^\bullet OH$ radicals, suggesting their potential applications in environmental remediation. Particularly, the visible light-responsive Bi-based photocatalysts are appealing for the application of environmental photocatalysis. In contrast, the applications of CdS, $Zn_xCd_{1-x}S$, and Ag-based semiconductors in environmental remediation are not encouraged due to the toxicity of Cd, high cost of Ag, and their low stability. Accordingly, it is clear

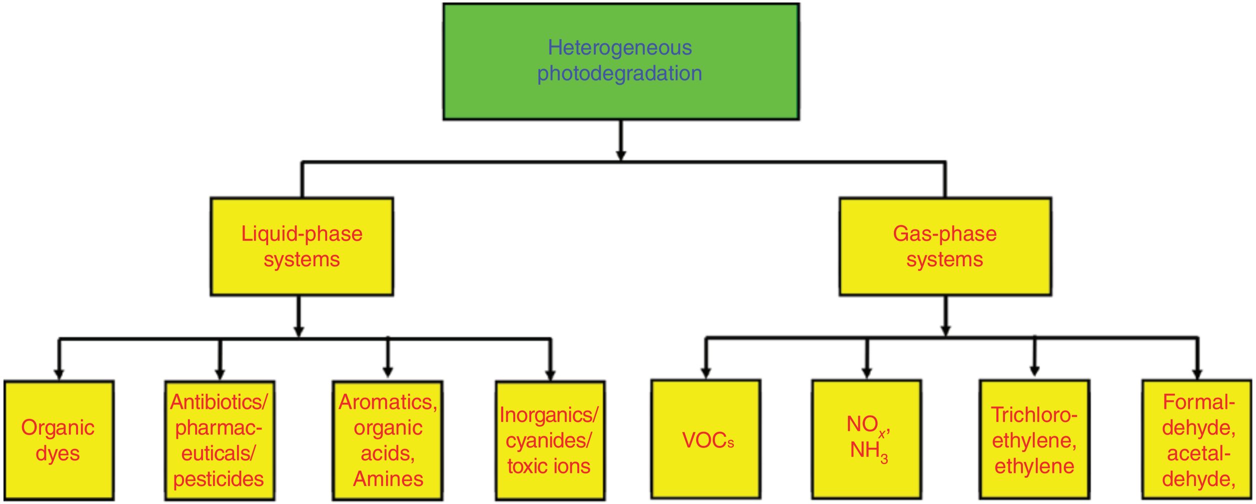

Figure 1.23 Heterogeneous photodegradation systems for various pollutants. Source: Li et al. [185].

that the thorough identification of ROS generation should be paid more attention in the investigations of photocatalytic environmental remediation.

In addition, due to the complex kinetics, bulk semiconductors commonly exhibit poor activity and stability to completely decompose the organic and inorganic contaminants. Many factors, such as light absorption, charge recombination dynamics, IFCT kinetics, surface structure and charge, and adsorption and photodegradation kinetics of photocatalysts, ROS generation, and O_2 reduction properties, play crucial roles in determining the overall photocatalytic degradation efficiency, all of which should be comprehensively considered for designing and optimizing environmental photocatalysts [370]. Accordingly, to effectively enhance the photocatalytic efficiency for durable degradation, a great number of semiconductor modification strategies have been exploited (Figure 1.24), such as creating semiconductor heterojunctions (type-II and multicomponent heterojunctions and homojunctions), constructing Schottky junctions or loading cocatalysts (e.g. coupling with metal nanoparticles and carbon nanomaterials), fabricating unique nanostructures (hollow one-dimensional (1D) nanorods/nanowires, 2D nanosheets, and three-dimensional (3D) hierarchical structures), loading suitable supports (e.g. activated carbon, Nafion, alumina, and silica), and designing the direct Z-scheme systems. Moreover, a combination of the different strategies seems to be very promising for heterogeneous photocatalytic degradation of pollutants, due to the simultaneously boosted light absorption, reactant adsorption, charge transport and separation, and surface catalysis.

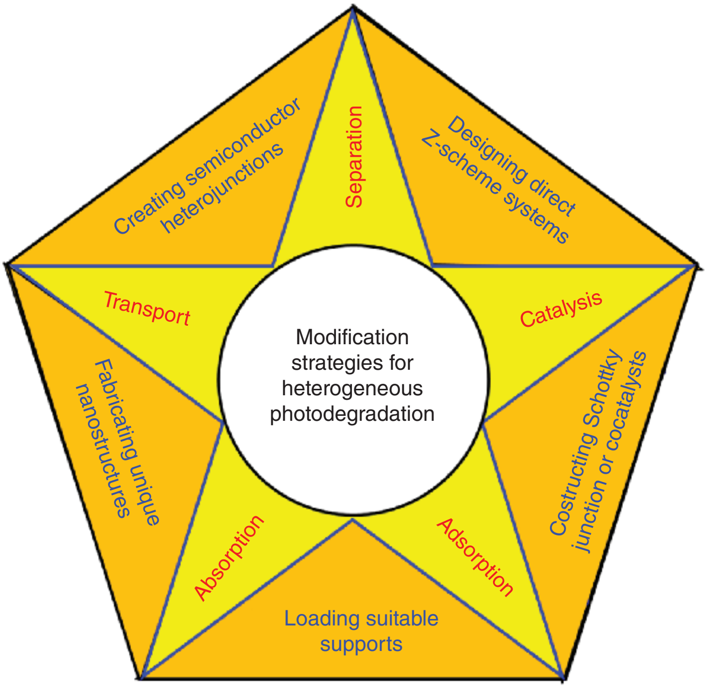

Figure 1.24 Semiconductor modification strategies for photocatalytic degradation. Source: Li et al. [185].

1.5.2 Evaluation of Solar Energy Photocatalysis

Evaluation of solar energy photocatalysis could be carried out according to the following three aspects: activity, photocatalytic mechanism, and semiconductor photocatalyst characterization. For the activity evaluation in different photocatalytic reactions, the stability and quantum efficiency should be examined in the practical applications. For the photocatalytic mechanism evaluation, the ROS species and reaction active sites should be carefully identified to elucidate the exact reaction mechanism. Additionally, the chemical composition, physical properties, and band

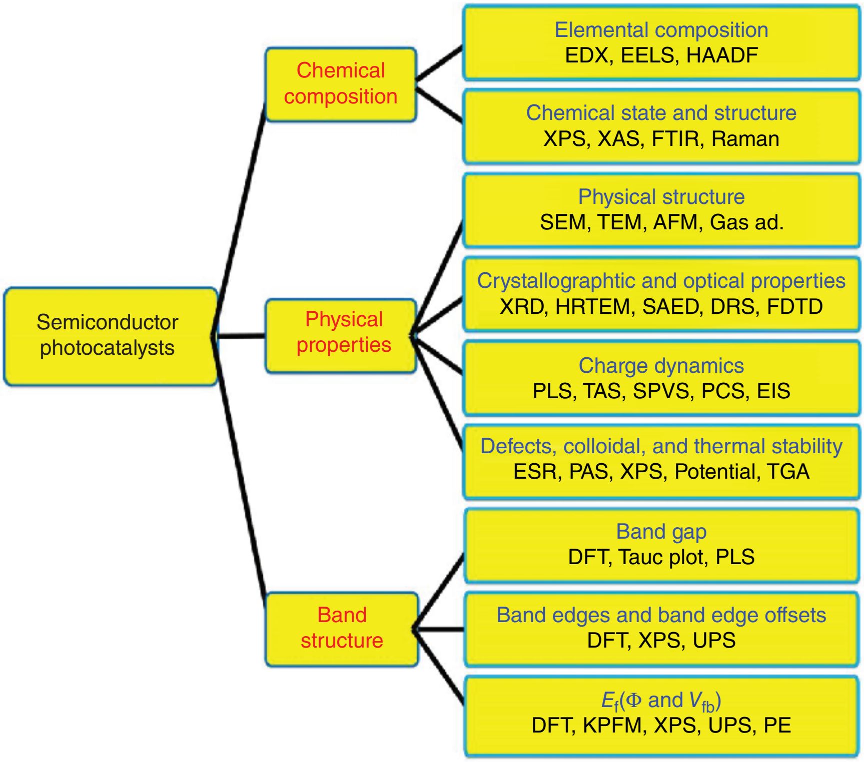

Figure 1.25 Characterization of some important properties of semiconductor photocatalysts. Source: Zhang et al. [378]. Abbreviations: E_f, Fermi level; f, work function; V_{fb}, flat-band potential; EDX, energy dispersive X-ray spectroscopy; EELS, electron energy-loss spectroscopy; HAADF, high-angle annular dark-field imaging; XPS, X-ray photoelectron spectroscopy; XAS, X-ray absorption spectroscopy; FTIR, Fourier transform infrared spectroscopy; SEM, scanning electron microscopy; TEM, transmission electron microscopy; AFM, atomic force microscopy; gas ad., gas adsorption–desorption analysis; XRD, X-ray diffraction; HRTEM, high-resolution transmission electron microscopy; SAED, selected area electron diffraction; DRS, diffuse reflectance spectroscopy; FDTD, finite-difference time-domain method; PLS, photoluminescence spectroscopy; TAS, transient absorption spectroscopy; SPVS, surface photovoltage spectroscopy; PCS, photocurrent spectroscopy; EIS, electrochemical impedance spectroscopy; ESR, electron spin resonance; PAS, positron annihilation spectroscopy; z potential, ζ potential; TGA, thermogravimetric analysis; DFT, density functional theory; UPS, ultraviolet photoelectron spectroscopy; KPFM, Kelvin probe force microscopy; PE, photoelectrochemical methods.

structure of semiconductor photocatalysts need to be properly analyzed by the different technologies listed in Figure 1.25 [378]. It should be noted that one or two technologies are applied to identify these properties. It is not necessary to use all these technologies to identify these properties in one time.

1.6 The Scope of This Book

So far, semiconductor photocatalysis technology has been widely used in many different fields, including photolysis of water for H_2 production, degradation of organic pollutants and heavy metal ions, or conversion of pollutants or CO_2 into solar fuel. As a new and effective way to deal with energy crisis and environmental problems, these areas have attracted growing attention, especially photocatalytic H_2 production and pollutant degradation. In recent years, the research on photocatalytic reduction of CO_2 and selective organic synthesis has gradually increased. Due to space limitation, this book focuses on the applications of different semiconductors in various photocatalytic research fields: photocatalytic decomposition of water for H_2 production, photocatalytic degradation of pollutants, and photocatalytic reduction of CO_2.

The book is roughly divided into six chapters. In Chapter 1, the fundamentals of solar energy photocatalysis are introduced. Chapter 2 focuses on various kinds of heterojunction systems for photocatalysis. In Chapter 3, the graphene-based photocatalysts are discussed. Chapter 4 focuses on the preparation of metal sulfide semiconductor photocatalysts and its application in the photocatalytic reactions. Chapter 5 and 6 focus on the preparation and applications of organic semiconductor photocatalysts and graphitic carbon nitride-based photocatalysts, respectively.

All in all, the selected content of this book is the hot research topics in semiconductor photocatalysts for different applications. The author hopes that this book will provide a professional, systematic, and up-to-date reference for researchers, who have been engaged in research in this field, as well as teachers and students. Solar energy photocatalysis is recognized as a very challenging research topic. We hope that this book can help you in the design, development, and improvement of new solar energy photocatalytic materials.

Acknowledgments

X. Li thanks National Natural Science Foundation of China (21975084, 51672089), Guangdong Provincial Applied Science and Technology Research and Development Program (2017B020238005), and the Ding Ying Talent Project of South China Agricultural University for their support.

References

1. Becquerel, A.E. (1839). Mémoire sur les effets électriques produits sous l'influence des rayons solaires. *Comptes Rendus* 9: 1839.
2. Brattain, W.H. and Garrett, C.G.B. (1955). Experiments on the interface between germanium and an electrolyte. *Bell Syst. Tech. J.* 34: 129–176.
3. Fujishima, A. and Honda, K. (1972). Electrochemical photolysis of water at a semiconductor electrode. *Nature* 238: 37–38.
4. Carey, J., Lawrence, J., and Tosine, H. (1976). Photodechlorination of PCB's in the presence of titanium dioxide in aqueous suspensions. *Bull. Environ. Contam. Toxicol.* 16: 697–701.
5. Frank, S.N. and Bard, A.J. (1977). Heterogeneous photocatalytic oxidation of cyanide ion in aqueous solutions at titanium dioxide powder. *J. Am. Chem. Soc.* 99: 303–304.
6. Schrauzer, G.N. and Guth, T.D. (1977). Photocatalytic reactions. 1. Photolysis of water and photoreduction of nitrogen on titanium dioxide. *J. Am. Chem. Soc.* 99: 7189–7193.
7. Kraeutler, B., Jaeger, C.D., and Bard, A.J. (1978). Direct observation of radical intermediates in the photo-Kolbe reaction – heterogeneous photocatalytic radical formation by electron spin resonance. *J. Am. Chem. Soc.* 100: 4903–4905.
8. Jaeger, C.D. and Bard, A.J. (1979). Spin trapping and electron spin resonance detection of radical intermediates in the photodecomposition of water at titanium dioxide particulate systems. *J. Phys. Chem.* 83: 3146–3152.
9. Kraeutler, B. and Bard, A.J. (1978). Heterogeneous photocatalytic preparation of supported catalysts. Photodeposition of platinum on titanium dioxide powder and other substrates. *J. Am. Chem. Soc.* 100: 4317–4318.
10. Kraeutler, B. and Bard, A.J. (1978). Heterogeneous photocatalytic synthesis of methane from acetic acid – new Kolbe reaction pathway. *J. Am. Chem. Soc.* 100: 2239–2240.
11. Bard, A.J. (1980). Photoelectrochemistry. *Science* 207: 139–144.
12. Bard, A.J. (1982). Design of semiconductor photoelectrochemical systems for solar energy conversion. *J. Phys. Chem.* 86: 172–177.
13. Halmann, M. (1978). Photoelectrochemical reduction of aqueous carbon dioxide on p-type gallium phosphide in liquid junction solar cells. *Nature* 275: 115–116.
14. Hemminger, J.C., Carr, R., and Somorjai, G.A. (1978). The photoassisted reaction of gaseous water and carbon dioxide adsorbed on the $SrTiO_3$ (111) crystal face to form methane. *Chem. Phys. Lett.* 57: 100–104.
15. Inoue, T., Fujishima, A., Konishi, S., and Honda, K. (1979). Photoelectrocatalytic reduction of carbon dioxide in aqueous suspensions of semiconductor powders. *Nature* 277: 637–638.
16. Kawai, T. and Sakata, T. (1980). Conversion of carbohydrate into hydrogen fuel by a photocatalytic process. *Nature* 286: 474–476.

17 Sato, S. and White, J.M. (1980). Photodecomposition of water over Pt/TiO_2 catalysts. *Chem. Phys. Lett.* 72: 83–86.

18 Wagner, F.T. and Somorjai, G.A. (1980). Photocatalytic hydrogen production from water on Pt-free $SrTiO_3$ in alkali hydroxide solutions. *Nature* 285: 559–560.

19 Wagner, F.T. and Somorjai, G.A. (1980). Photocatalytic and photoelectrochemical hydrogen production on strontium titanate single crystals. *J. Am. Chem. Soc.* 102: 5494–5502.

20 Bard, A.J. (1979). Photoelectrochemistry and heterogeneous photo-catalysis at semiconductors. *J. Photochem.* 10: 59–75.

21 Sato, S. and White, J.M. (1981). Photocatalytic water decomposition and water-gas shift reactions over NaOH-coated, platinized TiO_2. *J. Catal.* 69: 128–139.

22 Duonghong, D., Borgarello, E., and Graetzel, M. (1981). Dynamics of light-induced water cleavage in colloidal systems. *J. Am. Chem. Soc.* 103: 4685–4690.

23 Grätzel, M. (1981). Artificial photosynthesis: water cleavage into hydrogen and oxygen by visible light. *Acc. Chem. Res.* 14: 376–384.

24 Domen, K., Naito, S., Onishi, T. et al. (1982). Study of the photocatalytic decomposition of water vapor over a nickel(II) oxide-strontium titanate ($SrTiO_3$) catalyst. *J. Phys. Chem.* 86: 3657–3661.

25 Serpone, N., Borgarello, E., and Grätzel, M. (1984). Visible light induced generation of hydrogen from H_2S in mixed semiconductor dispersions, improved efficiency through inter-particle electron transfer. *J. Chem. Soc., Chem. Commun.*: 342–344.

26 Kakuta, N., Park, K.H., Finlayson, M.F. et al. (1985). Photoassisted hydrogen production using visible light and coprecipitated zinc sulfide.cntdot.cadmium sulfide without a noble metal. *J. Phys. Chem.* 89: 732–734.

27 Domen, K., Kudo, A., and Onishi, T. (1986). Mechanism of photocatalytic decomposition of water into H_2 and O_2 over NiO-$SrTiO_3$. *J. Catal.* 102: 92–98.

28 Domen, K., Kudo, A., Onishi, T. et al. (1986). Photocatalytic decomposition of water into hydrogen and oxygen over nickel(II) oxide-strontium titanate ($SrTiO_3$) powder. 1. Structure of the catalysts. *J. Phys. Chem.* 90: 292–295.

29 Anpo, M., Shima, T., Kodama, S., and Kubokawa, Y. (1987). Photocatalytic hydrogenation of propyne with water on small-particle titania: size quantization effects and reaction intermediates. *J. Phys. Chem.* 91: 4305–4310.

30 O'Regan, B. and Gratzel, M. (1991). A low-cost, high-efficiency solar cell based on dye-sensitized colloidal TiO_2 films. *Nature* 353: 737–740.

31 Choi, W., Termin, A., and Hoffmann, M.R. (1994). The role of metal ion dopants in quantum-sized TiO_2: correlation between photoreactivity and charge carrier recombination dynamics. *J. Phys. Chem.* 98: 13669–13679.

32 Wang, R., Hashimoto, K., Fujishima, A. et al. (1997). Light-induced amphiphilic surfaces. *Nature* 388: 431–432.

33 Kudo, A., Ueda, K., Kato, H., and Mikami, I. (1998). Photocatalytic O_2 evolution under visible light irradiation on $BiVO_4$ in aqueous $AgNO_3$ solution. *Catal. Lett.* 53: 229–230.

34 Kudo, A., Omori, K., and Kato, H. (1999). A novel aqueous process for preparation of crystal form-controlled and highly crystalline $BiVO_4$ powder from layered vanadates at room temperature and its photocatalytic and photophysical properties. *J. Am. Chem. Soc.* 121: 11459–11467.

35 Zou, Z., Ye, J., Sayama, K., and Arakawa, H. (2001). Direct splitting of water under visible light irradiation with an oxide semiconductor photocatalyst. *Nature* 414: 625–627.

36 Grätzel, M. (2001). Photoelectrochemical cells. *Nature* 414: 338–344.

37 Asahi, R., Morikawa, T., Ohwaki, T. et al. (2001). Visible-light photocatalysis in nitrogen-doped titanium oxides. *Science* 293: 269–271.

38 Abe, R., Sayama, K., Domen, K., and Arakawa, H. (2001). A new type of water splitting system composed of two different TiO_2 photocatalysts (anatase, rutile) and a IO_3^-/I^- shuttle redox mediator. *Chem. Phys. Lett.* 344: 339–344.

39 Khan, S.U.M., Al-Shahry, M., and Ingler, W.B. (2002). Efficient photochemical water splitting by a chemically modified n-TiO_2. *Science* 297: 2243–2245.

40 Yu, J.C., Yu, J.G., Ho, W.K. et al. (2002). Effects of F^- doping on the photocatalytic activity and microstructures of nanocrystalline TiO_2 powders. *Chem. Mater.* 14: 3808–3816.

41 Hitoki, G., Ishikawa, A., Takata, T. et al. (2002). Ta_3N_5 as a novel visible light-driven photocatalyst ($\lambda<600$ nm). *Chem. Lett.* 31: 736–737.

42 Hitoki, G., Takata, T., Kondo, J.N. et al. (2002). An oxynitride, TaON, as an efficient water oxidation photocatalyst under visible light irradiation ($\lambda\leq500$ nm). *Chem. Commun.* 38: 1698–1699.

43 Kudo, A., Tsuji, I., and Kato, H. (2002). $AgInZn_7S_9$ solid solution photocatalyst for H_2 evolution from aqueous solutions under visible light irradiation. *Chem. Commun.* 38: 1958–1959.

44 Zhang, L.Z. and Yu, J.C. (2003). A sonochemical approach to hierarchical porous titania spheres with enhanced photocatalytic activity. *Chem. Commun.* 39: 2078–2079.

45 Wang, X.C., Yu, J.C., Ho, C.M. et al. (2005). Photocatalytic activity of a hierarchically macro/mesoporous titania. *Langmuir* 21: 2552–2559.

46 Kato, H., Asakura, K., and Kudo, A. (2003). Highly efficient water splitting into H_2 and O_2 over lanthanum-doped $NaTaO_3$ photocatalysts with high crystallinity and surface nanostructure. *J. Am. Chem. Soc.* 125: 3082–3089.

47 Tsuji, I., Kato, H., Kobayashi, H., and Kudo, A. (2004). Photocatalytic H_2 evolution reaction from aqueous solutions over band structure-controlled $(AgIn)_xZn_{2(1-x)}S_2$ solid solution photocatalysts with visible-light response and their surface nanostructures. *J. Am. Chem. Soc.* 126: 13406–13413.

48 Maeda, K., Takata, T., Hara, M. et al. (2005). GaN:ZnO solid solution as a photocatalyst for visible-light-driven overall water splitting. *J. Am. Chem. Soc.* 127: 8286–8287.

49 Maeda, K., Teramura, K., Takata, T. et al. (2005). Overall water splitting on $(Ga_{1-x}Zn_x)(N_{1-x}O_x)$ solid solution photocatalyst: relationship between physical properties and photocatalytic activity. *J. Phys. Chem. B* 109: 20504–20510.

50 Maeda, K., Teramura, K., Lu, D.L. et al. (2006). Photocatalyst releasing hydrogen from water – enhancing catalytic performance holds promise for hydrogen production by water splitting in sunlight. *Nature* 440: 295–295.

51 Tada, H., Mitsui, T., Kiyonaga, T. et al. (2006). All-solid-state Z-scheme in CdS-Au-TiO_2 three-component nanojunction system. *Nat. Mater.* 5: 782–786.

52 Yu, J., Guo, H., Davis, S.A., and Mann, S. (2006). Fabrication of hollow inorganic microspheres by chemically induced self-transformation. *Adv. Funct. Mater.* 16: 2035–2041.

53 Yu, J., Liu, S., and Yu, H. (2007). Microstructures and photoactivity of mesoporous anatase hollow microspheres fabricated by fluoride-mediated self-transformation. *J. Catal.* 249: 59–66.

54 Zhang, X., Ai, Z., Jia, F., and Zhang, L. (2008). Generalized one-pot synthesis, characterization, and photocatalytic activity of hierarchical BiOX (X = Cl, Br, I) nanoplate microspheres. *J. Phys. Chem. C* 112: 747–753.

55 Williams, G., Seger, B., and Kamat, P.V. (2008). TiO_2-graphene nanocomposites. UV-assisted photocatalytic reduction of graphene oxide. *ACS Nano* 2: 1487–1491.

56 Tian, Y. and Tatsuma, T. (2005). Mechanisms and applications of plasmon-induced charge separation at TiO_2 films loaded with gold nanoparticles. *J. Am. Chem. Soc.* 127: 7632–7637.

57 Yang, H.G., Sun, C.H., Qiao, S.Z. et al. (2008). Anatase TiO_2 single crystals with a large percentage of reactive facets. *Nature* 453: 638–641.

58 Zong, X., Yan, H., Wu, G. et al. (2008). Enhancement of photocatalytic H_2 evolution on CdS by loading MoS_2 as cocatalyst under visible light irradiation. *J. Am. Chem. Soc.* 130: 7176–7177.

59 Wang, X., Maeda, K., Thomas, A. et al. (2009). A metal-free polymeric photocatalyst for hydrogen production from water under visible light. *Nat. Mater.* 8: 76–80.

60 Yan, H., Yang, J., Ma, G. et al. (2009). Visible-light-driven hydrogen production with extremely high quantum efficiency on Pt–PdS/CdS photocatalyst. *J. Catal.* 266: 165–168.

61 Wang, X.W., Liu, G., Chen, Z.G. et al. (2009). Enhanced photocatalytic hydrogen evolution by prolonging the lifetime of carriers in ZnO/CdS heterostructures. *Chem. Commun.* 45: 3452–3454.

62 Maeda, K., Higashi, M., Lu, D.L. et al. (2010). Efficient nonsacrificial water splitting through two-step photoexcitation by visible light using a modified oxynitride as a hydrogen evolution photocatalyst. *J. Am. Chem. Soc.* 132: 5858–5868.

63 Zhang, W., Wang, Y., Wang, Z. et al. (2010). Highly efficient and noble metal-free NiS/CdS photocatalysts for H_2 evolution from lactic acid sacrificial solution under visible light. *Chem. Commun.* 46: 7631–7633.

64 Varghese, O.K., Paulose, M., LaTempa, T.J., and Grimes, C.A. (2009). High-rate solar photocatalytic conversion of CO_2 and water vapor to hydrocarbon fuels. *Nano Lett.* 9: 731–737.

65 Yi, Z.G., Ye, J.H., Kikugawa, N. et al. (2010). An orthophosphate semiconductor with photooxidation properties under visible-light irradiation. *Nat. Mater.* 9: 559–564.

66 Liu, S., Yu, J., and Jaroniec, M. (2010). Tunable photocatalytic selectivity of hollow TiO_2 microspheres composed of anatase polyhedra with exposed {001} facets. *J. Am. Chem. Soc.* 132: 11914–11916.

67 Chen, X.B., Liu, L., Yu, P.Y., and Mao, S.S. (2011). Increasing solar absorption for photocatalysis with black hydrogenated titanium dioxide nanocrystals. *Science* 331: 746–750.

68 Li, Q., Guo, B., Yu, J. et al. (2011). Highly efficient visible-light-driven photocatalytic hydrogen production of CdS-cluster-decorated graphene nanosheets. *J. Am. Chem. Soc.* 133: 10878–10884.

69 Iwase, A., Ng, Y.H., Ishiguro, Y. et al. (2011). Reduced graphene oxide as a solid-state electron mediator in Z-scheme photocatalytic water splitting under visible light. *J. Am. Chem. Soc.* 133: 11054–11057.

70 Yu, J. and Ran, J. (2011). Facile preparation and enhanced photocatalytic H_2-production activity of $Cu(OH)_2$ cluster modified TiO_2. *Energy Environ. Sci.* 4: 1364–1371.

71 Yu, J., Hai, Y., and Cheng, B. (2011). Enhanced photocatalytic H_2-production activity of TiO_2 by $Ni(OH)_2$ cluster modification. *J. Phys. Chem. C* 115: 4953–4958.

72 Zhang, J., Yu, J., Zhang, Y. et al. (2011). Visible light photocatalytic H_2-production activity of CuS/ZnS porous nanosheets based on photoinduced interfacial charge transfer. *Nano Lett.* 11: 4774–4779.

73 Wang, W.N., An, W.J., Ramalingam, B. et al. (2012). Size and structure matter: enhanced CO_2 photoreduction efficiency by size-resolved ultrafine Pt nanoparticles on TiO_2 single crystals. *J. Am. Chem. Soc.* 134: 11276–11281.

74 Xiang, Q., Yu, J., and Jaroniec, M. (2012). Synergetic effect of MoS_2 and graphene as cocatalysts for enhanced photocatalytic H_2 production activity of TiO_2 nanoparticles. *J. Am. Chem. Soc.* 134: 6575–6578.

75 Zhang, J., Yu, J., Jaroniec, M., and Gong, J.R. (2012). Noble metal-free reduced graphene oxide-$Zn_xCd_{1-x}S$ nanocomposite with enhanced solar photocatalytic H_2-production performance. *Nano Lett.* 12: 4584–4589.

76 Yu, J., Wang, S., Low, J., and Xiao, W. (2013). Enhanced photocatalytic performance of direct Z-scheme g-C_3N_4-TiO_2 photocatalysts for the decomposition of formaldehyde in air. *Phys. Chem. Chem. Phys.* 15: 16883–16890.

77 Yu, J., Low, J., Xiao, W. et al. (2014). Enhanced photocatalytic CO_2-reduction activity of anatase TiO_2 by coexposed {001} and {101} facets. *J. Am. Chem. Soc.* 136: 8839–8842.

78 Zhang, J., Qi, L., Ran, J. et al. (2014). Ternary NiS/$Zn_xCd_{1-x}S$/reduced graphene oxide nanocomposites for enhanced solar photocatalytic H_2-production activity. *Adv. Energy Mater.* 4: 1301925.

79 Liu, J., Liu, Y., Liu, N. et al. (2015). Metal-free efficient photocatalyst for stable visible water splitting via a two-electron pathway. *Science* 347: 970–974.

80 Jin, J., Yu, J., Guo, D. et al. (2015). A hierarchical Z-scheme CdS-WO_3 photocatalyst with enhanced CO_2 reduction activity. *Small* 11: 5262–5271.

81 Chen, J., Wu, X.J., Yin, L. et al. (2015). One-pot synthesis of CdS nanocrystals hybridized with single-layer transition-metal dichalcogenide nanosheets for efficient photocatalytic hydrogen evolution. *Angew. Chem. Int. Ed.* 54: 1210–1214.

82 Ghosh, S., Kouame, N.A., Ramos, L. et al. (2015). Conducting polymer nanostructures for photocatalysis under visible light. *Nat. Mater.* 14: 505–511.

83 Ong, W.J., Tan, L.L., Chai, S.P., and Yong, S.T. (2015). Graphene oxide as a structure-directing agent for the two-dimensional interface engineering of sandwich-like graphene-g-C_3N_4 hybrid nanostructures with enhanced visible-light photoreduction of CO_2 to methane. *Chem. Commun.* 51: 858–861.

84 Yu, W., Xu, D., and Peng, T. (2015). Enhanced photocatalytic activity of g-C_3N_4 for selective CO_2 reduction to CH_3OH via facile coupling of ZnO: a direct Z-scheme mechanism. *J. Mater. Chem. A* 3: 19936–19947.

85 Low, J., Cheng, B., Yu, J., and Jaroniec, M. (2016). Carbon-based two-dimensional layered materials for photocatalytic CO_2 reduction to solar fuels. *Energy Storage Mater.* 3: 24–35.

86 Ma, T.Y., Cao, J.L., Jaroniec, M., and Qiao, S.Z. (2016). Interacting carbon nitride and titanium carbide nanosheets for high-performance oxygen evolution. *Angew. Chem. Int. Ed.* 55: 1138–1142.

87 Wang, Q., Hisatomi, T., Jia, Q. et al. (2016). Scalable water splitting on particulate photocatalyst sheets with a solar-to-hydrogen energy conversion efficiency exceeding 1%. *Nat. Mater.* 15: 611–615.

88 Zhang, B., Zheng, X.L., Voznyy, O. et al. (2016). Homogeneously dispersed multimetal oxygen-evolving catalysts. *Science* 352: 333–337.

89 Huang, Z.F., Song, J., Li, K. et al. (2016). Hollow cobalt-based bimetallic sulfide polyhedra for efficient all-pH-value electrochemical and photocatalytic hydrogen evolution. *J. Am. Chem. Soc.* 138: 1359–1365.

90 Zhou, X., Liu, R., Sun, K. et al. (2016). Solar-driven reduction of 1 atm of CO_2 to formate at 10% energy-conversion efficiency by use of a TiO_2-protected III-V tandem photoanode in conjunction with a bipolar membrane and a Pd/C cathode. *Acs Energy Lett.* 1: 764–770.

91 Fu, J., Zhu, B., Jiang, C. et al. (2017). Hierarchical porous O-doped g-C_3N_4 with enhanced photocatalytic CO_2 reduction activity. *Small* 13: 1603938.

92 Zhu, M., Cai, X., Fujitsuka, M. et al. (2017). Au/$La_2Ti_2O_7$ nanostructures sensitized with black phosphorus for plasmon-enhanced photocatalytic hydrogen production in visible and near-infrared light. *Angew. Chem. Int. Ed.* 56: 2064–2068.

93 Zhu, X., Zhang, T., Sun, Z. et al. (2017). Black phosphorus revisited: a missing metal-free elemental photocatalyst for visible light hydrogen evolution. *Adv. Mater.* 29: 1605776.

94 Ran, J., Gao, G., Li, F.T. et al. (2017). Ti_3C_2 MXene co-catalyst on metal sulfide photo-absorbers for enhanced visible-light photocatalytic hydrogen production. *Nat. Commun.* 8: 13907.

95 Chai, Z., Zeng, T.T., Li, Q. et al. (2016). Efficient visible light-driven splitting of alcohols into hydrogen and corresponding carbonyl compounds over a Ni-modified CdS photocatalyst. *J. Am. Chem. Soc.* 138: 10128–10131.

96 Che, W., Cheng, W., Yao, T. et al. (2017). Fast photoelectron transfer in (Cring)–C_3N_4 plane heterostructural nanosheets for overall water splitting. *J. Am. Chem. Soc.* 139: 3021–3026.

97 Zhang, Z.Y., Huang, J.D., Fang, Y.R. et al. (2017). A nonmetal plasmonic Z-scheme photocatalyst with UV- to NIR-driven photocatalytic protons reduction. *Adv. Mater.* 29: 1606688.

98 Hirakawa, H., Hashimoto, M., Shiraishi, Y., and Hirai, T. (2017). Photocatalytic conversion of nitrogen to ammonia with water on surface oxygen vacancies of titanium dioxide. *J. Am. Chem. Soc.* 139: 10929–10936.

99 Jiao, X.C., Chen, Z.W., Li, X.D. et al. (2017). Defect-mediated electron-hole separation in one-unit-cell $ZnIn_2S_4$ layers for boosted solar-driven CO_2 reduction. *J. Am. Chem. Soc.* 139: 7586–7594.

100 Xu, Y.F., Yang, M.Z., Chen, B.X. et al. (2017). A $CsPbBr_3$ perovskite quantum dot/graphene oxide composite for photocatalytic CO_2 reduction. *J. Am. Chem. Soc.* 139: 5660–5663.

101 Park, S., Chang, W.J., Lee, C.W. et al. (2017). Photocatalytic hydrogen generation from hydriodic acid using methylammonium lead iodide in dynamic equilibrium with aqueous solution. *Nat. Energy* 2: 16185.

102 Zhu, M.S., Kim, S., Mao, L. et al. (2017). Metal-free photocatalyst for H_2 evolution in visible to near-infrared region: black phosphorus/graphitic carbon nitride. *J. Am. Chem. Soc.* 139: 13234–13242.

103 Wen, J.Q., Xie, J., Zhang, H.D. et al. (2017). Constructing multifunctional metallic Ni interface layers in the g-C_3N_4 nanosheets/amorphous NiS heterojunctions for efficient photocatalytic H_2 generation. *ACS Appl. Mater. Interfaces* 9: 14031–14042.

104 Qi, Y., Zhao, Y., Gao, Y.Y. et al. (2018). Redox-based visible-light-driven Z-scheme overall water splitting with apparent quantum efficiency exceeding 10%. *Joule* 2: 2393–2402.

105 Pachfule, P., Acharjya, A., Roeser, J. et al. (2018). Diacetylene functionalized covalent organic framework (COF) for photocatalytic hydrogen generation. *J. Am. Chem. Soc.* 140: 1423–1427.

106 Chen, R.T., Pang, S., An, H.Y. et al. (2018). Charge separation via asymmetric illumination in photocatalytic Cu_2O particles. *Nat. Energy* 3: 655–663.

107 Ma, S., Deng, Y.P., Xie, J. et al. (2018). Noble-metal-free Ni_3C cocatalysts decorated CdS nanosheets for high efficiency visible-light-driven photocatalytic H_2 evolution. *Appl. Catal., B* 227: 218–228.

108 Shi, R., Ye, H.F., Liang, F. et al. (2018). Interstitial P-doped CdS with long-lived photogenerated electrons for photocatalytic water splitting without sacrificial agents. *Adv. Mater.* 30: 1705941.

109 Xu, F.Y., Meng, K., Zhu, B.C. et al. (2019). A new photocatalytic CO_2 reduction cocatalyst. *Adv. Funct. Mater.* 29: 1904256.

110 Fu, J.W., Xu, Q.L., Low, J.X. et al. (2019). Ultrathin 2D/2D WO_3/g-C_3N_4 step-scheme H_2-production photocatalyst. *Appl. Catal., B* 243: 556–565.

111 Low, J.X., Dai, B.Z., Tong, T. et al. (2019). In situ irradiated X-ray photoelectron spectroscopy investigation on a direct Z-scheme TiO_2/CdS composite film photocatalyst. *Adv. Mater.* 31: 5.

112 Kumar, P., Vahidzadeh, E., Thakur, W.K. et al. (2019). C_3N_5: A low bandgap semiconductor containing an azo-linked carbon nitride framework for photocatalytic, photovoltaic and adsorbent applications. *J. Am. Chem. Soc.* 141: 5415–5436.

113 Li, X.D., Sun, Y.F., Xu, J.Q. et al. (2019). Selective visible-light-driven photocatalytic CO_2 reduction to CH_4 mediated by atomically thin $CuIn_5S_8$ layers. *Nat. Energy* 4: 690–699.

114 Lee, B.H., Park, S., Kim, M. et al. (2019). Reversible and cooperative photoactivation of single-atom Cu/TiO_2 photocatalysts. *Nat. Mater.* 18: 620–626.

115 Shiraishi, Y., Takii, T., Hagi, T. et al. (2019). Resorcinol-formaldehyde resins as metal-free semiconductor photocatalysts for solar-to-hydrogen peroxide energy conversion. *Nat. Mater.* 18: 985–993.

116 Wang, Q., Nakabayashi, M., Hisatomi, T. et al. (2019). Oxysulfide photocatalyst for visible-light-driven overall water splitting. *Nat. Mater.* 18: 827–832.

117 Takata, T., Jiang, J., Sakata, Y. et al. (2020). Photocatalytic water splitting with a quantum efficiency of almost unity. *Nature* 581: 411–414.

118 Ni, M., Leung, M.K.H., Leung, D.Y.C., and Sumathy, K. (2007). A review and recent developments in photocatalytic water-splitting using TiO_2 for hydrogen production. *Renewable Sustainable Energy Rev.* 11: 401–425.

119 Wang, P., Huang, B., Qin, X. et al. (2008). Ag@AgCl: a highly efficient and stable photocatalyst active under visible light. *Angew. Chem. Int. Ed.* 47: 7931–7933.

120 Cao, S., Low, J., Yu, J., and Jaroniec, M. (2015). Polymeric photocatalysts based on graphitic carbon nitride. *Adv. Mater.* 27: 2150–2176.

121 Wen, J., Xie, J., Chen, X., and Li, X. (2017). A review on g-C_3N_4-based photocatalysts. *Appl. Surf. Sci.* 391: 72–123.

122 Ong, W.J., Tan, L.L., Ng, Y.H. et al. (2016). Graphitic carbon nitride (g-C_3N_4)-based photocatalysts for artificial photosynthesis and environmental remediation: are we a step closer to achieving sustainability? *Chem. Rev.* 116: 7159–7329.

123 Cao, S. and Yu, J. (2014). g-C_3N_4-based photocatalysts for hydrogen generation. *J. Phys. Chem. Lett.* 5: 2101–2107.

124 Xiang, Q., Cheng, B., and Yu, J. (2015). Graphene-based photocatalysts for solar-fuel generation. *Angew. Chem. Int. Ed.* 54: 11350–11366.

125 Yu, J., Jin, J., Cheng, B., and Jaroniec, M. (2014). A noble metal-free reduced graphene oxide-CdS nanorod composite for the enhanced visible-light photocatalytic reduction of CO_2 to solar fuel. *J. Mater. Chem. A* 2: 3407–3416.

126 Li, Q., Li, X., Wageh, S. et al. (2015). Graphene nanocomposite photocatalysts. *Adv. Energy Mater.* 5: 1500010.

127 Li, X., Yu, J., Wageh, S. et al. (2016). Graphene in photocatalysis: a review. *Small* 12: 6640–6696.

128 Zhou, P., Yu, J., and Jaroniec, M. (2014). All-solid-state Z-scheme photocatalytic systems. *Adv. Mater.* 26: 4920–4935.

129 Low, J., Jiang, C., Cheng, B. et al. (2017). A review of direct Z-scheme photocatalysts. *Small Methods* 1: 1700080.

130 He, K., Xie, J., Luo, X. et al. (2017). Enhanced visible light photocatalytic H_2 production over Z-scheme g-C_3N_4 nansheets/WO_3 nanorods nanocomposites loaded with $Ni(OH)_x$ cocatalysts. *Chin. J. Catal.* 38: 240–252.

131 Iqbal, S., Pan, Z., and Zhou, K. (2017). Enhanced photocatalytic hydrogen evolution from in situ formation of few-layered MoS_2/CdS nanosheet-based van der Waals heterostructures. *Nanoscale* 9: 6638–6642.

132 Xiang, Q., Yu, J., and Jaroniec, M. (2011). Preparation and enhanced visible-light photocatalytic H_2-production activity of graphene/C_3N_4 composites. *J. Phys. Chem. C* 115: 7355–7363.

133 Yuan, J., Wen, J., Zhong, Y. et al. (2015). Enhanced photocatalytic H_2 evolution over noble-metal-free NiS cocatalyst modified CdS nanorods/g-C_3N_4 heterojunctions. *J. Mater. Chem. A* 3: 18244–18255.

134 Li, X., Yu, J.G., Jaroniec, M., and Chen, X.B. (2019). Cocatalysts for selective photoreduction of CO_2 into solar fuels. *Chem. Rev.* 119: 3962–4179.

135 Wen, J., Li, X., Liu, W. et al. (2015). Photocatalysis fundamentals and surface modification of TiO_2 nanomaterials. *Chin. J. Catal.* 36: 2049–2070.

136 Kumar, S.G. and Rao, K.S.R.K. (2015). Tungsten-based nanomaterials (WO_3 & Bi_2WO_6): modifications related to charge carrier transfer mechanisms and photocatalytic applications. *Appl. Surf. Sci.* 355: 939–958.

137 Kuang, P.Y., Zheng, P.X., Liu, Z.Q. et al. (2016). Embedding Au quantum dots in rimous cadmium sulfide nanospheres for enhanced photocatalytic hydrogen evolution. *Small* 12: 6735–6744.

138 He, R.a., Cao, S., Zhou, P., and Yu, J. (2014). Recent advances in visible light Bi-based photocatalysts. *Chin. J. Catal.* 35: 989–1007.

139 Zhang, X.H., Peng, T.Y., and Song, S.S. (2016). Recent advances in dye-sensitized semiconductor systems for photocatalytic hydrogen production. *J. Mater. Chem. A* 4: 2365–2402.

140 Morris, A.J., Meyer, G.J., and Fujita, E. (2009). Molecular approaches to the photocatalytic reduction of carbon dioxide for solar fuels. *Acc. Chem. Res.* 42: 1983–1994.

141 Esswein, A.J. and Nocera, D.G. (2007). Hydrogen production by molecular photocatalysis. *Chem. Rev.* 107: 4022–4047.

142 Takeda, H. and Ishitani, O. (2010). Development of efficient photocatalytic systems for CO_2 reduction using mononuclear and multinuclear metal complexes based on mechanistic studies. *Coord. Chem. Rev.* 254: 346–354.

143 Windle, C.D. and Perutz, R.N. (2012). Advances in molecular photocatalytic and electrocatalytic CO_2 reduction. *Coord. Chem. Rev.* 256: 2562–2570.

144 Sprick, R.S., Bonillo, B., Clowes, R. et al. (2016). Visible-light-driven hydrogen evolution using planarized conjugated polymer photocatalysts. *Angew. Chem. Int. Ed.* 55: 1824–1828.

145 Muktha, B., Madras, G., Row, T.N.G. et al. (2007). Conjugated polymers for photocatalysis. *J. Phys. Chem. B* 111: 7994–7998.

146 Li, L., Cai, Z., Wu, Q. et al. (2016). Rational design of porous conjugated polymers and roles of residual palladium for photocatalytic hydrogen production. *J. Am. Chem. Soc.* 138: 7681–7686.

147 Zhou, Q. and Shi, G. (2016). Conducting polymer-based catalysts. *J. Am. Chem. Soc.* 138: 2868–2876.

148 Yeh, T.F., Syu, J.M., Cheng, C. et al. (2010). Graphite oxide as a photocatalyst for hydrogen production from water. *Adv. Funct. Mater.* 20: 2255–2262.

149 Chen, X. and Mao, S.S. (2007). Titanium dioxide nanomaterials: synthesis, properties, modifications, and applications. *Chem. Rev.* 107: 2891–2959.

150 Rehman, S., Ullah, R., Butt, A.M., and Gohar, N.D. (2009). Strategies of making TiO_2 and ZnO visible light active. *J. Hazard. Mater.* 170: 560–569.

151 Li, X., Yu, J., Low, J. et al. (2015). Engineering heterogeneous semiconductors for solar water splitting. *J. Mater. Chem. A* 3: 2485–2534.

152 Chen, X., Shen, S., Guo, L., and Mao, S.S. (2010). Semiconductor-based photocatalytic hydrogen generation. *Chem. Rev.* 110: 6503–6570.

153 Dong, F., Xiong, T., Sun, Y. et al. (2014). A semimetal bismuth element as a direct plasmonic photocatalyst. *Chem. Commun.* 50: 10386–10389.

154 Zhang, Q., Zhou, Y., Wang, F. et al. (2014). From semiconductors to semimetals: bismuth as a photocatalyst for NO oxidation in air. *J. Mater. Chem. A* 2: 11065–11072.

155 Zhao, Z., Zhang, W., Sun, Y. et al. (2016). Bi cocatalyst/Bi_2MoO_6 microspheres nanohybrid with SPR-promoted visible-light photocatalysis. *J. Phys. Chem. C* 120: 11889–11898.

156 Sun, Y., Zhao, Z., Dong, F., and Zhang, W. (2015). Mechanism of visible light photocatalytic NO_x oxidation with plasmonic Bi cocatalyst-enhanced $(BiO)_2CO_3$ hierarchical microspheres. *Phys. Chem. Chem. Phys.* 17: 10383–10390.

157 Dong, F., Zhao, Z., Sun, Y. et al. (2015). An advanced semimetal-organic Bi spheres-g-C_3N_4 nanohybrid with SPR-enhanced visible-light photocatalytic performance for NO purification. *Environ. Sci. Technol.* 49: 12432–12440.

158 Dong, F., Li, Q., Sun, Y., and Ho, W.K. (2014). Noble metal-like behavior of plasmonic Bi particles as a cocatalyst deposited on $(BiO)_2CO_3$ microspheres for efficient visible light photocatalysis. *ACS Catal.* 4: 4341–4350.

159 Xiong, T., Dong, X.a., Huang, H. et al. (2016). Single precursor mediated-synthesis of Bi semimetal deposited N-doped $(BiO)\ _2CO_3$ superstructures for highly promoted photocatalysis. *ACS Sustainable Chem. Eng.* 4: 2969–2979.

160 Zhai, Z.Y., Guo, X.N., Jin, G.Q., and Guo, X.Y. (2015). Visible light-induced selective photocatalytic aerobic oxidation of amines into imines on Cu/graphene. *Catal. Sci. Technol.* 5: 4202–4207.

161 Ni, Z.L., Zhang, W.D., Jiang, G.M. et al. (2017). Enhanced plasmonic photocatalysis by SiO_2@Bi microspheres with hot-electron transportation channels via Bi-O-Si linkages. *Chin. J. Catal.* 38: 1174–1183.

162 Ueno, K. and Misawa, H. (2013). Surface plasmon-enhanced photochemical reactions. *J. Photochem. Photobiol., C* 15: 31–52.

163 Linic, S., Christopher, P., and Ingram, D.B. (2011). Plasmonic-metal nanostructures for efficient conversion of solar to chemical energy. *Nat. Mater.* 10: 911–921.

164 Clavero, C. (2014). Plasmon-induced hot-electron generation at nanoparticle/metal-oxide interfaces for photovoltaic and photocatalytic devices. *Nat. Photonics* 8: 95–103.

165 Zhang, X.M., Chen, Y.L., Liu, R.S., and Tsai, D.P. (2013). Plasmonic photocatalysis. *Rep. Prog. Phys.* 76: 046401.

166 Long, R. and Prezhdo, O.V. (2014). Instantaneous generation of charge-separated state on TiO_2 surface sensitized with plasmonic nanoparticles. *J. Am. Chem. Soc.* 136: 4343–4354.

167 Cushing, S.K., Li, J., Meng, F. et al. (2012). Photocatalytic activity enhanced by plasmonic resonant energy transfer from metal to semiconductor. *J. Am. Chem. Soc.* 134: 15033–15041.

168 Ha, E., Lee, L.Y.S., Wang, J. et al. (2014). Significant enhancement in photocatalytic reduction of water to hydrogen by Au/Cu_2ZnSnS_4 nanostructure. *Adv. Mater.* 26: 3496–3500.

169 Jiang, R., Li, B., Fang, C., and Wang, J. (2014). Metal/semiconductor hybrid nanostructures for plasmon-enhanced applications. *Adv. Mater.* 26: 5274–5309.

170 Mo, Z., Xu, H., Chen, Z.G. et al. (2018). Gold/monolayer graphitic carbon nitride plasmonic photocatalyst for ultrafast electron transfer in solar-to-hydrogen energy conversion. *Chin. J. Catal.* 39: 760–770.

171 Li, Y.R., Guo, Y., Long, R. et al. (2018). Steering plasmonic hot electrons to realize enhanced full-spectrum photocatalytic hydrogen evolution. *Chin. J. Catal.* 39: 453–462.

172 Yang, X., Wang, Y., Xu, X. et al. (2017). Surface plasmon resonance-induced visible-light photocatalytic performance of silver/silver molybdate composites. *Chin. J. Catal.* 38: 260–269.

173 Yang, J.J., Liu, B.S., and Zhao, X.J. (2017). A visible-light-active Au-Cu(I)@$Na_2Ti_6O_{13}$ nanostructured hybrid pasmonic photocatalytic membrane for acetaldehyde elimination. *Chin. J. Catal.* 38: 2048–2055.

174 Warren, S.C. and Thimsen, E. (2012). Plasmonic solar water splitting. *Energy Environ. Sci.* 5: 5133–5146.

175 Creutz, C., Brunschwig, B.S., and Sutin, N. (2006). Interfacial charge-transfer absorption: 3. Application to semiconductor−molecule assemblies. *J. Phys. Chem. B* 110: 25181–25190.

176 Li, X., Yu, J., and Jaroniec, M. (2016). Hierarchical photocatalysts. *Chem. Soc. Rev.* 45: 2603–2636.

177 Wood, P.M. (1988). The potential diagram for oxygen at pH 7. *Biochem. J.* 253: 287–289.

178 Guan, L. and Chen, X. (2018). Photoexcited charge transport and accumulation in anatase TiO_2. *ACS Appl. Energy Mater.* 1: 4313–4320.

179 Zhang, J.Z. (2000). Interfacial charge carrier dynamics of colloidal semiconductor nanoparticles. *J. Phys. Chem. B* 104: 7239–7253.

180 Ravensbergen, J., Abdi, F.F., van Santen, J.H. et al. (2014). Unraveling the carrier dynamics of $BiVO_4$: a femtosecond to microsecond transient absorption study. *J. Phys. Chem. C* 118: 27793–27800.

181 Özgür, Ü., Alivov, Y.I., Liu, C. et al. (2005). A comprehensive review of ZnO materials and devices. *J. Appl. Phys.* 98: 041301.

182 Abdi, F.F., Savenije, T.J., May, M.M. et al. (2013). The origin of slow carrier transport in $BiVO_4$ thin film photoanodes: a time-resolved microwave conductivity study. *J. Phys. Chem. Lett.* 4: 2752–2757.

183 Zhang, J.F., Zhou, P., Liu, J.J., and Yu, J.G. (2014). New understanding of the difference of photocatalytic activity among anatase, rutile and brookite TiO_2. *Phys. Chem. Chem. Phys.* 16: 20382–20386.

184 Zhang, J., Wageh, S., Al-Ghamdi, A., and Yu, J. (2016). New understanding on the different photocatalytic activity of wurtzite and zinc-blende CdS. *Appl. Catal., B* 192: 101–107.

185 Li, X., Xie, J., Jiang, C. et al. (2018). Review on design and evaluation of environmental photocatalysts. *Front. Environ. Sci. Eng.* 12: 14.

186 He, R.A., Xu, D.F., Cheng, B. et al. (2018). Review on nanoscale Bi-based photocatalysts. *Nanoscale Horiz.* 3: 464–504.

187 Chen, S.Y. and Wang, L.W. (2012). Thermodynamic oxidation and reduction potentials of photocatalytic semiconductors in aqueous solution. *Chem. Mater.* 24: 3659–3666.

188 Yang, X., Cui, H., Li, Y. et al. (2013). Fabrication of Ag_3PO_4-graphene composites with highly efficient and stable visible light photocatalytic performance. *ACS Catal.* 3: 363–369.

189 Zhang, D., Tang, H., Wang, Y. et al. (2014). Synthesis and characterization of graphene oxide modified AgBr nanocomposites with enhanced photocatalytic activity and stability under visible light. *Appl. Surf. Sci.* 319: 306–311.

190 Li, J., Wei, L., Yu, C. et al. (2015). Preparation and characterization of graphene oxide/Ag_2CO_3 photocatalyst and its visible light photocatalytic activity. *Appl. Surf. Sci.* 358: 168–174.

191 Reddy, D.A., Lee, S., Choi, J. et al. (2015). Green synthesis of AgI-reduced graphene oxide nanocomposites: toward enhanced visible-light photocatalytic activity for organic dye removal. *Appl. Surf. Sci.* 341: 175–184.

192 Kudo, A. and Miseki, Y. (2009). Heterogeneous photocatalyst materials for water splitting. *Chem. Soc. Rev.* 38: 253–278.

193 Paracchino, A., Laporte, V., Sivula, K. et al. (2011). Highly active oxide photocathode for photoelectrochemical water reduction. *Nat. Mater.* 10: 456–461.

194 Gu, J., Yan, Y., Krizan, J.W. et al. (2014). *p*-Type $CuRhO_2$ as a self-healing photoelectrode for water reduction under visible light. *J. Am. Chem. Soc.* 136: 830–833.

195 Park, J.E., Hu, Y., Krizan, J.W. et al. (2018). Stable hydrogen evolution from an $AgRhO_2$ photocathode under visible light. *Chem. Mater.* 30: 2574–2582.

196 Di, T., Zhu, B., Zhang, J. et al. (2016). Enhanced photocatalytic H_2 production on CdS nanorod using cobalt-phosphate as oxidation cocatalyst. *Appl. Surf. Sci.* 389: 775–782.

197 Chen, S.S., Shen, S., Liu, G.J. et al. (2015). Interface engineering of a CoO_x/Ta_3N_5 photocatalyst for unprecedented water oxidation performance under visible-light-irradiation. *Angew. Chem. Int. Ed.* 54: 3047–3051.

198 Wang, P., Xia, Y., Wu, P. et al. (2014). Cu(II) as a general cocatalyst for improved visible-light photocatalytic performance of photosensitive Ag-based compounds. *J. Phys. Chem. C* 118: 8891–8898.

199 Wang, X., Wang, K., Feng, K. et al. (2014). Greatly enhanced photocatalytic activity of $TiO_{2-x}N_x$ by a simple surface modification of Fe(III) cocatalyst. *J. Mol. Catal. A: Chem.* 391: 92–98.

200 Yu, H., Xu, L., Wang, P. et al. (2014). Enhanced photoinduced stability and photocatalytic activity of AgBr photocatalyst by surface modification of Fe(III) cocatalyst. *Appl. Catal., B* 144: 75–82.

201 Peng, Y., Ji, J., and Chen, D. (2015). Ultrasound assisted synthesis of ZnO/reduced graphene oxide composites with enhanced photocatalytic activity and anti-photocorrosion. *Appl. Surf. Sci.* 356: 762–768.

202 Huang, M., Yu, J., Deng, C. et al. (2016). 3D nanospherical $Cd_xZn_{1-x}S$/reduced graphene oxide composites with superior photocatalytic activity and photocorrosion resistance. *Appl. Surf. Sci.* 365: 227–239.

203 Chen, J., Zhang, F., Zhao, Y.L. et al. (2016). Facile synthesis of CdS/C core-shell nanospheres with ultrathin carbon layer for enhanced photocatalytic properties and stability. *Appl. Surf. Sci.* 362: 126–131.

204 Cai, L., Xiong, X., Liang, N., and Long, Q. (2015). Highly effective and stable Ag_3PO_4-WO_3/MWCNTs photocatalysts for simultaneous Cr(VI) reduction and orange II degradation under visible light irradiation. *Appl. Surf. Sci.* 353: 939–948.

205 Wang, H., Li, J., Huo, P. et al. (2016). Preparation of Ag_2O/Ag_2CO_3/MWNTs composite photocatalysts for enhancement of ciprofloxacin degradation. *Appl. Surf. Sci.* 366: 1–8.

206 Miao, J., Xie, A., Li, S. et al. (2016). A novel reducing graphene/polyaniline/cuprous oxide composite hydrogel with unexpected photocatalytic activity for the degradation of Congo red. *Appl. Surf. Sci.* 360: 594–600.

207 Xu, X., Gao, Z., Cui, Z. et al. (2016). Synthesis of Cu_2O Octadecahedron/TiO_2 quantum dot heterojunctions with high visible light photocatalytic activity and high stability. *ACS Appl. Mater. Interfaces* 8: 91–101.

208 Liu, Y., Zhang, B., Luo, L. et al. (2015). TiO_2/Cu_2O Core/ultrathin shell nanorods as efficient and stable photocatalysts for water reduction. *Angew. Chem. Int. Ed.* 54: 15260–15265.

209 Liu, L., Yang, W., Sun, W. et al. (2015). Creation of $Cu_2O@TiO_2$ composite photocatalysts with *p–n* heterojunctions formed on exposed Cu_2O facets, their energy band alignment study, and their enhanced photocatalytic activity under illumination with visible light. *ACS Appl. Mater. Interfaces* 7: 1465–1476.

210 Liu, J., Wen, M., Chen, H. et al. (2014). Assembly of TiO_2-on-Cu_2O nanocubes with narrow-band Cu_2O-induced visible-light-enhanced photocatalytic activity. *ChemPlusChem* 79: 298–303.

211 Lalitha, K., Sadanandam, G., Kumari, V.D. et al. (2010). Highly stabilized and finely dispersed Cu_2O/TiO_2: a promising visible sensitive photocatalyst for continuous production of hydrogen from glycerol: water mixtures. *J. Phys. Chem. C* 114: 22181–22189.

212 Beigi, A.A., Fatemi, S., and Salehi, Z. (2014). Synthesis of nanocomposite CdS/TiO_2 and investigation of its photocatalytic activity for CO_2 reduction to CO and CH_4 under visible light irradiation. *J. CO_2 Util.* 7: 23–29.

213 Xiao, F.X., Miao, J., Wang, H.Y., and Liu, B. (2013). Self-assembly of hierarchically ordered CdS quantum dots-TiO_2 nanotube array heterostructures as efficient visible light photocatalysts for photoredox applications. *J. Mater. Chem. A* 1: 12229–12238.

214 Tian, F., Hou, D., Hu, F. et al. (2017). Pouous TiO_2 nanofibers decorated CdS nanoparticles by SILAR method for enhanced visible-light-driven photocatalytic activity. *Appl. Surf. Sci.* 391: 295–302.

215 Yang, G., Yang, B., Xiao, T., and Yan, Z. (2013). One-step solvothermal synthesis of hierarchically porous nanostructured CdS/TiO_2 heterojunction with higher visible light photocatalytic activity. *Appl. Surf. Sci.* 283: 402–410.

216 Fujishima, M., Nakabayashi, Y., Takayama, K. et al. (2016). High coverage formation of CdS quantum dots on TiO_2 by the photocatalytic growth of preformed seeds. *J. Phys. Chem. C* 120: 17365–17371.

217 Pan, X. and Xu, Y.J. (2015). Graphene-templated bottom-up fabrication of ultralarge binary CdS-TiO_2 nanosheets for photocatalytic selective reduction. *J. Phys. Chem. C* 119: 7184–7194.

218 Ma, K., Yehezkeli, O., Domaille, D.W. et al. (2015). Enhanced hydrogen production from DNA-assembled Z-scheme TiO_2-CdS photocatalyst systems. *Angew. Chem. Int. Ed.* 54: 11490–11494.

219 Wei, Y., Jiao, J., Zhao, Z. et al. (2015). Fabrication of inverse opal TiO_2-supported Au@CdS core-shell nanoparticles for efficient photocatalytic CO_2 conversion. *Appl. Catal., B* 179: 422–432.

220 Wei, Y., Jiao, J., Zhao, Z. et al. (2015). 3D ordered macroporous TiO_2-supported Pt@CdS core-shell nanoparticles: design, synthesis and efficient photocatalytic conversion of CO_2 with water to methane. *J. Mater. Chem. A* 3: 11074–11085.

221 Dong, W., Pan, F., Xu, L. et al. (2015). Facile synthesis of CdS@TiO_2 core-shell nanorods with controllable shell thickness and enhanced photocatalytic activity under visible light irradiation. *Appl. Surf. Sci.* 349: 279–286.

222 Liu, S., Zhang, N., Tang, Z.R., and Xu, Y.J. (2012). Synthesis of one-dimensional CdS@TiO_2 core-shell nanocomposites photocatalyst for selective redox: the dual role of TiO_2 shell. *ACS Appl. Mater. Interfaces* 4: 6378–6385.

223 Butburee, T., Bai, Y., Pan, J. et al. (2014). Step-wise controlled growth of metal@TiO_2 core-shells with plasmonic hot spots and their photocatalytic properties. *J. Mater. Chem. A* 2: 12776–12784.

224 Tanaka, A., Fuku, K., Nishi, T. et al. (2013). Functionalization of Au/TiO_2 plasmonic photocatalysts with Pd by formation of a core-shell structure for effective dechlorination of chlorobenzene under irradiation of visible light. *J. Phys. Chem. C* 117: 16983–16989.

225 Wu, X.F., Song, H.Y., Yoon, J.M. et al. (2009). Synthesis of core-shell Au@TiO_2 nanoparticles with truncated wedge-shaped morphology and their photocatalytic properties. *Langmuir* 25: 6438–6447.

226 Ji, L., McDaniel, M.D., Wang, S.J. et al. (2015). A silicon-based photocathode for water reduction with an epitaxial $SrTiO_3$ protection layer and a nanostructured catalyst. *Nat. Nanotechnol.* 10: 84–90.

227 Yu, H., Chen, F., Chen, F., and Wang, X. (2015). In situ self-transformation synthesis of g-C_3N_4-modified CdS heterostructure with enhanced photocatalytic activity. *Appl. Surf. Sci.* 358: 385–392.

228 Liu, L., Qi, Y., Hu, J. et al. (2015). Efficient visible-light photocatalytic hydrogen evolution and enhanced photostability of core@shell Cu_2O@g-C_3N_4 octahedra. *Appl. Surf. Sci.* 351: 1146–1154.

229 Zhang, J., Wang, Y., Jin, J. et al. (2013). Efficient visible-light photocatalytic hydrogen evolution and enhanced photostability of core/shell CdS/g-C_3N_4 nanowires. *ACS Appl. Mater. Interfaces* 5: 10317–10324.

230 Le Formal, F., Tetreault, N., Cornuz, M. et al. (2011). Passivating surface states on water splitting hematite photoanodes with alumina overlayers. *Chem. Sci.* 2: 737–743.

231 Song, G., Xin, F., Chen, J., and Yin, X. (2014). Photocatalytic reduction of CO_2 in cyclohexanol on CdS-TiO_2 heterostructured photocatalyst. *Appl. Catal., A* 473: 90–95.

232 Zhai, J., Tao, X., Pu, Y. et al. (2010). Core/shell structured ZnO/SiO_2 nanoparticles: preparation, characterization and photocatalytic property. *Appl. Surf. Sci.* 257: 393–397.

233 Chen, J.J., Wu, J.C.S., Wu, P.C., and Tsai, D.P. (2012). Improved photocatalytic activity of shell-isolated plasmonic photocatalyst Au@SiO_2/TiO_2 by promoted LSPR. *J. Phys. Chem. C* 116: 26535–26542.

234 Yoo, J.B., Yoo, H.J., Lim, B.W. et al. (2012). Controlled synthesis of monodisperse SiO_2-TiO_2 microspheres with a yolk-shell structure as effective photocatalysts. *ChemSusChem* 5: 2334–2340.

235 Zhang, X., Zhu, Y., Yang, X. et al. (2013). Enhanced visible light photocatalytic activity of interlayer-isolated triplex Ag@SiO_2@TiO_2 core-shell nanoparticles. *Nanoscale* 5: 3359–3366.

236 Yao, X. and Liu, X. (2014). One-pot synthesis of Ag/AgCl@SiO_2 core-shell plasmonic photocatalyst in natural geothermal water for efficient photocatalysis under visible light. *J. Mol. Catal. A: Chem.* 393: 30–38.

237 Nadrah, P., Gaberscek, M., and Sever Skapin, A. (2017). Selective degradation of model pollutants in the presence of core@shell TiO_2@SiO_2 photocatalyst. *Appl. Surf. Sci.* 405: 389–394.

238 Zhu, S. and Wang, D. (2017). Photocatalysis: basic principles, diverse forms of implementations and emerging scientific opportunities. *Adv. Energy Mater.* 7: 1700841.

239 Lian, Z., Xu, P., Wang, W. et al. (2015). C_{60}-Decorated CdS/TiO_2 mesoporous architectures with enhanced photostability and photocatalytic activity for H_2 evolution. *ACS Appl. Mater. Interfaces* 7: 4533–4540.

240 Luo, G., Jiang, X., Li, M. et al. (2013). Facile fabrication and enhanced photocatalytic performance of Ag/AgCl/rGO heterostructure photocatalyst. *ACS Appl. Mater. Interfaces* 5: 2161–2168.

241 Tong, R., Liu, C., Xu, Z. et al. (2016). Efficiently enhancing visible light photocatalytic activity of faceted TiO_2 nanocrystals by synergistic effects of core-shell structured Au@CdS nanoparticles and their selective deposition. *ACS Appl. Mater. Interfaces* 8: 21326–21333.

242 Hu, Z. and Yu, J.C. (2013). Pt_3Co-loaded CdS and TiO_2 for photocatalytic hydrogen evolution from water. *J. Mater. Chem. A* 1: 12221–12228.

243 Liu, S., Yang, M.Q., and Xu, Y.J. (2014). Surface charge promotes the synthesis of large, flat structured graphene-(CdS nanowire)-TiO_2 nanocomposites as versatile visible light photocatalysts. *J. Mater. Chem. A* 2: 430–440.

244 Wang, P., Ming, T., Wang, G. et al. (2014). Cocatalyst modification and nanonization of Ag/AgCl photocatalyst with enhanced photocatalytic performance. *J. Mol. Catal. A: Chem.* 381: 114–119.

245 Park, H., Kirn, Y.K., and Choi, W. (2011). Reversing CdS preparation order and its effects on photocatalytic hydrogen production of CdS/Pt-TiO_2 hybrids under visible light. *J. Phys. Chem. C* 115: 6141–6148.

246 Osterloh, F.E. (2007). Inorganic materials as catalysts for photochemical splitting of water. *Chem. Mater.* 20: 35–54.

247 Kumar, S.G. and Rao, K.S.R.K. (2017). Comparison of modification strategies towards enhanced charge carrier separation and photocatalytic degradation activity of metal oxide semiconductors (TiO_2, WO_3 and ZnO). *Appl. Surf. Sci.* 391: 124–148.

248 Bai, S., Jiang, J., Zhang, Q., and Xiong, Y. (2015). Steering charge kinetics in photocatalysis: intersection of materials syntheses, characterization techniques and theoretical simulations. *Chem. Soc. Rev.* 44: 2893–2939.

249 Bai, S., Jiang, W., Li, Z., and Xiong, Y. (2015). Surface and interface engineering in photocatalysis. *ChemNanoMat* 1: 223–239.

250 Zhang, P., Wang, T., Chang, X., and Gong, J. (2016). Effective charge carrier utilization in photocatalytic conversions. *Acc. Chem. Res.* 49: 911–921.

251 Devi, L.G. and Kavitha, R. (2016). A review on plasmonic metal-TiO_2 composite for generation, trapping, storing and dynamic vectorial transfer of photogenerated electrons across the Schottky junction in a photocatalytic system. *Appl. Surf. Sci.* 360: 601–622.

252 Song, S., Cheng, B., Wu, N. et al. (2016). Structure effect of graphene on the photocatalytic performance of plasmonic Ag/Ag_2CO_3-rGO for photocatalytic elimination of pollutants. *Appl. Catal., B* 181: 71–78.

253 Qi, L., Yu, J., Liu, G., and Wong, P.K. (2014). Synthesis and photocatalytic activity of plasmonic Ag@AgCl composite immobilized on titanate nanowire films. *Catal. Today* 224: 193–199.

254 Zhou, X., Liu, G., Yu, J., and Fan, W. (2012). Surface plasmon resonance-mediated photocatalysis by noble metal-based composites under visible light. *J. Mater. Chem.* 22: 21337–21354.

255 Wang, X., Li, S., Ma, Y. et al. (2011). H_2WO_4 center dot H_2O/Ag/AgCl composite nanoplates: a plasmonic Z-scheme visible-light photocatalyst. *J. Phys. Chem. C* 115: 14648–14655.

256 Low, J., Yu, J., Li, Q., and Cheng, B. (2014). Enhanced visible-light photocatalytic activity of plasmonic Ag and graphene co-modified Bi_2WO_6 nanosheets. *Phys. Chem. Chem. Phys.* 16: 1111–1120.

257 Jiang, J., Yu, J., and Cao, S. (2016). Au/PtO nanoparticle-modified g-C_3N_4 for plasmon-enhanced photocatalytic hydrogen evolution under visible light. *J. Colloid Interface Sci.* 461: 56–63.

258 Yu, S., Wilson, A.J., Kumari, G. et al. (2017). Opportunities and challenges of solar-energy-driven carbon dioxide to fuel conversion with plasmonic catalysts. *ACS Energy Lett.* 2: 2058–2070.

259 Madhusudan, P., Zhang, J., Yu, J. et al. (2016). One-pot template-free synthesis of porous $CdMoO_4$ microspheres and their enhanced photocatalytic activity. *Appl. Surf. Sci.* 387: 202–213.

260 Lei, C.S., Zhu, X.F., Zhu, B.C. et al. (2017). Superb adsorption capacity of hierarchical calcined Ni/Mg/Al layered double hydroxides for Congo red and Cr(VI) ions. *J. Hazard. Mater.* 321: 801–811.

261 Lei, C., Zhu, X., Zhu, B. et al. (2016). Hierarchical NiO-SiO_2 composite hollow microspheres with enhanced adsorption affinity towards Congo red in water. *J. Colloid Interface Sci.* 466: 238–246.

262 He, R., Zhang, J., Yu, J., and Cao, S. (2016). Room-temperature synthesis of BiOI with tailorable (0 0 1) facets and enhanced photocatalytic activity. *J. Colloid Interface Sci.* 478: 201–208.

263 Chen, F., Liu, S.W., and Yu, J.G. (2016). Efficient removal of gaseous formaldehyde in air using hierarchical titanate nanospheres with in situ amine functionalization. *Phys. Chem. Chem. Phys.* 18: 18161–18168.

264 He, R., Cao, S., Yu, J., and Yang, Y. (2016). Microwave-assisted solvothermal synthesis of $Bi_4O_5I_2$ hierarchical architectures with high photocatalytic performance. *Catal. Today* 264: 221–228.

265 Chen, M., Huang, Y., and Lee, S.C. (2017). Salt-assisted synthesis of hollow Bi_2WO_6 microspheres with superior photocatalytic activity for NO removal. *Chin. J. Catal.* 38: 348–356.

266 Yang, J., Wang, D., Han, H., and Li, C. (2013). Roles of cocatalysts in photocatalysis and photoelectrocatalysis. *Acc. Chem. Res.* 46: 1900–1909.

267 Ran, J., Zhang, J., Yu, J. et al. (2014). Earth-abundant cocatalysts for semiconductor-based photocatalytic water splitting. *Chem. Soc. Rev.* 43: 7787–7812.

268 Yu, J., Zhang, J., and Liu, S. (2010). Ion-exchange synthesis and enhanced visible-light photoactivity of CuS/ZnS nanocomposite hollow spheres. *J. Phys. Chem. C* 114: 13642–13649.

269 Ran, J., Yu, J., and Jaroniec, M. (2011). $Ni(OH)_2$ modified CdS nanorods for highly efficient visible-light-driven photocatalytic H_2 generation. *Green Chem.* 13: 2708–2713.

270 Chen, W., Chu, M., Gao, L. et al. (2015). $Ni(OH)_2$ loaded on TaON for enhancing photocatalytic water splitting activity under visible light irradiation. *Appl. Surf. Sci.* 324: 432–437.

271 Xu, Y. and Xu, R. (2015). Nickel-based cocatalysts for photocatalytic hydrogen production. *Appl. Surf. Sci.* 351: 779–793.

272 Zou, X. and Zhang, Y. (2015). Noble metal-free hydrogen evolution catalysts for water splitting. *Chem. Soc. Rev.* 44: 5148–5180.

273 Zhou, X., Jin, J., Zhu, X.J. et al. (2016). New $Co(OH)_2$/CdS nanowires for efficient visible light photocatalytic hydrogen production. *J. Mater. Chem. A* 4: 5282–5287.

274 Chai, B., Liu, C., Wang, C.L. et al. (2017). Photocatalytic hydrogen evolution activity over $MoS_2/ZnIn_2S_4$ microspheres. *Chin. J. Catal.* 38: 2067–2075.

275 Chen, F., Yang, H., Wang, X., and Yu, H. (2017). Facile synthesis and enhanced photocatalytic H_2-evolution performance of NiS_2-modified g-C_3N_4 photocatalysts. *Chin. J. Catal.* 38: 296–304.

276 He, K., Xie, J., Yang, Z. et al. (2017). Earth-abundant WC nanoparticles as an active noble-metal-free cocatalyst for highly boosted photocatalytic H_2 production over g-C_3N_4 nanosheets under visible light. *Catal. Sci. Technol.* 7: 1193–1202.

277 Jiang, D.C., Zhu, L., Irfan, R.M. et al. (2017). Integrating noble-metal-free NiS cocatalyst with a semiconductor heterojunction composite for efficient photocatalytic H_2 production in water under visible light. *Chin. J. Catal.* 38: 2102–2109.

278 Liu, C., Zhang, Y., Dong, F. et al. (2017). Chlorine intercalation in graphitic carbon nitride for efficient photocatalysis. *Appl. Catal., B* 203: 465–474.

279 Ma, S., Xu, X.M., Xie, J., and Li, X. (2017). Improved visible-light photocatalytic H_2 generation over CdS nanosheets decorated by NiS_2 and metallic carbon black as dual earth-abundant cocatalysts. *Chin. J. Catal.* 38: 1970–1980.

280 Wen, J., Xie, J., Shen, R. et al. (2017). Markedly enhanced visible-light photocatalytic H_2 generation over g-C_3N_4 nanosheets decorated by robust nickel phosphide ($Ni_{12}P_5$) cocatalysts. *Dalton Trans.* 46: 1794–1802.

281 Xu, W.C. and Wang, H.X. (2017). Earth-abundant amorphous catalysts for electrolysis of water. *Chin. J. Catal.* 38: 991–1005.

282 Liang, Q.S., Shi, F.B., Xiao, X.F. et al. (2018). In situ growth of CoP nanoparticles anchored on black phosphorus nanosheets for enhanced photocatalytic hydrogen production. *ChemCatChem* 10: 2179–2183.

283 Ma, B.J., Zhang, R.S., Lin, K.Y. et al. (2018). Large-scale synthesis of noble-metal-free phosphide/CdS composite photocatalysts for enhanced H_2 evolution under visible light irradiation. *Chin. J. Catal.* 39: 527–533.

284 Wang, Q.Z., Niu, T.J., Wang, L. et al. (2018). NiFe layered double-hydroxide nanoparticles for efficiently enhancing performance of $BiVO_4$ photoanode in photoelectrochemical water splitting. *Chin. J. Catal.* 39: 613–618.

285 Low, J., Yu, J., and Ho, W. (2015). Graphene-based photocatalysts for CO_2 reduction to solar fuel. *J. Phys. Chem. Lett.* 6: 4244–4251.

286 Cao, S. and Yu, J. (2016). Carbon-based H_2-production photocatalytic materials. *J. Photochem. Photobiol., C* 27: 72–99.

287 Low, J., Yu, J., Jaroniec, M. et al. (2017). Heterojunction photocatalysts. *Adv. Mater.*: 1601694.

288 Moniz, S.J.A., Shevlin, S.A., Martin, D.J. et al. (2015). Visible-light driven heterojunction photocatalysts for water splitting – a critical review. *Energy Environ. Sci.* 8: 731–759.

289 Wang, H., Zhang, L., Chen, Z. et al. (2014). Semiconductor heterojunction photocatalysts: design, construction, and photocatalytic performances. *Chem. Soc. Rev.* 43: 5234–5244.

290 Fu, J.W., Yu, J.G., Jiang, C.J., and Cheng, B. (2018). g-C_3N_4-Based heterostructured photocatalysts. *Adv. Energy Mater.* 8: 1701503.

291 Du, H., Liu, Y.N., Shen, C.C., and Xu, A.W. (2017). Nanoheterostructured photocatalysts for improving photocatalytic hydrogen production. *Chin. J. Catal.* 38: 1295–1306.

292 Zhang, Z., Huang, Y., Liu, K. et al. (2015). Multichannel-improved charge-carrier dynamics in well-designed hetero-nanostructural plasmonic photocatalysts toward highly efficient solar-to-fuels conversion. *Adv. Mater.* 27: 5906–5914.

293 Zhao, Y., Huang, X., Tan, X. et al. (2016). Fabrication of BiOBr nanosheets@TiO_2 nanobelts *p*–*n* junction photocatalysts for enhanced visible-light activity. *Appl. Surf. Sci.* 365: 209–217.

294 Yang, S., Xu, D., Chen, B. et al. (2016). Synthesis and visible-light-driven photocatalytic activity of *p*–*n* heterojunction $Ag_2O/NaTaO_3$ nanocubes. *Appl. Surf. Sci.* 383: 214–221.

295 Sun, B., Zhou, G., Gao, T. et al. (2016). NiO nanosheet/TiO_2 nanorod-constructed *p*–*n* heterostructures for improved photocatalytic activity. *Appl. Surf. Sci.* 364: 322–331.

296 Li, Y., Wang, B., Liu, S. et al. (2015). Synthesis and characterization of Cu_2O/TiO_2 photocatalysts for H_2 evolution from aqueous solution with different scavengers. *Appl. Surf. Sci.* 324: 736–744.

297 Duo, F., Wang, Y., Mao, X. et al. (2015). A $BiPO_4$/BiOCl heterojunction photocatalyst with enhanced electron-hole separation and excellent photocatalytic performance. *Appl. Surf. Sci.* 340: 35–42.

298 Tian, N., Huang, H., and Zhang, Y. (2015). Mixed-calcination synthesis of $CdWO_4$/g-C_3N_4 heterojunction with enhanced visible-light-driven photocatalytic activity. *Appl. Surf. Sci.* 358: 343–349.

299 Feng, Y., Yan, X., Liu, C. et al. (2015). Hydrothermal synthesis of CdS/Bi_2MoO_6 heterojunction photocatalysts with excellent visible-light-driven photocatalytic performance. *Appl. Surf. Sci.* 353: 87–94.

300 Cao, C., Xiao, L., Chen, C., and Cao, Q. (2015). Synthesis of novel Cu_2O/BiOCl heterojunction nanocomposites and their enhanced photocatalytic activity under visible light. *Appl. Surf. Sci.* 357: 1171–1179.

301 Guo, X., Chen, Y.B., Qin, Z.X. et al. (2018). Facet-selective growth of cadmium sulfide nanorods on zinc oxide microrods: intergrowth effect for improved photocatalytic performance. *ChemCatChem* 10: 153–158.

302 Wang, B., Zhang, J.T., and Huang, F. (2017). Enhanced visible light photocatalytic H_2 evolution of metal-free g-C_3N_4/SiC heterostructured photocatalysts. *Appl. Surf. Sci.* 391: 449–456.

303 Teng, W., Tan, X.J., Li, X.Y., and Tang, Y.B. (2017). Novel Ag_3PO_4/MoO_3 *p–n* heterojunction with enhanced photocatalytic activity and stability under visible light irradiation. *Appl. Surf. Sci.* 409: 250–260.

304 Li, P., Zhou, Y., Zhao, Z. et al. (2015). Hexahedron prism-anchored octahedronal CeO_2: crystal facet-based homojunction promoting efficient solar fuel synthesis. *J. Am. Chem. Soc.* 137: 9547–9550.

305 Jiang, G., Wei, M., Yuan, S., and Chang, Q. (2016). Efficient photocatalytic reductive dechlorination of 4-chlorophenol to phenol on {001}/{101} facets co-exposed TiO_2 nanocrystals. *Appl. Surf. Sci.* 362: 418–426.

306 Huang, M., Yu, J., Hu, Q. et al. (2016). Preparation and enhanced photocatalytic activity of carbon nitride/titania(001 vs 101 facets)/reduced graphene oxide(g-C_3N_4/TiO_2/rGO) hybrids under visible light. *Appl. Surf. Sci.* 389: 1084–1093.

307 Lu, D., Zhang, G., and Wan, Z. (2015). Visible-light-driven g-C_3N_4/Ti^{3+}-TiO_2 photocatalyst co-exposed {001} and {101} facets and its enhanced photocatalytic activities for organic pollutant degradation and Cr(VI) reduction. *Appl. Surf. Sci.* 358: 223–230.

308 Zhang, J., Zhang, L.L., Shi, Y.X. et al. (2017). Anatase TiO_2 nanosheets with coexposed {101} and {001} facets coupled with ultrathin SnS_2 nanosheets as a face-to-face *n-p-n* dual heterojunction photocatalyst for enhancing photocatalytic activity. *Appl. Surf. Sci.* 420: 839–848.

309 Xia, P.F., Zhu, B.C., Cheng, B. et al. (2018). 2D/2D g-C_3N_4/MnO_2 nanocomposite as a direct Z-scheme photocatalyst for enhanced photocatalytic activity. *ACS Sustainable Chem. Eng.* 6: 965–973.

310 Lv, J.L., Zhang, J.F., Liu, J. et al. (2018). Bi SPR-promoted Z-scheme Bi_2MoO_6/CdS-diethylenetriamine composite with effectively enhanced visible light photocatalytic hydrogen evolution activity and stability. *ACS Sustainable Chem. Eng.* 6: 696–706.

311 Xu, Q., Zhu, B., Jiang, C. et al. (2018). Constructing 2D/2D Fe_2O_3/g-C_3N_4 direct Z-scheme photocatalysts with enhanced H_2 generation performance. *Sol. RRL* 2: 1800006.

312 Tang, H., Fu, Y., Chang, S. et al. (2017). Construction of Ag_3PO_4/Ag_2MoO_4 Z-scheme heterogeneous photocatalyst for the remediation of organic pollutants. *Chin. J. Catal.* 38: 337–347.

313 Fu, Y.H., Li, Z.J., Liu, Q.Q. et al. (2017). Construction of carbon nitride and MoS_2 quantum dot 2D/0D hybrid photocatalyst: direct Z-scheme mechanism for improved photocatalytic activity. *Chin. J. Catal.* 38: 2160–2170.

314 Song, S., Meng, A., Jiang, S. et al. (2017). Construction of Z-scheme Ag_2CO_3/N-doped graphene photocatalysts with enhanced visible-light photocatalytic activity by tuning the nitrogen species. *Appl. Surf. Sci.* 396: 1368–1374.

315 Ma, Y.J., Bian, Y., Liu, Y. et al. (2018). Construction of Z-scheme system for enhanced photocatalytic H_2 evolution based on CdS quantum dots/CeO_2 nanorods heterojunction. *ACS Sustainable Chem. Eng.* 6: 2552–2562.

316 Yu, W., Chen, J., Shang, T. et al. (2017). Direct Z-scheme g-C_3N_4/WO_3 photocatalyst with atomically defined junction for H_2 production. *Appl. Catal., B* 219: 693–704.

317 Meng, A.Y., Zhu, B.C., Zhong, B. et al. (2017). Direct Z-scheme TiO_2/CdS hierarchical photocatalyst for enhanced photocatalytic H_2-production activity. *Appl. Surf. Sci.* 422: 518–527.

318 Xu, F.Y., Zhang, L.Y., Cheng, B., and Yu, J.G. (2018). Direct Z-scheme TiO_2/NiS core-shell hybrid nanofibers with enhanced photocatalytic H_2-production activity. *ACS Sustainable Chem. Eng.* 6: 12291–12298.

319 Li, J., Zhang, M., Li, Q., and Yang, J. (2017). Enhanced visible light activity on direct contact Z-scheme g-C_3N_4-TiO_2 photocatalyst. *Appl. Surf. Sci.* 391: 184–193.

320 Zhu, C., Zhang, L., Jiang, B. et al. (2016). Fabrication of Z-scheme Ag_3PO_4/MoS_2 composites with enhanced photocatalytic activity and stability for organic pollutant degradation. *Appl. Surf. Sci.* 377: 99–108.

321 Hu, T.P., Li, P.F., Zhang, J.F. et al. (2018). Highly efficient direct Z-scheme WO3/CdS-diethylenetriamine photocatalyst and its enhanced photocatalytic H_2 evolution under visible light irradiation. *Appl. Surf. Sci.* 442: 20–29.

322 Lu, D.Z., Wang, H.M., Zhao, X.N. et al. (2017). Highly efficient visible-light-induced photoactivity of Z-scheme g-C_3N_4/Ag/MoS_2 ternary photocatalysts for organic pollutant degradation and production of hydrogen. *ACS Sustainable Chem. Eng.* 5: 1436–1445.

323 Pan, L., Zhang, J., Jia, X. et al. (2017). Highly efficient Z-scheme WO_{3-x} quantum dots/TiO_2 for photocatalytic hydrogen generation. *Chin. J. Catal.* 38: 253–259.

324 Li, J., Yuan, H., and Zhu, Z. (2016). Improved photoelectrochemical performance of Z-scheme g-C_3N_4/Bi_2O_3/$BiPO_4$ heterostructure and degradation property. *Appl. Surf. Sci.* 385: 34–41.

325 Cui, M., Yu, J., Lin, H. et al. (2016). In-situ preparation of Z-scheme AgI/Bi_5O_7I hybrid and its excellent photocatalytic activity. *Appl. Surf. Sci.* 387: 912–920.

326 Hu, J.Y., Zhang, S.S., Cao, Y.H. et al. (2018). Novel highly active anatase/rutile TiO_2 photocatalyst with hydrogenated heterophase interface structures for photoelectrochemical water splitting into hydrogen. *ACS Sustainable Chem. Eng.* 6: 10823–10832.

327 Luo, J., Zhou, X., Ma, L., and Xu, X. (2016). Rational construction of Z-scheme Ag_2CrO_4/g-C_3N_4 composites with enhanced visible-light photocatalytic activity. *Appl. Surf. Sci.* 390: 357–367.

328 He, R.A., Zhou, J.Q., Fu, H.Q. et al. (2018). Room-temperature in situ fabrication of Bi_2O_3/g-C_3N_4 direct Z-scheme photocatalyst with enhanced photocatalytic activity. *Appl. Surf. Sci.* 430: 273–282.

329 Xin, L., Jin, A.L., Jia, Y.S. et al. (2017). Synergy of adsorption and visible-light photocatalytic degradation of methylene blue by a bifunctional Z-scheme heterojunction of WO_3/g-C_3N_4. *Appl. Surf. Sci.* 405: 359–371.

330 Ge, H.N., Xu, F.Y., Cheng, B. et al. (2019). S-Scheme heterojunction TiO_2/CdS nanocomposite nanofiber as H_2-production photocatalyst. *ChemCatChem* 11: 10.

331 Xu, Q.L., Zhang, L.Y., Yu, J.G. et al. (2018). Direct Z-scheme photocatalysts: principles, synthesis, and applications. *Mater. Today* 21: 1042–1063.

332 Di, T.M., Xu, Q.L., Ho, W.K. et al. (2019). Review on metal sulphide-based Z-scheme photocatalysts. *ChemCatChem* 11: 1394–1411.

333 Lee, J., Ye, H., Pan, S., and Bard, A.J. (2008). Screening of photocatalysts by scanning electrochemical microscopy. *Anal. Chem.* 80: 7445–7450.

334 Ye, H., Lee, J., Jang, J.S., and Bard, A.J. (2010). Rapid screening of $BiVO_4$-based photocatalysts by scanning electrochemical microscopy (SECM) and studies of their photoelectrochemical properties. *J. Phys. Chem. C* 114: 13322–13328.

335 Katz, J.E., Gingrich, T.R., Santori, E.A., and Lewis, N.S. (2009). Combinatorial synthesis and high-throughput photopotential and photocurrent screening of mixed-metal oxides for photoelectrochemical water splitting. *Energy Environ. Sci.* 2: 103–112.

336 Park, H.S., Kweon, K.E., Ye, H. et al. (2011). Factors in the metal doping of $BiVO_4$ for improved photoelectrocatalytic activity as studied by scanning electrochemical microscopy and first-principles density-functional calculation. *J. Phys. Chem. C* 115: 17870–17879.

337 Greeley, J., Jaramillo, T.F., Bonde, J. et al. (2006). Computational high-throughput screening of electrocatalytic materials for hydrogen evolution. *Nat. Mater.* 5: 909–913.

338 Ye, H., Park, H.S., and Bard, A.J. (2011). Screening of electrocatalysts for photoelectrochemical water oxidation on W-doped $BiVO_4$ photocatalysts by scanning electrochemical microscopy. *J. Phys. Chem. C* 115: 12464–12470.

339 Haber, J.A., Cai, Y., Jung, S. et al. (2014). Discovering Ce-rich oxygen evolution catalysts, from high throughput screening to water electrolysis. *Energy Environ. Sci.* 7: 682–688.

340 Xiang, C., Suram, S.K., Haber, J.A. et al. (2014). High-throughput bubble screening method for combinatorial discovery of electrocatalysts for water splitting. *ACS Comb. Sci.* 16: 47–52.

341 Yu, W., Zhang, J., and Peng, T. (2016). New insight into the enhanced photocatalytic activity of N-, C- and S-doped ZnO photocatalysts. *Appl. Catal., B* 181: 220–227.

342 Zhu, B., Zhang, J., Jiang, C. et al. (2017). First principle investigation of halogen-doped monolayer g-C_3N_4 photocatalyst. *Appl. Catal., B* 207: 27–34.

343 Zhang, X., Zhao, X., Wu, D. et al. (2016). $MnPSe_3$ monolayer: a promising 2D visible-light photohydrolytic catalyst with high carrier mobility. *Adv. Sci.* 3: 1600062.

344 Yan, Q., Yu, J., Suram, S.K. et al. (2017). Solar fuels photoanode materials discovery by integrating high-throughput theory and experiment. *Proc. Natl. Acad. Sci. U.S.A.* 114: 3040–3043.

345 Zhou, L., Yan, Q., Shinde, A. et al. (2015). High throughput discovery of solar fuels photoanodes in the CuO–V_2O_5 system. *Adv. Energy Mater.* 5: 1500968.

346 Bard, A. and Fox, M. (1995). Artificial photosynthesis: solar splitting of water to hydrogen and oxygen. *Acc. Chem. Res.* 28: 141–145.

347 Maeda, K. (2013). Z-Scheme water splitting using two different semiconductor photocatalysts. *ACS Catal.* 3: 1486–1503.

348 Sasaki, Y., Nemoto, H., Saito, K., and Kudo, A. (2009). Solar water splitting using powdered photocatalysts driven by Z-schematic interparticle electron transfer without an electron mediator. *J. Phys. Chem. C* 113: 17536–17542.

349 Zhang, L.J., Li, S., Liu, B.K. et al. (2014). Highly efficient CdS/WO_3 photocatalysts: Z-scheme photocatalytic mechanism for their enhanced photocatalytic H_2 evolution under visible light. *ACS Catal.* 4: 3724–3729.

350 Liu, H., Yuan, J., and Shangguan, W. (2006). Photochemical reduction and oxidation of water including sacrificial reagents and Pt/TiO_2 catalyst. *Energy Fuels* 20: 2289–2292.

351 Cheng, D., Negreiros, F.R., Aprà, E., and Fortunelli, A. (2013). Computational approaches to the chemical conversion of carbon dioxide. *ChemSusChem* 6: 944–965.

352 Li, X., Wen, J., Low, J. et al. (2014). Design and fabrication of semiconductor photocatalyst for photocatalytic reduction of CO_2 to solar fuel. *Sci. China Mater.* 57: 70–100.

353 Li, H., Lei, Y., Huang, Y. et al. (2011). Photocatalytic reduction of carbon dioxide to methanol by Cu_2O/SiC nanocrystallite under visible light irradiation. *J. Nat. Gas Chem.* 20: 145–150.

354 Li, X., Liu, H., Luo, D. et al. (2012). Adsorption of CO_2 on heterostructure CdS(Bi_2S_3)/TiO_2 nanotube photocatalysts and their photocatalytic activities in the reduction of CO_2 to methanol under visible light irradiation. *Chem. Eng. J.* 180: 151–158.

355 Yu, J., Wang, K., Xiao, W., and Cheng, B. (2014). Photocatalytic reduction of CO_2 into hydrocarbon solar fuels over g-C_3N_4-Pt nanocomposite photocatalysts. *Phys. Chem. Chem. Phys.* 16: 11492–11501.

356 Wang, K., Li, Q., Liu, B. et al. (2015). Sulfur-doped g-C_3N_4 with enhanced photocatalytic CO_2-reduction performance. *Appl. Catal. B: Environ.* 176–177: 44–52.

357 Liu, Y.Y., Huang, B.B., Dai, Y. et al. (2009). Selective ethanol formation from photocatalytic reduction of carbon dioxide in water with $BiVO_4$ photocatalyst. *Catal. Commun.* 11: 210–213.

358 Mao, J., Peng, T.Y., Zhang, X.H. et al. (2012). Selective methanol production from photocatalytic reduction of CO_2 on $BiVO_4$ under visible light irradiation. *Catal. Commun.* 28: 38–41.

359 Zhao, Y., Chen, G., Bian, T. et al. (2015). Defect-rich ultrathin ZnAl-layered double hydroxide nanosheets for efficient photoreduction of CO_2 to CO with water. *Adv. Mater.* 27: 7824–7831.

360 Zhang, Z., Wang, Z., Cao, S.W., and Xue, C. (2013). Au/Pt nanoparticle-decorated TiO_2 nanofibers with plasmon-enhanced photocatalytic activities for solar-to-fuel conversion. *J. Phys. Chem. C* 117: 25939–25947.

361 Xu, Q., Yu, J., Zhang, J. et al. (2015). Cubic anatase TiO_2 nanocrystals with enhanced photocatalytic CO_2 reduction activity. *Chem. Commun.* 51: 7950–7953.

362 Wang, W., Xu, D., Cheng, B. et al. (2017). Hybrid carbon@TiO_2 hollow spheres with enhanced photocatalytic CO_2 reduction activity. *J. Mater. Chem. A* 5: 5020–5029.

363 Huang, Q., Yu, J., Cao, S. et al. (2015). Efficient photocatalytic reduction of CO_2 by amine-functionalized g-C_3N_4. *Appl. Surf. Sci.* 358: 350–355.

364 Liu, S., Xia, J., and Yu, J. (2015). Amine-functionalized titanate nanosheet-assembled yolk@shell microspheres for efficient cocatalyst-free visible-light photocatalytic CO_2 reduction. *ACS Appl. Mater. Interfaces* 7: 8166–8175.

365 Neatu, S., Macia-Agullo, J.A., Concepcion, P., and Garcia, H. (2014). Gold-copper nanoalloys supported on TiO_2 as photocatalysts for CO_2 reduction by water. *J. Am. Chem. Soc.* 136: 15969–15976.

366 Pastor, E., Pesci, F.M., Reynal, A. et al. (2014). Interfacial charge separation in Cu_2O/RuO_x as a visible light driven CO_2 reduction catalyst. *Phys. Chem. Chem. Phys.* 16: 5922–5926.

367 Tsai, C.W., Chen, H.M., Liu, R.S. et al. (2011). Ni@NiO core-shell structure-modified nitrogen-doped $InTaO_4$ for solar-driven highly efficient CO_2 reduction to methanol. *J. Phys. Chem. C* 115: 10180–10186.

368 Zhai, Q., Xie, S., Fan, W. et al. (2013). Photocatalytic conversion of carbon dioxide with water to methane: platinum and copper(I) oxide co-catalysts with a core-shell structure. *Angew. Chem. Int. Ed.* 52: 5776–5779.

369 Hamdy, M.S., Amrollahi, R., Sinev, I. et al. (2014). Strategies to design efficient silica-supported photocatalysts for reduction of CO_2. *J. Am. Chem. Soc.* 136: 594–597.

370 Hoffmann, M., Martin, S., Choi, W., and Bahnemann, D. (1995). Environmental applications of semiconductor photocatalysis. *Chem. Rev.* 95: 69–96.

371 Chen, C., Ma, W., and Zhao, J. (2010). Semiconductor-mediated photodegradation of pollutants under visible-light irradiation. *Chem. Soc. Rev.* 39: 4206–4219.

372 Park, H., Park, Y., Kim, W., and Choi, W. (2013). Surface modification of TiO_2 photocatalyst for environmental applications. *J. Photochem. Photobiol., C* 15: 1–20.

373 Chatterjee, D. and Dasgupta, S. (2005). Visible light induced photocatalytic degradation of organic pollutants. *J. Photochem. Photobiol., C* 6: 186–205.

374 Zhang, H., Chen, G., and Bahnemann, D.W. (2009). Photoelectrocatalytic materials for environmental applications. *J. Mater. Chem.* 19: 5089–5121.

375 Chong, M.N., Jin, B., Chow, C.W.K., and Saint, C. (2010). Recent developments in photocatalytic water treatment technology: a review. *Water Res.* 44: 2997–3027.

376 Zhao, B.X. and Zhang, P.Y. (2009). Photocatalytic decomposition of perfluorooctanoic acid with beta-Ga_2O_3 wide bandgap photocatalyst. *Catal. Commun.* 10: 1184–1187.

377 Li, X.Y., Zhang, P.Y., Jin, L. et al. (2012). Efficient photocatalytic decomposition of perfluorooctanoic acid by indium oxide and its mechanism. *Environ. Sci. Technol.* 46: 5528–5534.

378 Zhang, L., Ran, J., Qiao, S.Z., and Jaroniec, M. (2019). Characterization of semiconductor photocatalysts. *Chem. Soc. Rev.* 48: 5184–5206.